01 Oct 1995

Strength of flexural members using structural grade 80 of A653 and grade E of A611 steels

Shaojie Wu

Wei-Wen Yu
Missouri University of Science and Technology, wwy4@mst.edu

Roger A. LaBoube
Missouri University of Science and Technology, laboube@mst.edu

Civil Engineering Study 95-5
Cold-Formed Steel Series

First Progress Report

STRENGTH OF FLEXURAL MEMBERS USING STRUCTURAL GRADE 80 OF A653 AND GRADE E OF A611 STEELS

by

Shaojie Wu
Research Associate

Wei-Wen Yu
Roger A. LaBoube
Project Directors

A Research Project Sponsored by
the American Iron and Steel Institute

October, 1995

Department of Civil Engineering
University of Missouri-Rolla
Rolla, Missouri

ABSTRACT

This first progress report reviews earlier research on ASTM A653 Structural Grade 80 steel (formerly ASTM A446 Grade E) and similar steels used for cold-formed structural members, and summarizes the results of the tension coupon tests recently carried out at the University of Missouri-Rolla. The review focuses on experimental study and structural performance of members made of such steels, including ultimate strength of structural members as affected by the increases in yield strength of base metal, reduction in ductility of base metal, thickness of base metal, flat width-to-thickness ratio of elements, type of deck profile, and base metal rolling direction. The cold-formed structural members considered in this study include beams, decks, connections, and columns. The results obtained from the tension coupon tests include the 0.2% offset yield strength and tensile strength, stress-strain relationship, 2-inch gage length percent elongation, local and uniform percent elongations of the A653 Structural Grade 80 steel in two orthotropic directions.

It is noted that limited information on the A653 Structural Grade 80 steel and similar steels is available in published literature. Searching for such information continues. Available test data and evaluation of the data indicate that cold-formed structural members (mainly beams and connections) made of the A653 Structural Grade 80 steel may be designed based on a stress level that is higher than 75% of the specified yield and tensile strengths of the steel.

The tension coupon tests indicated that the 0.2% offset yield and tensile strengths of the A653 Structural Grade 80 steel both in the rolling direction and perpendicular to the rolling direction increase with the decreases in thickness of steel sheets, while the ductility of the steel decreases with the decreases in thickness of steel sheets. The material properties perpendicular to the rolling direction are significantly different from those in the rolling direction.

TABLE OF CONTENT

LIST OF TABLES

LIST OF TABLES

LIST OF FIGURES

1. INTRODUCTION

1.1 BACKGROUND

As per the Specification for the Design of Cold-Formed Steel Structural Members (AISI 1986) and the Load and Resistance Factor Design Specification for Cold-Formed Steel Structural Members (AISI 1991), ASTM A653 Structural Grade 80 steel (earlier ASTM A446 Grade E steel) is allowed to be used for cold-formed structural members of particular configurations. The unique properties of the Structural Grade 80 steel, as compared to the conventional steels used for cold-formed members, is that it has a high specified yield strength (F_y=80 ksi (552 MPa)) and a low tensile-to-yield strength ratio (F_u/F_y=1.03). The ductility of the steel is unspecified (Yu 1991). As a result of these characteristics, the use of the Structural Grade 80 steel has been limited in the areas where the members are cold-formed with large radii and the connections are not highly stressed, such as roofing, floor decks, wall panels, and bridge deck forms.

Due to the lack of ductility and low tensile-to-yield strength ratio (hereafter referred to as F_u/F_y ratio) of the Structural Grade 80 steel and considering the required ductility for adequate structural performance, the AISI Specifications permit the use of Structural Grade 80 steel provided that (1) the yield strength, F_y, used for design of elements, members, and structural assemblies, is taken as 75% of the specified minimum yield point or 60 ksi (414 MPa), whichever is less, and (2) the tensile strength, F_u, used for design of connections and joints, is taken as 75% of the specified minimum tensile strength or 62 ksi (428 MPa), whichever is less. This simple reduction of the specified strengths by 25% for designing both members and connections indicates that the structural performance of the cold-formed members and connections made of Structural Grade 80 steel has not been fully understood. A more detailed investigation on structural performance as affected by high yield and tensile strengths, low ductility, and low F_u/F_y ratio of the Structural Grade 80 steel is needed.

1.2 OBJECTIVE AND SCOPE

In September 1994, a research project entitled "Strength of Flexural Members Using Structural Grade 80 of A653 and Grade E of A611 Steels" was initiated at the University of Missouri-Rolla under the sponsorship of American Iron and Steel Institute. The objective of the overall research is to study the structural performance and strength of the cold-formed steel members and connections made of ASTM A653 Structural Grade 80 steel. In addition, appropriate design criteria will be developed for consideration in the AISI Specifications.

The overall research consists of three phases: preliminary study (first phase); experimental investigation (second phase); and development of design recommendations (third phase). The preliminary study includes several major tasks: (1) collecting available test data and publications relative to the use and design of Structural Grade 80 steel, (2) analyzing the available test data with an emphasis given to the type of failure mode, and (3) comparing the available test data with the current AISI design approach and other design specifications. This first progress report summarizes the results of the preliminary study. It contains a literature review on Structural Grade 80 steel and similar steels, evaluation of available test data, and a summary of the results of the tension coupon tests. The report focuses on the geometric parameters used in earlier research (such as thickness and flat-width-to-thickness ratio (hereafter referred to as w/t ratio)), strength, ductility, type of failure mode of test specimens, and comparison between test results and the values predicted using the AISI Specifications. The results of the tension coupon tests include 0.2% offset yield and tensile strengths, stress-strain relationship, 2-inch gage length percent elongation, local and uniform elongations.

2. LITERATURE REVIEW

A broad range of published literature on earlier experimental studies of ASTM A653 Structural Grade 80 steel and steels similar to the Structural Grade 80 steel has been searched. The sources of the literature include published conference papers, industry and university research reports, journal papers, and several unpublished papers and reports. The literature was published over a time period from the 1970's to the present. Research conducted both domestically and abroad has been reviewed. The review focuses on the experimental study of material properties of the Structural Grade 80 steel and similar steels and the structural performance of the members made of such steels, including buckling and post-buckling behavior and ultimate strength of the members as affected by the increases in strength of base metal, reduction in ductility of base metal, thickness of base metal, flat width-to-thickness ratio of elements, type of deck profile, and base metal rolling direction. The test specimens include tensile coupons, perforated sheets and wall studs, beams and deck panels, columns, and connections.

A brief review of earlier research on steels having low ductility, low tensile-to-yield strength ratio, and/or high strength is presented in Section 2.1. The literature review on the Structural Grade 80 steel and similar steels is presented in three different sections. Section 2.2 deals with tests of material properties, including tensile tests on perforated sheets and wall studs. Section 2.3 discusses tests of members, such as beams and columns. Section 2.4 deals with tests of connections. In each section, earlier tests of the Structural Grade 80 steel are reviewed first, followed by the tests of steels similar to the Structural Grade 80 steel. The review follows the chronological order of the published literature.

2.1 EARLIER RESEARCH ON STEELS HAVING LOW-DUCTILITY, LOW TENSILE-TO-YIELD STRENGTH RATIO, AND/OR HIGH STRENGTH

(a) Dhalla and Winter (1971a,b,c, 1974a,b) studied different low ductility steels to investigate ductility

requirements on structural performance of cold-formed members. The study included coupon tests, connection tests (perforated, bolted, and welded), and finite element analyses of perforated steel sheets. Bending and compression tests were not included in the investigation. The study recognized local elongation of low ductility steels due to necking, as seen in hot-rolled steels, and its effect on structural performance of cold-formed steel members. As a result, two elongation parameters, local elongation (including fracture) in a 1/2-inch (12.7 mm) gage length (namely necking zone) and uniform elongation (excluding fracture) in a 2-inch (50.8 mm) gage length, were introduced. Based on the elongations, a low ductility steel can be evaluated for its suitability in developing complete plastification of a critical section in a tension member with stress concentrations.

Experimental and analytical studies concluded that a sheet steel has sufficient ductility to wipe out stress concentrations and completely plastify critical section in a thin rectangular plate with perforation or in a bolted or welded connection, if the steel has an uniform elongation of 3% and a F_u/F_y ratio of about 1.10, but has a small local elongation (necking strain), such as the A653 Structural Grade 80 steel in rolling direction (longitudinal direction). The same conclusion could be reached if a steel has a local elongation larger than 20%, but the uniform elongation is less than 3% and the F_u/F_y ratio is 1.01.

(b) Macadam et al. (1988) tested simple beams and columns made of two steels. One steel (virgin ductile steel) had a yield strength ranging from 69.4 to 72.5 ksi (478.5 to 499.9 MPa) in the rolling direction (longitudinal direction) and a F_u/F_y ratio ranging from 1.04 to 1.06. The other steel (cold-reduced steel) had a higher yield strength ranging from 79.9 to 83.4 ksi (550.9 to 575.0 MPa) in the rolling direction and a lower F_u/F_y ratio ranging from 1.01 to 1.03. The virgin ductile steel satisfied all the ductility requirements of the AISI Specifications. The cold-reduced steel had a 2-inch gage length elongation of 9%, an uniform elongation of 0.8%, but a very large local elongation of 33.8%. The yield strength in compression in the rolling direction was about 85% of that in tension for the virgin ductile steel and about 81% of that in tension for the cold-reduced steel due to Bauschinger effect. The tensile properties perpendicular to the rolling direction (transverse direction) were similar to those in the rolling direction. The thickness of the

virgin ductile steel specimens was 0.101 inches (2.565 mm) and the thickness of the cold-reduced steel specimens was 0.096 inches (2.438 mm). The w/t ratio for stiffened flanges ranged from 17.00 to 42.27 and the ratio for unstiffened flanges ranged from 6.90 to 16.70.

The beam tests concluded that the AISI Specification (1986) for flexural members with regard to effective width, lateral-torsional buckling, and nominal flexural strength based on first yielding are applicable to members made of low strain hardening ductile steels (F_u/F_y ratio is less than 1.08). The ratio of measured beam flexural strength to calculated strength (M_{test}/M_{calc}) was 0.97 (for cross-section capacity provisions) and 0.98 (for lateral-torsional buckling provisions) for the cold-reduced steel specimens when using the tested yield strength in tension for the strength calculation, while the ratio became 1.12 and 1.19, respectively, when using the tested yield strength in compression for the calculation. The ratios for the virgin ductile steel specimens are all larger than those for the cold-reduced steel specimens, ranging from 1.02 to 1.41. The stub column tests indicated that the ratio of measured column strength to calculated strength was 0.84 for the virgin ductile steel specimens and 0.87 for the cold-reduced steel specimens when using the tested yield strength in tension for the calculation, while the ratio became 0.96 and 1.04, respectively, when using the tested yield strength in compression for the calculation.

(c) Pan and Yu (1988) conducted tests on I-shaped beams and stub columns using high strength ductile steels. The tests focused on the effect of high yield strength on effective width of unstiffened compression elements. The w/t ratios of the specimens ranged from 5.65 to 53.28 for unstiffened flanges, with 6.50 to 23.24 for beams using 80 and 100 ksi (552 and 690 MPa) steels, 5.65 to 39.46 for stub columns using 80 ksi steel, 6.81 to 49.10 for stub columns using 100 ksi steel, and 9.64 to 53.28 for stub columns using 140 ksi (965 MPa) steel. The thickness of the specimens varied from 0.046 to 0.088 inches, with 0.065 and 0.088 inches (1.651 and 2.235 mm) for beams and 0.046, 0.065, and 0.088 inches (1.168, 1.651, and 2.235 mm) for stub columns. The yield strength in tension ranged from 77.1 to 165.1 ksi (531.6 to 1138.4 MPa) and the yield strength in compression from 84.3 to 153.3 ksi (581.3 to 1057.0 MPa). The difference between the yield strengths in tension and compression is not significant. The elongation in a 2-inch gage

length ranged from 4.30 to 20.40% (20.40% for 80 ksi steel, 8.10% for 100 ksi steel used for beams, 10.10% for 100 ksi steel used for stub columns, and 4.30% for 140 ksi steel).

The beam tests revealed that the calculated beam strength using the AISI Specification (1986) agreed well with the tested flexural strength of all the beams based on first yielding in compression flange, with a mean ratio of measured beam strength to calculated strength, M_{test}/M_{calc}, ranging from 1.03 for 80 ksi steel to 0.98 for 100 ksi steel. And, for the stub column tests, the mean ratio of measured column strength to calculated strength, P_{test}/P_{calc}, was 0.97 for 80 ksi steel, 0.92 for 100 ksi steel, and 0.82 for 140 ksi steel. The effective width is apparently affected by the increases in yield strength. Measured edge strains on the stub columns indicated that the maximum edge stresses were smaller than the yield strength at failure, and the ratio of the maximum edge stress to the yield strength decreases with the increases in w/t ratio and yield strength. An equation was developed to modify the yield strength and was used to evaluate both beam and stub column strengths. The equation provided excellent correlation with experimental results for all the w/t ratios and yield strengths used in the tests. The average ratio of measured strength to modified calculated strength ranged from 0.99 to 1.05 for 80 and 100 ksi steels (with a 2-inch gage length elongation ranging from 8.10% to 20.40%), whereas for 140 ksi steel (with a 2-inch gage length elongation of 4.30%), the ratio was 0.96. This indicates that member flexural strength based on first yielding may be affected more strongly by the increases in yield strength of the base material than by the ductility of the material.

2.2 TESTS OF MATERIAL PROPERTIES OF STRUCTURAL GRADE 80 STEEL AND SIMILAR STEELS

2.2.1 Tests of Structural Grade 80 Steel

Dhalla and Winter (1971b) tested nine coupons made of A653 Structural Grade 80 steel ('Z' steel designated in the reference) as part of the tests of material properties of several low ductility steels. The Structural Grade 80 steel specimens had a thickness of 0.038 (0.965 mm) inches. The coupon tests indicated

that the properties of the Structural Grade 80 steel differed significantly in the longitudinal direction (parallel to rolling direction, six coupons) and in the transverse direction (perpendicular to rolling direction, three coupons). The average values are listed in the following table.

Loading Direction With Respect To Rolling Direction	0.2% Offset Yield Strength F_y (ksi/MPa)	Tensile Strength F_u (ksi/MPa)	F_u/F_y Ratio	Elongation In 2-inch Gage Length (including necking) (%)	Elongation in 1/2-inch gage length (including necking) (%)	Elongation in 2-1/2-inch gage length (excluding necking) (%)
Longitudinal (parallel to rolling)	75.5/520.6	81.7/563.3	1.08	4.38	9.86	2.74
Transverse (perpendicular to rolling)	99.4/685.4	99.8/688.1	1.00	1.34	4.15	0.48

As shown in Fig. 2.2.1, the Structural Grade 80 steel (Z steel) had significantly more strain in the strain hardening range (uniform strain) in the longitudinal direction than in the transverse direction. The average uniform elongation in a 2-1/2-inch (63.5 mm) gage length was 2.74% in the longitudinal direction and 0.48% in the transverse direction. The strain corresponding to necking (local strain) was small in both directions as shown in the figure. The average local elongation in a 1/2-inch (12.7 mm) gage length (including fracture) was 9.86% in the longitudinal direction and 4.15% in the transverse direction.

To study the ductility requirement for the low ductility Structural Grade 80 steel in achieving tensile strength of cold-formed steel sheets with a stress raiser, Dhalla and Winter (1971b) conducted tension tests for seven perforated sheets made of the Structural Grade 80 steel (the ratio of the hole diameter to the width of the tension coupon ranged from 0.04 to 0.32 for the coupons loaded in the longitudinal direction and

from 0.10 to 0.33 for the coupons loaded in the transverse direction). The thickness of the sheets was 0.038 inches (0.965 mm). It was found that for the Structural Grade 80 steel in the longitudinal direction (five sheets), the ratio of the average stress on net area at ultimate load to the material tensile strength determined from the coupon tests ranged from 0.99 to 1.17, while in the transverse direction (two sheets), the ratio was 0.94 when the sheets failed in a semi-brittle manner. The strength of the sheets, which was based on the tensile strength of the base material, appears to depend on the ductility of the material. Smaller ductility seems to result in a smaller strength ratio, but the strength ratio still reached 1.00 for the sheets loaded in the rolling direction.

2.2.2 Tests of Steels Similar to Structural Grade 80 Steel

(a) Maricic (1979) summarized several typical high strength sheet steels on the Australian market at that time. He indicated that the steels with a yield strength of 550 MPa (79.8 ksi) and a thickness ranging from 0.400 to 0.950 mm (0.016 to 0.037 inches) had a minimum elongation of 2% in a 50 mm (2 inches) gage length.

(b) Hancock (1995) reported test results on the ductility of the G550 steel conforming to Australia Standard AS1397. The Australia G550 Steel was considered to be similar to the ASTM A653 Structural Grade 80 steel. According to AS1397, the G550 steel has a minimum elongation of 2% in a 2-inch gage length. It is indicated that G550 steel may or may not satisfy the Dhalla and Winter's uniform and local elongation requirements, depending on the thickness of the steel. While 0.900 mm (0.035 inches) thick G550 steel satisfies the uniform and local elongation requirements, 0.420 mm (0.017 inches) thick G550 steel does not. Tensile coupon tests on 0.420, 0.480, 0.600, 0.800, and 1.000 mm (0.017, 0.019, 0.024, 0.031, and 0.039 inches) thick steels showed that the 0.600, 0.800, and 1.000 mm thick steels satisfied the uniform elongation requirement (not less than 3%), but only the 1.000 mm thick steel satisfied the local elongation requirement (not less than 20%) as shown in following table.

Coupon Thickness (mm/inch)	Uniform Elongation (%)	Local Elongation in 10-mm (0.40-inch) gage length (%)	Tensile to Yield Strength Ratio
0.420/0.017	1.30	12.80	#
0.480/0.019	1.80	13.50	#
0.600/0.024	3.90	18.00	1.02
0.800/0.031	8.10	19.50	1.06
1.000/0.039	8.60	20.60	1.12

Note: "#" means that data was not determined accurately due to rounding of stress-strain curve with resultant low 0.2% proof stress.

Tensile tests on wall studs having holes in the flange and web (a 36 mm (1.417 inches) circular hole in the web and a 20 mm (0.787 inches) circular hole in each flange) were carried out to study the effect of thickness on tensile strength of the G550 steel sheets with stress raiser. The test results indicated that the ratio of ultimate net section strength of the wall studs to the coupon tensile strength varied from 0.94 to 0.97, increasing with the increases in thickness of the G550 steel sheets.

2.3 TESTS OF STRUCTURAL MEMBERS MADE OF STRUCTURAL GRADE 80 STEEL AND SIMILAR STEELS

2.3.1 Members Made of Structural Grade 80 Steel

Six Butler Manufacturing Company's BR-II rib corrugated Hi-Ten galvanized sheet steel panels, made of

ASTM A653 Structural Grade 80 steel, were tested under uniform loads (MRI 1978). The measured thickness of the base metal ranged from 0.015 to 0.016 inches (0.381 to 0.406 mm) (29 gage, nominal thickness of base metal of 0.015 inches (0.381 mm)). Tension coupons were cut from the tested panels, and tensile tests of the coupons indicated that yield strength of the material ranged from 109.9 to 113.4 ksi (758.0 to 781.6 MPa) and the tensile strength was exactly the same as the yield strength for all the coupons. Note that the actual yield strength was much higher than the specified nominal yield strength of 80 ksi (552 MPa). The percent elongation in a 2-inch gage length ranged from 2 to 3%. According to the product catalog of the Butler panels as shown in Fig. 2.3.1, the flat width-to-thickness ratio (w/t ratio) of the top compression flange of the rib (stiffened flange) was 85.42, while the w/t ratios of the edge subelement of the pan, middle subelement of the pan, and entire pan are 170.83, 133.33, and 608.33, respectively. Local and uniform elongations and modulus of elasticity of the steel were not available in the reference.

Among the six tested panels, two were three-span continuous panels with each span length of 7'-6" (2286 mm), two were two-span continuous panels with each span length of 7'-6", and two were five-span continuous panels with each span length of 5' (1524 mm). Purlins were used as intermediate supports. All the panels were simply supported on the purlins and edge frames. Fasteners were used to attach the panels only on the purlins and the end girts. Uniform load was applied through a vacuum plenum chamber that was connected to suction fans. Among each set of two panels, one panel was loaded under positive pressure, and another loaded under negative pressure.

It was found that the failure of the panels under positive pressure was due to buckling of compressed panel ribs (trapezoidal shape as shown in Fig. 2.3.1) over the purlin locations, while the failure of the panels under negative pressure was due to pulling fasteners through panels. The buckles were elastic in nature since they recovered when pressure on the panels was reduced. Deflections at different spans were measured and plotted against load pressure. The load-deflection relationships of all the test panels indicated that the behavior of the panels was almost linear prior to failure. Predicted ultimate strength of the panels and comparison between the tested and predicted strengths were not available in the reference.

2.3.2 Members Made of Steels Similar to Structural Grade 80 Steel

(a) Mahendran (1992) tested corrugated and trapezoidal roof panels under fatigue loading to study fatigue behavior of connections between fasteners and steel panels. The specimens were made of Australian G550 steel with a minimum yield strength of 550 MPa (79.8 ksi) and a base metal thickness of 0.420 mm (0.017 inches). The depth of the corrugated profile was 16 mm (0.629 inches) and the depth of the trapezoidal profile was 29 mm (1.142 inches). A concentrated load was applied at the ribbed crest in the middle of the panel. Effect of an overload at earlier stage of fatigue life on panel behavior was studied. Ductility of the steel is not available in the reference.

Static tests were carried out prior to fatigue tests. The static tests indicated that for the corrugated profile, the crests dimpled in a rhombus shape and underwent a localized plastic mechanism, while for trapezoidal profile, the crests did not undergo a localized plastic mechanism, but instead underwent only a localized yielding around the fastener holes. This yielding eventually lead to a pull through failure. The ultimate load per fastener of the trapezoidal panels was 1500 N (337.2 lb) and was higher than that of the corrugated panels (between 870 and 920 N (195.6 to 206.8 lb)). Comparison of measured strength with predicted strength for the static tests was not available in the reference.

Prior to fatigue tests, an overload, 900 N (202.3 lb) on the corrugated panels and 1300 N (292.3 lb) on the trapezoidal panels, was applied on specimens to form a dimple or permanent deformation on the crests. Fatigue tests indicated that an early formed localized plastic mechanism in the corrugated panels reduced local panel stiffness and increased strain along yield lines, eventually resulting in a shortened fatigue life as compared to the tests without the overload. However for the trapezoidal panels, the overload caused a local membrane action which increased the local panel stiffness and lengthened fatigue life as compared to the tests without the overload.

(b) Salaheldin and Schmidt (1992) conducted tests on simply supported corrugated deck panels (profile type

A) and trapezoidal deck panels (profile type B) loaded by a concentrated load at the center of each deck. The average yield strength and modulus of elasticity obtained from coupon tests were 600 MPa (87.0 ksi, similar to the Australian G550 steel) and 200 GPa (29006.5 ksi), respectively. The geometric properties of the panels and the test program are shown in Fig. 2.3.2. Ductility of the steel is not available in the reference.

In all the test specimens, the formation of a local plastic mechanism at the ribs progressed from the load location toward longitudinal edges of the panels, indicating a considerable post-buckling strength of the panels. The measured maximum deflection corresponding to the ultimate strength ranged between 4 and 5 inches (101.6 and 127.0 mm) for all the test specimens. The study indicated that for long span panels, a considerable redistribution of stress with the increases in central deflection occurred across the panels, while for short span panels, the stresses were concentrated at the center of the panels where the load was located. The tests showed that the increases in the depth of the profile reduced the ability of the panels to redistribute the longitudinal membrane stresses across the width of the panels.

(c) A total of thirteen channel section columns were tested by Kwon and Hancock (1991, 1992) to study the behavior and strength of the columns undergoing distortional and mixed local-distortional buckling. The channel section was formed by a press brake. Six columns consisted of simple lipped channel without intermediate stiffener in the web, and seven columns consisted of simple lipped channel with an intermediate stiffener in the web. The columns were tested under fixed-end boundary conditions. The channels were made of cold-reduced zinc-coated steel conforming to AS1397 Grade G500. The steel had a tested mean yield strength of 590.3 MPa (85.6 ksi), a tested mean tensile strength of 621.7 MPa (90.2 ksi), a mean tensile-to-yield strength ratio of 1.06, and a mean base metal thickness of 1.100 mm (0.043 inches). The ratio of the measured ultimate stress in the columns at failure to the actual yield strength ranged from 0.24 to 0.27 for the columns without intermediate stiffener in the web and from 0.28 to 0.36 for the columns with intermediate stiffener in the web. The ratio of the measured buckling stress to the yield strength ranged from 0.08 to 0.15 for the columns without intermediate stiffener in the web and from 0.12 to 0.27

for the columns with intermediate stiffener in the web. The post-buckling strength reserve was large for all the columns.

The strengths of the columns were evaluated using the AISI Specification (1986) and the actual yield strength of the base metal material. The ratio of tested column strength to the predicted strength ranged from 0.85 to 1.03, with a mean ratio of 0.90.

(d) Comprehensive research on cold-formed profiled steel decks having intermediate stiffeners was carried out in Australia by Bernard et al. (1992a,b, 1993c). The decks were made of cold-reduced aluminum/zinc coated Grade G550 steel which has a minimum yield strength of 550 MPa (79.8 ksi) and a minimum elongation of 2%. According to Hancock (1995), the AS1397 Grade G550 steel is similar to ASTM A653 Structural Grade 80 steel. Measured elastic modulus of the Grade G550 steel with coating was 220 GPa (31907.2 ksi), while a higher modulus of 230 GPa (33358.5 ksi) was measured for the base metal alone. The mean measured 0.2% yield strength of uncoated base metal was 653 MPa (94.7 ksi) and the mean measured tensile strength was 656 MPa (95.1 ksi), resulting in a F_u/F_y ratio of 1.01. The base metal thickness varied from 0.580 to 0.588 mm (about 0.023 inches). The net longitudinal residual stress (the stress in the middle-plane of a sheet, calculated based on measured surface stresses on two sides of the sheet) and the surface flexural residual stresses (measured using foil strain gages on two sides of a sheet) were obtained from several tested decks and found to be in an order of 5 to 10 MPa (0.7 to 1.5 ksi) for the longitudinal residual stress and 80 to 120 MPa (11.6 to 17.4 ksi) for the flexural residual stress. The distribution of the longitudinal residual stress did not show a clear pattern based on a small number of test specimens and the stresses were less than the mean critical elastic buckling stress of each specimen by an order of magnitude, therefore, the residual stresses were not considered in the analyses. Both local and uniform elongations were not available in the reference.

The decks consisted of hat sections. Only one stiffener was located at the center of each compression flange as shown in Fig. 2.3.3. A total of twelve decks with four trapezoidal ribs of V shaped stiffeners, and a total

of nine decks with three trapezoidal ribs of flat-hat shaped stiffeners were tested. In another group of specimens, a total of six decks with four trapezoidal ribs without stiffeners, and a total of two decks with three trapezoidal ribs without stiffeners were tested as shown in Fig. 2.3.3. The stiffener height ranged from 3 to 12 mm (0.118 to 0.472 inches). The w/t ratio of the subelements for the decks with V shaped stiffeners ranged from 64.20 to 71.70, while the w/t ratio was 79.20 for the decks with flat-hat shaped stiffeners. The w/t ratio of the compression flange without a stiffener ranged from 74.20 to 223.30. The height of the hat section was about 54 mm (2.126 inches) for all the decks. The detailed geometries of the hat sections are shown in Fig. 2.3.3. The test set-up as shown in Fig. 2.3.4 was designed such that the deck specimen was subjected to uniform bending over the entire length of the specimen.

Both local and distortional buckling modes of V shaped and flat-hat shaped decks are shown in Figures 2.3.5 and 2.3.6. Only the local buckling mode was found in the decks without stiffeners. Numerical analyses based on the finite strip method for thin-walled members were conducted to determine critical moments and were found to compare well with measured buckling moments and buckled wave lengths. The analyses for the decks with V shaped stiffeners indicated that when measured imperfection of the compression flange was considered in the finite strip models, the estimated moments compared well with the measured values, otherwise, the numerical values underestimated the tested values for small stiffeners. The analyses for the decks with flat-hat stiffeners was not sensitive to the imperfection. Both local and particularly distortional buckled waveforms were observed to move along the length of the specimens during the tests. As moment increased, more waveforms popped up into the flanges. When distortional buckles occurred prior to local buckles, the local buckles were not superimposed on the distortional buckles. But when distortional buckles occurred after local buckles, the local buckles were superimposed on the distortional buckles. For all the tests, the measured critical buckling moments were less than the measured ultimate moment (average 35% of the ultimate moment for the decks with V shaped stiffeners and 65% of the ultimate moment for the decks with flat-hat shaped stiffeners). Post-buckling strength reserve was apparently available in the decks.

All tests were terminated with a brittle failure involving a spatial plastic mechanism centered on either a local or a distortional buckled cell (a buckled wave). The measured ultimate strength was compared to the code-predicted strength. As shown in Tables 2.3.1 and 2.3.2, according to the AISI Specification (1991), for the decks without stiffeners (ST21A through ST23B)) and the decks with small V shaped stiffeners (IST43A through IST48B), the tested strength was larger than the code-predicted strength. However, for the decks with larger V shaped stiffeners (IST48A through IST412B) and the decks with flat-hat shaped stiffeners (TS3A1 through TS3B6), the test strength was lower than the code-predicted strength. In the latter case, an interaction between local and distortional buckling was observed, in which the buckling process was characterized as local buckling first followed by distortional buckling. Actual yield strength was used for the computations.

The study concluded that the European code (Eurocode 3/Annexe A) consistently underestimates the ultimate strength of the decks as compared to the tested strength as shown in Tables 2.3.3 and 2.3.4. The tested strength is about 20% larger than the code-predicted strength. Similar results, as calculated using the AISI Specification (1991), were predicted using the Australia Standard as shown in Tables 2.3.5 and 2.3.6, but the standard deviation as predicted using the Australia Standard is much higher than that as predicted using the European code.

An unified approach, which determines the ultimate strength involving an interaction between local and distortional buckling, was developed by Pekoz and was used to check against the tested strength. The results indicate that the unified approach is conservative as shown in Table 2.3.7. Bernard et al. (1993c) then modified the Pekoz's approach by introducing a higher post-buckling stress for determining the effective section modulus. The results are still conservative by more than 15% as shown in Tables 2.3.8 and 2.3.9. The distortional buckling stress used in the Bernard's calculation was based on the finite strip analyses.

Using the same material and test program, Bernard et al. (1993a) tested twelve Condeck rolled panels as

shown in Fig. 2.3.7. Half of the tested panels were loaded in positive bending and the others in negative bending. Six Condeck panels (three in positive bending and three in negative bending) had a base metal thickness of 1.000 mm (0.039 inches), and six Condeck HP panels (three in positive bending and three in negative bending) had a base metal thickness of 0.750 mm (0.030 inches). The buckling modes observed from tests and numerical analyses were shown in Fig. 2.3.8. Residual stress was considered when the test results were interpreted. Compression flange curling, as observed in the central pan of the test panels in negative bending, was taken into account in the numerical analyses.

For the Condecks, it was found that the flange curling had an effect on the redistribution of stress. The redistribution caused by flange curling was more pronounced than any redistribution accompanying the onset of buckling for the specimens loaded in negative bending. Both local and distortional buckling strengths obtained from numerical analyses compared well with the test results when flange curling was considered in the models. The ultimate strength in negative bending and in local buckling mode, based on Australia Standard AS1538 (Winter's formula for effective width), was also affected by flange curling. When flange curling was not considered (larger effective width for compression flange was resulted in), the code-predicted ultimate strength was higher than the tested strength, but when the flange curling was considered (ignoring central pan results in a smaller effective width for compression flange), the code-predicted strength was close to the test strength. Calculation of flange curling was based on the Eurocode 3/Annex A. Final failure in all the tests occurred through a spatial plastic collapse mechanism. Measured ultimate moments were all higher than the buckling moments, indicating an apparent post-buckling strength reserve.

Bernard et al. (1993b) also tested eight Bondek rolled panels (four for Bondek 1 and four for Bondek 2 as shown in Fig. 2.3.9), using the same material and test program as used for the tests mentioned above. For both products, two specimens had a thickness of 0.750 mm (0.030 inches) and the other two had a thickness of 1.000 mm (0.039 inches). For the two specimens with same thickness, one was tested in positive bending and the other in negative bending. The buckling modes observed from tests and numerical analyses are shown in Fig. 2.3.10. In all of the tested specimens, local buckling was evident, often occurring after

distortional buckling in negative bending. In the negative bending, specimens were found to buckle in the distortional mode. When residual stress was used to modify experimental buckling moments, the tested moments agreed well with numerical results (based on finite strip method). Final failure in all the tests occurred through a spatial plastic collapse mechanism. Measured ultimate moments were all higher than buckling moments, indicating an apparent post-buckling strength reserve. Based on the Australia Standard AS1538 (which considers effective web width and reduced maximum stress) and treating the pans as having no intermediate stiffeners in negative bending, the estimates for both positive and negative ultimate moments in local buckling mode were found to be conservative. These values were found to be unconservative if distortional buckling was considered in conjunction with the local buckling.

(e) Daudet and Klippstein (1994) tested C-channel stub columns made of cold-reduced steels which, according to the authors, were in compliance with ASTM A653 Structural Grade 80 steel for chemical composition. The cold-reduced specimens were compared with stub column specimens made of unreduced steel. Among all the specimens, six columns were made of a steel with a yield strength ranging from 84.0 to 88.9 ksi (579.3 to 613.1 MPa), a F_u/F_y ratio ranging from 1.02 to 1.09, a 2-inch gage length elongation between 6 and 7%, and a 1/2 gage length local elongation ranging from 16 to 24%. The elongations appear to be larger than those of the Structural Grade 80 steel as found by Dhalla and Winter. The thickness of the six specimens varied from 0.074 to 0.076 inches (1.867 to 1.925 mm) and the w/t ratio for stiffened flanges ranged from 21.75 to 107.10.

It was found that there was no difference in the local buckling behavior of stub columns using reduced steel as compared to the stub columns using unreduced steel. The performance of the stub columns using reduced steel appeared not to be influenced by the F_u/F_y ratio and ductility. Based on the AISI Specification (1986) and using the measured yield strength, the ratio of measured ultimate load to code-predicted ultimate load ranged from 0.68 to 0.74. When using 75% of measured yield strength, the ratio varied from 0.82 to 0.91.

(f) Davies and Cowen (1994) carried out a series of tests on storage rack components (connections and

columns) and conducted a full-scale test on a pallet rack frame fabricated from cold-reduced steel. The thickness of the components was 2 mm (0.079 inches) and 3.3 mm (0.130 inches). The yield strength was 474.3 MPa (68.8 ksi) for the 2 mm steel and 504.8 MPa (73.2 ksi) for the 3.3 mm steel. The elongation of the 2 mm steel was not reported, while the elongation of the 3.3 mm steel was 10%. The F_u/F_y ratio was 1.00 for the 2 mm steel and 1.01 for the 3 mm steel. To compare the components made of cold-reduced steel with the components made of ductile steel, another group of specimens made of hot-rolled steel were also tested. The hot-rolled steel had similar yield strength but larger elongation as compared to the cold-reduced steel. The w/t ratio of the stiffened flanges ranged from 15.15 to 47.50.

The study indicated that the failure in the connections made of the cold-reduced steel involved local distortion of columns and eventually tearing around perforations, indicating a ductile failure mode. The hot rolled steel resulted in only slightly stronger connections than the cold-reduced steel. The column tests showed a distortional buckling failure mode. There was little difference in failure load between the cold-reduced and the hot-rolled steel columns. It was found that the use of cold-reduced steel with low ductility had no detrimental effect on the performance of columns in compression. In the full-scale racking frame test, the failure started at one of the connections, which distorted and rotated when failure load was reached, indicating a ductile failure mode. Measured failure load of 29.9 kN (6.7 kips) per beam was slightly higher than the theoretical value of 28.0 kN (6.3 kips) per beam. The authors concluded, based on the tests and other similar experiences, that a formal ductility requirement is not needed for cold-formed sections and the requirement for a particular F_u/F_y ratio is not necessary.

(g) Xu (1995) conducted a series of fatigue tests on three different roof panels: namely arctangent (corrugated), trapezoidal, and ribbed profiles as shown in Fig. 2.3.11. The sheeting material conformed to the Australia Standard AS1397 (G550 steel) and had a mean yield strength of 610 MPa (88.5 ksi) in the longitudinal direction (metal forming direction) and 784 MPa (113.7 ksi) in the transverse direction. The elastic modulus of the sheeting was 210 GPa (30456.9 ksi) and the base metal thickness was 0.43 mm (0.017 inches). The mean total strain at final fracture was about 2% in the longitudinal direction and only

0.5% in the transverse direction. The w/t ratio of the stiffened flanges ranged from 55.81 to 302.33. Screw fasteners were used to fasten the panels on the test rig.

Prior to fatigue tests, a series of static tests were performed and a finite element analyses of the test panels were carried out to study the failure mode of the panels. It was found that both corrugated and trapezoidal panels experienced a local plastic collapse in the vicinity of a fastener at the central support of a two span test setup, and then demonstrated a large cross-sectional distortion and finally went into a strain hardening stage, while the ribbed panels had a sudden fracture failure mode with cracks forming under a screw-fastener head at the central support as shown in Fig. 2.3.12. The corrugated and trapezoidal panels indicated a ductile failure mode, while the ribbed panels showed a brittle failure mode.

The finite element analyses indicated that prior to local plastic collapse, the corrugated panels in the vicinity of the fasteners at the central support was loaded in membrane compression, and local bending moment in the steel sheet around the fastener was small. As the panels reached a local plastic collapse, the local bending moment in the steel sheet at the fastener increased rapidly. After forming a local plastic collapse, the local membrane stress changed from compression stress to tension stress. For the trapezoidal and ribbed panels, when midspan loads were small, the local bending moment in the steel sheet around the fasteners was dominant, but when the trapezoidal panels approached a local plastic collapse, or the ribbed panels reached an ultimate state, a tensile membrane stress in the longitudinal direction (parallel to ribs) became dominant.

The fatigue tests revealed that for the corrugated panels, when midspan loads were small, cracks initiated from the edge of the fastener hole and propagated toward all the directions from the hole. As midspan loads were increased, cracks initiated from the hole edge and propagated in only longitudinal (parallel to span) and transverse (perpendicular to span) directions or initiated slightly away from the hole edge and propagated only in the transverse direction. When applied loads were increased to form a local plastic collapse around the fastener, cracks initiated from the edges of a dimple (yield lines) around the fastener

and propagated only in the transverse direction. For the trapezoidal and ribbed panels, when applied loads were small and local bending moment in the steel sheet around fasteners was dominant, cracks initiated from the hole edge and propagated in only longitudinal and transverse directions. When applied loads were higher and both local bending moment in the steel sheet around fasteners and tensile membrane stress were dominant, cracks initiated slightly away from the hole edge and propagated only in the transverse direction.

2.4 TESTS OF CONNECTIONS MADE OF STRUCTURAL GRADE 80 STEEL AND SIMILAR STEELS

2.4.1 Connections Made of Structural Grade 80 Steel

(a) Dhalla and Winter (1971b) conducted tension tests of single bolted, longitudinally welded, and transversely welded connections made of A653 Structural Grade 80 steel ('Z' steel as designated in the reference) as part of an overall research on the ductility requirement for cold-formed steel structural members. The specimens had a thickness of 0.038 inches (0.965 mm). The material properties of the steel are shown in Section 2.2.1.

For the tests of single bolted connections, it was found that for the Structural Grade 80 steel in the longitudinal direction (nine specimens), failure occurred in a ductile manner as seen in ductile steels, while in the transverse direction (four specimens), the net section of the specimens developed an average 75% of predicted ultimate strength and showed a transverse cleavage fracture (semi-brittle manner) rather than a ductile inclined shear fracture. All of the Structural Grade 80 steel connections tended to result in a lower strength ratio (ratio of measured strength in shear, bearing, and net section tearing to the tensile strength of the steel) than other low ductility steel connections (which had local elongation larger than 20%) in the test series. When compared to ductile steel connections, shear and bearing strengths of low ductility steel connections were somewhat lower than those of ductile steel connections, but the tensile strength in net section seemed unaffected by the lower ductility. It appears that local elongation of a steel may be

important for shear and bearing strengths of connections. Since local strain in thin sheets may be very large around the fastener at failure due to bearing and shearing, a larger local elongation capacity may be needed.

For the tests of longitudinal fillet weld connections, the specimens were all loaded in the rolling direction (longitudinal direction, three specimens). Among the three specimens, two failed in an inclined tearing of sheet outside the fillet weld. The ratio of tensile strength of the connection to the tensile strength of the steel was 0.91 (for lap length of 2.85 inches (72.39 mm)) and 1.05 (for lap length of 3.75 inches (95.25 mm)). One specimen failed in shear at the fillet weld (for lap length of 2.50 inches (63.50 mm)).

For the tests of transverse fillet weld connections, all the specimens were loaded in the rolling direction (longitudinal direction). A total of eight specimens were tested (two fully welded, two partially welded, two unsymmetrically welded, and two doubly lapped) as shown in Fig. 2.4.1. All the specimens except for the two partially welded specimens failed in sheet and fractured around the contour of the fillet weld toe (heat affected zone, type c failure in Fig. 2.4.1). The ratio of tensile strength of the connection to the tensile strength of the steel was 0.84 and 0.86 for the two fully welded specimens, 0.87 and 0.88 for the two unsymmetrically welded specimens, and 0.84 and 0.86 for the two doubly lapped specimens. The fracture of the two partially welded specimens followed the contour of the partial weld toe and then extended into the unwelded base metal as shown in Fig. 2.4.1 (b), resulting in a higher strength ratio of 0.92 and 0.94. The lower strength ratios of the welded connections were considered to be attributed to the partial annealing of the base metal under the welding heat.

(b) Pekoz and McGuire (1979) summarized a series of tests on different welded connections. The tested strengths of the connections were compared to calculated strengths. Among all the connections tested, the ones using 24 gage (0.028 inches) and 28 gage (0.019 inches) steel sheets and welded with arc spot (puddle) welds were made of A653 Structural Grade 80 steel. Others were made of more ductile steel--A653 Structural Grade 33 steel (formerly ASTM A446 Grade A steel). The actual tensile strength of the 28 gage sheet steel ranged from 98.0 to 109.8 ksi, and that of the 24 gage sheet steel was 107.6 ksi. All the

calculated strengths of the connections were based on the actual tensile strengths of the steels used. The same equations were used for both Grade 80 and Grade 33 steels for predicting the strengths of the connections. For fourteen 28 gage steel connections welded with single sheet arc spot welds, the ratio of tested to calculated strength of the connections ranged from 0.62 to 1.24, with an average ratio of 0.93 and a standard deviation of 0.200. The failure modes of these fourteen connections were basically sheet bearing, shearing of the sheet behind the weld, and combinations of the two in which the weld plowed toward the end of the sheet. For six 24 gage steel connections welded with single sheet arc spot welds, the ratio of tested to calculated strength ranged from 0.65 to 1.28, with an average ratio of 1.13 and a standard deviation of 0.240. The failure modes of these six connections were similar to those of the 28 gage steel connections. Four 28 gage steel connections welded with double sheet arc spot welds failed in pure shearing in the welds. The ratio of tested to calculated strength of the connections ranged from 0.98 to 1.19, with an average of 1.07 and a standard deviation of 0.090. Three 28 gage steel connections welded with double sheet arc spot welds failed in tearing of the sheets along the contour of the welds with the tearing spreading across the sheet. The ratio of tested to calculated strength ranged from 0.86 and 0.93, with an average of 0.90.

2.4.2 Connections Made of Steels Similar to Structural Grade 80 Steel

Seleim and LaBoube (1994) conducted tests on various bolted connections made of cold-reduced low ductility steels. Test specimens had thicknesses of 0.040 and 0.070 inches (1.016 and 1.778 mm). The average yield strength was 70.4 ksi (485.6 MPa) for the 0.040 inch thick steel and 66.4 ksi (457.7 MPa) for the 0.070 inch thick steel. The F_u/F_y ratio was 1.08 for the 0.040 inch thick steel and 1.07 for the 0.070 inch thick steel. The uniform elongation for both thicknesses did not satisfy the AISI Specification requirement (less than 3%, varying from 0.70 to 2.55%). The local elongation of the 0.040 inch thick steel did not satisfy the AISI Specification requirement (less than 20%, varying from 12.70 to 18.80% except for one 20.90%), while the local elongation of the 0.070 inch thick steel satisfied the requirement (varying from 22.30 to 29.85%). The percent elongation in a 2-inch gage length for both thicknesses ranged from 4.95 to 9.35% (do not satisfy the AISI Specification requirement of greater than 10%).

For eleven specimens that failed in edge shearing, the ratio of measured ultimate load to predicted load ranged from 1.12 to 1.41 for both thickness steels. The predicted load was determined based on the AISI Specification (1986). Since edge shearing failure involved shearing a small portion of sheet in contact with fastener, the local elongation may play a major part in reaching a high ultimate strength.

For twenty-five specimens (thirteen made of the 0.040 inch thick steel and twelve made of the 0.070 inch thick steel) that failed in bearing, the ratio of measured ultimate load to predicted load ranged from 1.04 to 1.16 for the 0.070 inch thick steel, while the ratio varied from 0.89 to 1.09 for the 0.040 inch thick steel. The thinner steel (0.040 inch thick steel) appeared to result in a strength ratio that is relatively lower than the strength ratio of the thicker steel (0.070 inch thick steel), probably due to the lower local and uniform elongations of the thinner steel. Since bearing failure caused tearing of a larger area of sheet at a 45 degree angle out of the sheet plane, the low uniform elongation of the steel may be responsible for the relatively lower strength ratios as compared to the strength ratios of the specimens that failed in the edge shearing. Additional stress concentration due to sheet bending may also have added to the bearing area along bent lines (yield lines) of the sheet.

For three specimens (made of the 0.040 inch thick steel) that failed in edge shearing plus net section fracture (similar to block shear failure), the ratios of measured ultimate load to predicted load (based on edge shearing) were 1.23, 1.29, and 1.57. Relatively large local elongation of the steel may be important for reaching a high ultimate strength. For eight specimens (four made of the 0.040 inch thick steel and four made of the 0.070 inch thick steel) that failed in edge bearing plus shearing and net section fracture (also similar to block shear failure), the ratio of measured ultimate load to predicted load (based on bearing) ranged from 0.84 to 0.97 for the thinner steel, while 1.00 to 1.04 (except for one 0.99) for the thicker steel. Again, the lower local and uniform elongations of the thinner steel may be responsible for the slightly lower strength ratios as compared to those of the thicker steel.

3. EVALUATION OF EARLIER TEST RESULTS

The available test data on the flexural strength of deck panels made of ASTM A653 Structural Grade 80 steel and similar steels presented in the previous section were evaluated using the commercially available computer programs CFS (Glauz 1990), PANEL86 (Tondelli Engineering 1991), and RIBUMR (Kile 1995). The programs were developed based on the Specification for the Design of Cold-Formed Steel Structural Members (AISI 1986). Safety factors were eliminated from the computer results as to obtain unfactored nominal flexural strength for sections and uniformly distributed load strength for multi-span deck panels. The evaluation focuses on the comparison of the test data with the values predicted using the Specification to study the correlations between the two. The effect of yield strength and ductility on the effective width of compressed steel sheets and on the effective yield moment of hat sections is discussed. In the following discussion, Section 3.1 presents the evaluation of test results on single-span deck panels. Section 3.2 evaluates the test results on multi-span deck panels. Finally, Section 3.3 discusses the effect of yield strength and ductility of base metal materials on the effective width of stiffened compressed elements and on the effective yield moment of hat sections.

3.1 EVALUATION OF EARLIER TEST RESULTS ON SINGLE-SPAN DECK PANELS

Six deck panels tested in Australia (Bernard et al. 1992a, 1993c) were evaluated using the Specification for the Design of Cold-Formed Steel Structural Members (AISI 1986). Among the six panels, four panels had four ribs in each section, and the other two panels had three ribs in each section. Each individual rib shows a hat shape with two sloped webs and no intermediate stiffeners in the top compressed flange as shown in Fig. 2.3.3. Figure 3.1.1 shows the coordinates for the end sections of the panels. The coordinates of two end sections are averaged and listed in a table which is also shown in Fig. 3.1.1 for all the six panels. The base metal material of the panels is similar to the Structural Grade 80 steel with a mean yield strength of 653 MPa (94.7 ksi) and a mean tensile strength of 656 MPa (95.1 ksi). The mean thickness of the base

metal sheet is 0.585 mm (0.023 inches). The local, uniform, and 2-inch gage length percent elongations for the tension coupons were not indicated in the Bernard's reports, but the material properties of the same steel were given by Hancock (1995) as referred to Section 2.2.2 (b). Each test panel had a single span and was subjected to pure bending as shown in Fig. 2.3.4.

The ultimate moments of the panels obtained from the tests, $M_{u,test}$, are listed in Table 3.1.1. Shown in the same table are the calculated effective yield moments of the panels, $M_{y,91\ code}$, based on the Load and Resistance Factor Design Specification for Cold-Formed Steel Structural Members (AISI 1991), and the calculated effective yield moments, $M_{y,86\ code}$, based on the Specification for the Design of Cold-Formed Steel Structural Members (AISI 1986). The moments, $M_{y,91\ code}$, were calculated by Bernard et al. (1993c) and the moments, $M_{y,86\ code}$, were calculated using the computer program CFS (Glauz 1990). The effective yield moments are determined based on the first yielding in the effective section of the panels (without considering the lateral-torsional buckling of the panels). The actual yield strength was used in the calculation. The inelastic reserve capacity of the panels is not considered in the calculation. The slight difference between $M_{y,91\ code}$ and $M_{y,86\ code}$ may be due to a slight difference in interpreting the original dimensions of the specimens when calculating the latter. Also shown in the table are the calculated nominal effective design moments of the panels, $M_{n,60\ ksi}$, using 60 ksi (413.7 MPa) as design yield stress according to the AISI Specifications for the design of the members made of A653 Structural Grade 80 steel.

The ratio of the ultimate moment obtained from the tests to the calculated effective yield moment, $M_{u,test}/M_{y,86\ code}$, is computed and listed in Table 3.1.1 for all the panels. The ratio ranges from 1.04 to 1.27, with a mean value of 1.15 and a standard deviation of 0.101. Note that the ultimate tested moments of all the panels are larger than the calculated effective yield moments. A certain amount of inelastic reserve strength may exist in the panels as the failure of the panels was represented by a spatial plastic mechanism formed in the test specimens. The strain of the base metal corresponding to the yield strength was about 0.48%, which is far less than the uniform and local elongations of the material (Hancock 1995). In Hancock's paper, the sheet material with a thickness of 0.024 inches (0.610 mm) had uniform elongation

of 3.90% and a local elongation of 18.00%.

The computer results indicate that all six panels reached the first yielding at the top extreme fiber in compression, and the webs in all the panels are not fully effective at the first yielding. The ratio of the bottom extreme fiber stress (in tension) to the top extreme fiber yield stress (in compression), f_t/f_c, ranges from 0.424 to 0.449. As a result, the panels did not appear to fail in fracture of the base material in tension.

The ratio of the ultimate tested moment to the calculated nominal effective design moment, $M_{u,test}/M_{n,60\ ksi}$, is also computed and listed in Table 3.1.1 for all the panels. The ratio ranges from 1.32 to 1.60, with a mean value of 1.46 and a standard deviation of 0.125. The ultimate tested moments of all the panels are apparently much larger than the calculated moments. The ratio of the bottom extreme fiber stress (in tension) to the top extreme fiber stress (60 ksi in compression), f_t/f_c, ranges from 0.517 to 0.553. The effective section modulus, S_x, based on the actual yield strength of 94.7 ksi ranges from 0.195 to 0.282, while based on the stress of 60 ksi, S_x ranges from 0.244 to 0.351 $in.^3$. The section modulus based on the higher stress of 94.7 ksi is lower than that based on the lower stress of 60 ksi due to the reduced effective width of the compressed flange and the reduced effective depth of the webs at the higher stress, but the effect of such reduction in section modulus does not offset the beneficial effect of increasing the stress from 60 ksi to 94.7 ksi on the effective yield moment. Thus, the effective yield moment, $M_{y,86\ code}$, is larger than the nominal effective design moment, $M_{n,60\ ksi}$, as indicated in the table.

Some comments for the high ratio of the ultimate tested moment to the calculated effective yield moment are as follows. Since the calculated effective yield moment is determined based on the first yielding in a section, the maximum compressive or tensile strain within the section may just reach the yield strain (corresponding to the yield strength of base material), but may still be much less than the ultimate strain (corresponding to either crushing stress when sheet material is in compression or fracture of base metal when sheet material is in tension). If the yield tension or compression strain can be sustained by the

remaining effective elements of the section, the section may be able to carry more moment until a part of the section at the maximum strain location (beyond the yield strain) no longer has the ability to resist further strain. That part of the section will either crush under compression to form a plastic mechanism or fracture in tension. This flexural failure mode may depend on the type of section, but may often be possible for regular hat sections since all the compressed elements in a hat section are stiffened elements interconnected transversely even when some of the elements are partially effective to resist stresses due to an earlier buckling at a lower moment. As a result, a higher compressive or tensile yield strength in flexural members (with small or no shear forces) can be possibly reached in a regular hat section, and the section may even be able to carry a strain that is larger than the yield strain to result in an inelastic reserve strength. The 'regular' hat section refers to that the elements in a hat section do not have very large w/t or h/t ratios so that flange curling may not significantly change the shape of the section and reduce the total depth of the section. Small w/t ratio can also reduce shear lag effect as to make sections more effective.

3.2 EVALUATION OF EARLIER TEST RESULTS ON MULTI-SPAN DECK PANELS

Six Butler Manufacturing Company's BR-II rib corrugated Hi-Ten galvanized deck panels reported by Midwest Research Institute (MRI 1978) were evaluated using the Specification for the Design of Cold-Formed Steel Structural Members (AISI 1986). The test specimens were multi-span deck panels. A detailed description of the panels can be found in Section 2.3.1 and the dimensions of the panels are shown in Fig. 2.3.1. The panels were made of A653 Structural Grade 80 steel. The mean thickness of the panels is 0.016 inches (0.399 mm) and the mean yield strength of the base metal material is 111.5 ksi (768.5 MPa). The percent elongation in a 2-1/2 inch gage length ranges from 2% to 3% with a mean value of 2.40%. The yield strain of the base metal material corresponding to the yield strength is about 0.58%.

The section properties of the panels were analyzed using the computer program PANEL86 (Tondelli 1991) and the actual yield strength of 111.5 ksi. The effective yield moment in the positive bending (narrow rib flange is in compression) is determined as 2.68 k-in/foot (0.99 kN-m/m) and the effective yield moment in

the negative bending (the flanges with the intermediate stiffeners are in compression) is calculated as 2.38 k-in/foot (0.88 kN-m/m). As a comparison, a design stress of 60 ksi as specified in the AISI Specifications for the design of the members made of Structural Grade 80 steel was used to determine the nominal effective design moment of the test panels. The nominal effective design moment in the positive bending is found to be 2.05 k-in/foot (0.76 kN-m/m), while in the negative bending, the nominal effective design moment is 1.93 k-in/foot (0.71 kN-m/m). Under the actual yield strength and the design stress of 60 ksi, the webs of the panels are not fully effective in either positive or negative bending, and all the intermediate stiffeners in the flanges under the negative bending are considered as not adequate to perform as stiffeners. The ratio of the extreme fiber tension stress to the extreme fiber compression stress, f_t/f_c, is 0.140 in the positive bending and 0.476 in the negative bending under the yield strength of 111.5 ksi, while the ratio is 0.201 and 0.684 in the positive and negative bending, respectively, under the design stress of 60 ksi. This indicates that the first yielding in the panels occurs at the extreme fiber in compression in both positive and negative bending.

The ultimate tested pressures, $W_{u,test}$, are listed in Table 3.2.1. Also shown in the table are the calculated yield load, $W_{y,86\ code}$, based on the AISI Specification (1986) and the actual yield strength of 111.5 ksi, and the calculated nominal design load, $W_{n,60\ ksi}$, based on the AISI Specification (1986) and the design stress of 60 ksi. The ratio of the ultimate tested pressure to the calculated yield load, $W_{u,test}/W_{y,86\ code}$, ranges from 1.07 to 1.73 with a mean value of 1.32 and a standard deviation of 0.233, while the ratio of the ultimate tested pressure to the calculated design load, $W_{u,test}/W_{n,60\ ksi}$, ranges from 1.32 to 2.26 with a mean value of 1.67 and a standard deviation of 0.331. The failure mode of the panels was characterized by panel rib crushing in the positive bending and by panel pulled through fasteners in the negative bending (suction). No fracture of base metal material was observed in the tested panels. This may be attributed to the fact that the extreme fiber tension stress in the panel section is small as compared to the extreme fiber compression stress in the section in both positive and negative bending (quite small f_t/f_c ratios as shown earlier). As a result, the failure of the panels was initiated from crushing the compressed elements of the panel section rather than fracturing the tension elements.

It is clear from Table 3.2.1 that the ultimate tested pressures are larger than the calculated yield loads and the calculated nominal design loads. The calculated yield and nominal design loads were determined by the first yielding at the extreme fiber of the sections. Apparently, this is a conservative approach since the section of the panels may develop inelastic reserve strength, and moment redistribution may be possible in the multi-span deck panels. For all the test panels in consideration, it is found that the section where the first yielding occurs is always located at the first interior supports from the end spans of a panel.

As discussed by Yu (1991), partial plastification of beam cross section and moment redistribution in multi-span deck panels were observed in earlier tests even after webs of the panels crippled. The amount of moment redistribution may depend on the base material, type and shape of section, and number of spans. As long as fracture of base material does not occur, the partial plastic rotation of the sections at the interior supports may help to develop a global membrane tensile stress fields in the panels, resulting in an increase in load-carrying capacity. Comparing the $M_{u,test}/M_{y,86\ code}$ ratios (in Table 3.1.1) to the $W_{u,test}/W_{y,60\ ksi}$ ratios (in Table 3.2.1), the strength reserve in the multi-span panels appear to be larger than that in the single-span panels.

3.3 DISCUSSION OF POTENTIAL EFFECT OF YIELD STRENGTH AND DUCTILITY OF BASE MATERIAL ON EFFECTIVE YIELD MOMENT

The section of a deck panel usually consists of multiple hat-shaped sections. When such deck panel, either in single-span or multi-span, is subjected to uniform loads, the overall stability of the panel, such as lateral-torsional buckling, often does not control the moment capacity of the panel. In the region where little or no shear exists along the length of the panel, the strength of that region is controlled by the moment capacity of the hat sections.

In a hat section subjected to bending, one part of the section is in tension and another part is in compression. On one side of the neutral axis, a flange of the section is subjected to maximum tensile strain

and stress, while the flange on the other side is subjected to maximum compressive strain and stress. Thus, if the ductility of the base material is low and the yield strength is high, the failure of the section may be initiated either by fracture of extreme fiber in tension soon after yielding is reached in the tension flange, or by crushing the compressed flange and flange-web corners with a very large R/t ratio before corner yield stress is reached. In either situation, the moment capacity of the section may be affected. An early fracture of a low ductility material can not result in a desirable inelastic reserve strength of a hat section, and usually reduces the ability to redistribute moment in a multi-span panel. An early crush of the compressed elements, prior to yielding, apparently reduces the effective yield moment. Therefore, higher yield strength and lower ductility of a base metal material may affect the moment capacity of a deck panel.

On the other hand, if the extreme fiber tensile stress in a hat section is always smaller than the extreme fiber compressive stress in both positive and negative bending throughout entire loading process, the fracture of the base material prior to crushing the compressed elements may not be possible. As a result, the lower ductility of a base material may not be a dominating factor to affect the effective yield moment of the hat section. Thus, the effective yield moment is controlled by the first yielding in the extreme fiber in compression. As long as the inner radius of the flange-web corners is not too large, the corners may not crush prior to the crushing of the remaining effective flat of the flange and can enforce enough edge restraints on the flat of the flange as to allow it to reach the yield strength. In this situation, it is possible for a hat section made of high yield strength and low ductility steel to reach the expected effective yield moment.

The effect of yield strength on the effective width of a stiffened flat sheet in compression can be seen in Fig. 3.3.1 and Fig. 3.3.2, based on the effective width formula in the AISI Specification (1986). In each figure, three curves represent the w/t ratios equal to 60, 140, and 220. Figure 3.3.1 indicates that for the yield strength larger than 60 ksi, the effective width-to-thickness ratio b/t decreases slowly with the increases in the yield strength, and the difference in the b/t ratios among the three curves is small. Figure 3.3.2 also shows that for the yield strength larger than 60 ksi, the decreases in the effective width-to-flat width ratio

b/w is relatively small with the increases in the yield strength, except that the difference in the b/w ratios among the three curves is quite large. The larger the w/t ratio, the less effective the stiffened compression flange (lower b/w ratio). The two figures demonstrate that for the yield strength larger than 60 ksi, the decreases in the effective width of a stiffened flat sheet become smaller with the increases in yield strength.

A relationship between the effective moment and the top fiber compression stress for a hat section is shown in Fig. 3.3.3. The effective moment is calculated based on the AISI Specification (1986). The vertical coordinate on the right side of the figure represents the distance between the top extreme compressed fiber to the neutral axis of the section (Y_c). The hat section has a total depth of 2 inches and a total tension flange of 2 inches (two sides). The thickness of the section is 0.030 inches (0.763 mm) and the inner radius R is 0.125 inches (3.176 mm). It is shown in the figure that the effective moment of the section increases almost linearly with the increases in the stress in the top compressed flange, even up to a compressive stress of 120 ksi (827.4 MPa). This illustrates the effectiveness of using high yield strength material to achieve a higher effective moment if the stress in the section can reach the yield strength of the base material. This is because the effective width of the top compressed flange decreases very little at higher stress levels, resulting in little change in Y_c as shown in Fig. 3.3.3. With the little reduction in the effective width of the compressed flange and Y_c, the effective section modulus reduces very little, which can not offset the relatively larger increases in the yield strength. Note in the figure that the difference in the effective moments for three different w/t ratios (60, 140, and 220) is small under a same compressive stress in the top flange due to the small difference in the effective width of the compressed flange under a same compressive stress as shown in Fig. 3.3.1. Thus, using a large w/t ratio for the top compressed flange is apparently not economical as far as effective moment of the section is concerned.

Figure 3.3.3 indicates that except for the compressive stress less than 20 ksi (137.9 MPa), the maximum stress in the section always occurs at the top compressed flange of the section (Y_c is larger than 1 in.). At a compressive stress of 120 ksi, the corresponding compressive strain in the top flange is about 0.61%. This strain level may be less than the tensile strain of base material at fracture, but may reach a crushing strain

of the remaining effective flange and flange-to-web corners of the section. In this way, the tensile strain ductility of a base material may not be relevant to the effective yield moment of the section if the first yielding occurs in the top compressed flange.

4. COUPON TESTS OF A653 STRUCTURAL GRADE 80 STEEL

The ASTM A653 Structural Grade 80 steel has a minimum specified 0.2% offset yield strength of 80 ksi and a minimum specified tensile strength of 82 ksi. The percent elongation in a 2-1/2 inch gage length is unspecified. Since the Structural Grade 80 steel does not satisfy the ductility requirements specified in the AISI Specifications, more information on the material properties of the steel, such as local and uniform elongations, is needed in order to fully understand the material behavior of the steel. Tested material properties are also need for calculating the flexural and web crippling strengths of beams and the ultimate strength of connections made of the Structural Grade 80 steel in the next phases of this project. Thus, a total of seventy-six coupon tests on the ASTM A653 Structural Grade 80 steel were performed at the Department of Civil Engineering at the University of Missouri-Rolla. This section summarizes the results of the tests.

4.1 BASIC INFORMATION OF THE SHEET STEEL

Four types of ASTM A653 Structural Grade 80 steel sheets, namely 22, 24, 26, and 28 gages, were donated by the Wheeling Corrugating Company, Wheeling, West Virginia. The width of the sheets ranges from 38" to 42-1/2" (965.2 to 1079.5 mm) and all the sheets have a length of 10 feet (3048.0 mm). All the sheets are flat and galvanized. The chemical compositions for the steel used in this research project are listed as follows:

Gage Number	Carbon	Manganese	Sulfur	Phosphorus
22	0.047%	0.29%	0.005%	0.009%
24	0.062%	0.37%	0.010%	0.008%
26	0.050%	0.27%	0.008%	0.015%
28	0.061%	0.40%	0.014%	0.015%

4.2 PREPARATION OF TEST COUPONS

Four steel sheets, with each sheet for each gage number, were selected for making standard test coupons. Scratches and damages on the surface of the sheets were not found for the selected sheets. The sheets were handled carefully so that no buckling could occur and no deep scratches were made on the surface of the sheets prior to cutting coupons. Before the coupons were cut from the sheets, Acetone was used to thoroughly clean off the grease on both surfaces of each sheet.

The test coupons were cut from the sheets as shown in Fig. 4.2.1. A total of twelve coupons were cut in the rolling direction (longitudinal direction) of each sheet, with four on the left, four in the middle, and four on the right separated with a quarter width of the sheet as shown. A total of eight coupons were cut in the direction perpendicular to the rolling direction (transverse direction), with four on the left and four on the right separated with half width of the sheet as shown. The coupons in the longitudinal and transverse directions were separated by a distance of 12 inches (304.8 mm). Two sets of coupons with different dimensions were cut from each sheet. One set of coupons had an overall dimension of 2-1/8" (53.98 mm) wide and 10-1/4" (260.35 mm) long, for making the ASTM standard 2-1/2" (63.50 mm) long narrow width coupons as shown in Fig. 4.2.2. These coupons were used to study the stress-strain relationship of the material and the elongation in a 2-inch gage length, and will be referred to as "short" coupons in the following discussion. The other set of coupons had an overall dimension of 2-1/8" wide and 11-1/4" (285.75 mm) long, for making the 3-1/2" (88.90 mm) long narrow width coupons (other dimensions of the coupons are exactly the same as the 2-1/2" long narrow width coupons). These coupons were mainly used to study local and uniform elongations of the material and will be referred to as "long" coupons in the following discussion. The stress-strain relationship and 2-inch gage length elongation can also be produced from the long coupons. The coupons were carefully marked on the sheets with metal scriber so that they were parallel to both directions.

The symbol of the coupons is defined as follows. Each long coupon is labeled as "LTxx-Xx" or "TTxx-Xx". LT means (L)ongitudinal (T)ension in the rolling direction, and TT means (T)ransverse (T)ension in the direction perpendicular to the rolling direction. The first two numbers "xx" indicates gage number (22, 24, 26, or 28). The upper character "X" indicates the coupon is located on the (L)eft, (M)iddle, or (R)ight of a sheet. The last number "x" indicates the number of coupons in either left, middle, or right groups. For example, LT22-L1 means that the coupon was cut in the longitudinal direction, 22 gage, on the left of a sheet, and the number 1 coupon among four coupons on the left. An illustration of the symbols is shown in Fig. 4.2.1. For the short coupons, the labeling is the same as the long ones, except an upper character "S" is appended at the end of each label. For example, LT22-L1S has the same meaning as the long one indicated above, except that it represents a short coupon. The number of actual tested coupons is listed as follows:

Type of Coupon	Gage	LTxx-Lx	LTxx-Mx	LTxx-Rx	TTxx-Lx	TTxx-Rx
Long	22	2	2	2	2	2
	24	2	2	2	2	2
	26	2	2	2	2	2
	28	2	2	2	2	2
Short	22	3	2	2	2	2
	24	2	x	2	2	2
	26	2	x	3	2	2
	28	2	x	2	2	2
Total		17	10	17	16	16

The coupons were machined to the required dimensions according to the ASTM A370 and E8. For the long

coupons, a 3-1/2" long narrow width was made, instead of 2-1/2" long, as suggested by Dhalla (1971b) and Yu (1991) in order to study the local and uniform elongations. After the coupons were machined, a Hydrochloric Acid solution with a 7.5% concentration was used to dissolve the galvanized coatings at one end of each long coupon. The depth of the coated area dissolved on each coupon was about 1/4 to 1/2 inches (6.35 to 12.70 mm). The thickness for all the long coupons was then measured by a caliper with an accuracy up to 0.001" (0.025 mm). The measurement was done soon after the coatings were resolved as to avoid rusting on the surface. The thickness for the 22, 24, 26, and 28 gage sheets is 0.029", 0.024", 0.017", and 0.015" (0.737, 0.610, 0.432, and 0.381 mm) respectively.

For the purpose of measuring 3-inch and 1-inch gage length elongations used for calculating the local and uniform elongations, fifteen thin lines perpendicular to the longitudinal edge of the narrow strip of each coupon were marked at a 1/4" interval with a metal scriber, separating the 3-1/2" long narrow strip into fourteen segments. The distance between the first line on the left and each line on the right was measured with the caliper prior to testing, including the distance between the two line markers 3-inch apart near the ends of the strip and the distance between the two line markers 1-inch apart in the middle of the strip. For the short coupons, two thin lines with a distance of 2 inches apart were marked in the middle of the narrow strip. The distance between the two lines were also measured prior to testing and the value will be used to compute the measured 2-inch gage length elongation and compare it with the data recorded from an MTS extensometer in the test. In order to avoid fracture occurring at the ends of the narrow strip of the coupons, fine sand papers were used to slightly reduce the width of the strip near the middle of each coupon. Care was taken to ensure that the reduced width still satisfies the ASTM A370 dimension requirement (0.500"±0.010") (12.70 mm±0.254 mm), with an usual width falling between 0.497" and 0.502" (12.62 and 12.75 mm). The width of the narrow strip was then measured at three different locations for the long coupons, two near the opposite ends of the strip at the line markers 3-inch apart and the smallest width near the middle due to the sand paper removal. For the short coupons, the width was measured at the two line markers 2-inch apart and at the middle portion of each coupon with the smallest width. The average of three measurements is listed in Tables 4.4.1 to 4.4.8 for all the coupons and is used to calculate the stress.

4.3 TEST PROCEDURE

The MTS 880 Test System located at the Engineering Research Lab of the University of Missouri-Rolla, as shown in Fig. 4.3.1, was used to carry out the coupon test. It consists of a loading frame with top and bottom grips (on the right in the picture), various control panels (in the middle of the picture), and a data acquisition system (on the left in the picture) with a real time computer monitor (not shown in the picture). The System uses the close-loop control scheme with three main control modes, namely load, strain, and displacement controls which are automatically operated in the System (including the grip hydraulic system). An option of collecting three samples per second in the data acquisition system was selected.

For each coupon test, the displacement control mode was first used to set up the net distance between the two grips as shown in Fig. 4.3.2. The coupon was first placed and griped in the lower grip while the alignment of the coupon on both upper and lower grips were undertaken. An MTS 2-inch gage length extensometer with a 50% strain measuring capacity was mounted in the middle of the coupon as shown in the figure. The two knife edges of the extensometer were aligned at two scribed line markers 2-inch apart where the distance between the markers were measured prior to testing. Prior to fastening the upper grip, the force, strain, and displacement conditioners were nulled. The upper grip was then tightened. The data acquisition system was switched to collect data immediately before the test was started. The entire test process was controlled under the displacement mode so that an unloading branch in the stress-strain relationship can be obtained. Soon after each test, the distance between the two line markers 2-inch apart with a fracture in-between was measured again, and the 2-inch gage length percent elongation was computed and compared to the recorded data from the extensometer. This was done for both long and short coupons. For the long coupons, additional post-fracture measurement was carried out on the distance between the 3-inch gage length line markers and the distance between the 1-inch gage length line markers in order to calculate the local and uniform elongations.

According to the ASTM A370 and E8, the speed of the strain rate in the standard tension coupon test should

be larger than $3.11x10^{-6}$ (in./in.)/sec and less than $5.65x10^{-5}$ (in./in.)/sec. A trial-and-error process was carried out to set up a strain rate for the coupon tests. It was found that there was basically no difference in the final strain readings under the rate of $3.11x10^{-5}$ (in./in.)/sec and that of $5.65x10^{-5}$ (in./in.)/sec. Thus, the upper limit of the required strain rate was used throughout the tests. The time used for running each test ranged from about 4.5 to 11 minutes for the short coupons, and from about 5 to 13 minutes for the long coupons. This corresponds to a time duration of $7.5x10^{4}$ sec. set up in the System under the displacement control mode at the range 1 (from zero to full movement (5") of the lower grip) for the short coupons, for the long coupons, a time duration of $8.0x10^{4}$ sec. was set up.

4.4 TEST RESULTS

Prior to presenting the local and uniform elongations of the ASTM A653 Structural Grade 80 steel, the results on the yield and tensile strengths, the recorded stress-strain curves and measured 2-inch gage length percent elongation are discussed first, followed by a discussion of failure mode of the coupons.

(a) Yield and Tensile Strengths

The yield strength of the ASTM A653 Structural Grade 80 steel is defined by the 0.2% offset yield strength since this full hard steel does not exhibit a sharp yield point. To obtain the 0.2% offset yield strength, the stress-strain curves of the steels were generated from the recorded load and strain data. Two typical stress-strain curves of 22 gage sheet steel are shown in Fig. 4.4.1 (longitudinal direction) and Fig. 4.4.2 (transverse direction). First of all, a linear regression analysis was performed on the data of the stress-strain curve up to a 60% of ultimate strength to produce the initial stiffness (modulus of elasticity) of the curve. Based on the initial stiffness, a straight line with the same stiffness can be generated and originated from the 0.2% offset strain. The straight line intersects the stress-strain curve. The 0.2% offset yield strength of the steel can then be found at the intersection point as shown in the figures. The tensile strength of the steel corresponds to the ultimate load capacity of the coupon and can be directly read from the stress-strain curve.

The 0.2% offset yield strength and tensile strength are listed in Tables 4.4.1 to 4.4.8 for all the coupons tested. The star symbol "*" shown in the tables indicates that the data is not available. The average values are calculated in each direction for each gage steel. The strength values for the long and short coupons are listed in the separated tables. Little difference exists between the strength values of the long coupons and those of the short coupons. This can also be seen from the typical stress-strain curves shown in Fig. 4.4.3 and Fig. 4.4.4, where the curves of the long and short coupons are compared. It is seen from the tables that in both longitudinal and transverse directions, the yield and tensile strengths of the steel increase with the decreases in thickness of steel sheets. Figure 4.4.5 shows the relationship between the yield and tensile strengths vs. the thickness of the steel sheet. The strength values in the figure are those average values of both long and short coupons listed in the tables. It is clear from the figure that the 22 gage sheet steel with a thickness of 0.029" has the lowest yield and tensile strengths, while the 26 and 28 gage sheet steels with a thickness of 0.017" and 0.015", respectively, have the highest values. The yield and tensile strengths in the transverse direction are much higher than those in the longitudinal direction for all the steel sheets. The average ratio of tensile to yield strength is less than 1.05 for all the steel sheets in both longitudinal and transverse directions, with the ratio in the transverse direction being much lower than that in the longitudinal direction.

(b) Stress-Strain Relationships and 2-Inch Gage Length Percent Elongation

Figures 4.4.6 to 4.4.9 compare the typical stress-strain curves in both longitudinal and transverse directions for each gage steel. In all the cases shown, the yield and tensile strengths in the transverse direction of the steels are much higher than those in the longitudinal direction, while the ductility in the transverse direction is much lower than that in the longitudinal direction. The figures and Tables 4.4.1 to 4.4.8 indicate that the 2-inch gage length percent elongation in the transverse direction at fracture is about half of that in the longitudinal direction. All the steel sheets clearly demonstrated an orthotropic behavior. These characteristics of the steel sheets may have effect on the strength of the structural members in two-way loading situation. All the data in the parentheses listed in the tables are the 2-inch gage length percent

elongations measured by a caliper. The average values indicated in the tables were calculated based on the recorded data from the extensometer rather than from the measured data. The star symbol "*" shown in the tables indicates that the data is not available.

The relationship between the 2-inch gage length percent elongation and the thickness of the steel sheets can be seen in Figures 4.4.10 and 4.4.11. Figure 4.4.10 compares the stress-strain curves of four different steel sheets in the longitudinal direction, while Figure 4.4.11 compares the stress-strain curves of four different steel sheets in the transverse direction. It is noticed that the ultimate strain at fracture increases with the increases in thickness of the sheets in both longitudinal and transverse directions. In the longitudinal direction, the ductility of the 22 gage steel sheet, when excluding necking strain, is higher than the ductility of the other three gage steel sheets, while this is not significant in the transverse direction. There appears no substantial difference in ductility between the 26 and 28 gage steel sheets. The above observations can also be seen from the 2-inch gage length percent elongation values listed in Tables 4.4.1 to 4.4.8. A plot using all the average 2-inch gage length percent elongation values listed in the table is shown in Fig. 4.4.12. The data from both long and short coupons are included. The decrease of 2-inch gage length percent elongation with the decreases in thickness is apparently shown in the figure.

It is clear that the A653 Structural Grade 80 sheet steel does not possess a clear sharp yield point. The yielding is gradually developed before the tensile strength is reached. The strain hardening of the steel appears to be very small. After the tensile strength is reached, the stress decreases with the increases in strain.

(c) Failure Mode

The failure of the coupons is typically characterized by the necking along an inclined line with respect to the loading direction as shown in Fig. 4.4.13. In this figure, the coupons from four different sheets in both longitudinal and transverse directions are included. Figure 4.4.14 compares the failure modes between the

long and short coupons for the 22 and 28 gage steel sheets in both longitudinal and transverse directions. It is noticed that there is no difference in failure modes between the long and short coupons. The failure of the coupons did not appear to be brittle. Only two coupons of the 22 gage steel sheet in the transverse direction indicated a partial brittle failure mode as shown in Fig. 4.4.15, where a horizontal fracture was formed at one edge of the necking line. After a short length of penetration of the horizontal fracture, it changed the path and followed an inclined fracture line. The real time computer monitoring of the stress-strain relationship indicated that the onset of decreasing stress in the stress-strain curves corresponded to the initiation of necking in the coupon. From the onset of necking, the fracture along the necking line was quickly formed. The width of the necking band in all the coupons was very small. The relatively small necking strain in the longitudinal tension, as shown in Fig. 4.4.10, may not be significant, but the relatively large plastic strain prior to necking in the longitudinal tension and the relatively large necking strain in the transverse tension, as shown in Fig. 4.4.11, may be both valuable in developing effective yield moment of beams. Figure 4.4.16 shows the formation of a necking in a 22 gage coupon prior to fracture. A discussion on the necking theory for sheet material and the development of the angle of the inclined necking line can be found in Dodd and Bai's book (1987).

(d) Local and Uniform Percent Elongations

The local and uniform percent elongations were calculated based on the formulas given by Yu (1991). The computed values are listed in Tables 4.4.1 to 4.4.4 for all the long coupons. The star symbol "*" shown in the tables indicates that the data is not available. It is indicated in the tables that with the decrease of the thickness of the steel sheets, the local percent elongation tends to decrease in both longitudinal and transverse directions, but this is not significant for the uniform elongation in the two directions. An exception is that the uniform percent elongation of the 28 gage sheet in the longitudinal direction is relatively larger than that of the 26 gage sheet. For all the long coupons indicated, the local percent elongation of the steel is less than 12.0% and the uniform percent elongation is less than 1.3%. Figure 4.4.17 shows the relationship between the local and uniform elongations and the thickness of the steel

sheets. It is shown in the figure that both local and uniform elongations in the transverse direction are smaller than those in the longitudinal direction, with a larger difference for the local elongation. The uniform elongation in both longitudinal and transverse directions is much smaller than the local elongation. Therefore, the local elongation may have more impact on reducing stress concentration and developing yield flexural strength of beams. Measurements on reduced width of the narrow strip after tests were carried out on several failed coupons in order to observe the region of local elongation. It was found that relatively large reduction in the width of the narrow strip occurred in a half inch length near a fracture (1/4" on each side of the fracture). This is confirmed with Dhalla's finding (1971b). It indicates that large plastic strain can be formed in a relatively large region outside the necking band.

5. SUMMARY

Based on the previous discussion, some tentative observations are summarized as follows:

(1) It is noted that very limited information on ASTM A653 Structural Grade 80 steel is available in the published literature. Information on steels similar to A653 Structural Grade 80 steel, such as Australia Standard AS1397 G550 and G500 steels, has been found in the literature.

(2) Earlier limited tests on A653 Structural Grade 80 steel included coupon tests, tests on perforated sheets, connection tests (both bolted and welded), and tests of roof deck panels. There was a great difference between tensile properties of the Structural Grade 80 steel in the rolling direction (longitudinal direction) and perpendicular to the rolling direction (transverse direction). The ductility in the transverse direction is smaller than that in the longitudinal direction. The uniform elongation (in strain hardening range) and local elongation (necking strain) of the steel are small. The tests on tension coupons, perforated sheets, and connections indicated that failure of the specimens was ductile in nature in the longitudinal direction and semi-brittle in the transverse direction. The ratio of tested strength of specimen to coupon tensile strength ranged from 0.84 to 1.17 in the longitudinal direction, with the ratio being 0.94 for perforated sheets in the transverse direction. There is no detailed comparison between measured strength and calculated strength on roof deck panels. The post-buckling behavior observed in the roof panel tests was apparent.

(3) Tests on hat shaped panels made of Australia G550 steel, which is similar to the A653 Structural Grade 80 steel, indicated that the AISI Specification (1991) predicts well the flexural strength of the panels without stiffeners (local buckling only) under pure bending, using the actual yield strength. The webs of the panels were considered to be partially effective in the calculation. The AISI Specification also predicts well the flexural strength of the panels with small stiffeners at the middle of the compression flanges when distortional buckling was dominant, while it overestimates the strength when local buckling followed by

distortional buckling was dominant. The equation considering interaction between local and distortional buckling, developed by Pekoz (1986), was found to be conservative. Post-buckling behavior of the panels was observed in all the tests. Imperfection, residual stress, and flange curling may affect member flexural strength in some cases.

(4) Maximum stress in the compression flange of members made of high strength steel may not reach the yield strength of the steel. As a result, flexural strength based on first yielding appears not to be strongly affected by ductility of the base metal, but it is affected by the increases in strength of the base metal and the increases in the w/t ratio of the compressed elements.

(5) Significant post-buckling strength reserve was observed in the tests on roof panels made of Australia G550 steel and loaded under concentrated loads.

(6) Static tests on roof panels made of Australian G550 steel under line or point concentrated load indicated that the failure mode of the panels depended on the geometric profiles of the panels. Considerable post-buckling strength reserve was observed from the tests. Ductile failure mode was apparent for the trapezoidal and corrugated panels with fasteners at the crests, but not for ribbed panels fastened at the crests as indicated in Fig. 2.3.12.

(7) Development of full tensile strength in net section made of Australian G550 steel was found to be dependent on the thickness of specimens, which is related to ductility of the base metal. However, the percentage of tensile strength achieved in perforated wall stud tests was found to be greater than 90% for the thickness ranging from 0.420 to 1.000 mm (0.017 to 0.039 inches).

(8) The lower strain hardening ratio and large local elongation (but small uniform elongation) of low ductile steels may not detrimentally affect the development of full tensile strength in net section.

(9) Edge shearing, bearing, and net section tearing failure modes in cold-formed steel connections seem to be affected by local elongation of a low ductility steel. Larger local elongation appears to help redistribute local higher stress and reduce stress concentration, resulting in a higher ratio of tested strength of connection to tensile strength of base metal.

(10) For all the test panels and specimens reviewed, the yield strength ranged from 68.8 to 165.1 ksi (474.3 to 1138.4 MPa), the thickness of material ranged from 0.015 to 0.130 inches (0.381 to 3.302 mm), the w/t ratio ranged from 15.15 to 302.33 for stiffened compression element and from 5.65 to 53.27 for unstiffened compression element, and the height of deck panel varied from 0.630 to 2.126 inches (16.002 to 54.000 mm).

(11) The evaluation of the available test data indicates that multi-span panels made of the Structural Grade 80 steel and similar steels may carry more uniform loads than single-span panels due to possible partial plastification in sections and moment redistribution in panels. The effective yield moment of the beams made of such steel can be possibly reached. The ductility of the steel may have less effect on the effective yield moment if the sections are designed in such a way that the first yielding can only be reached in the compression flange.

(12) The tension coupon tests of the Structural Grade 80 sheet steel indicated that the 0.2% offset yield and tensile strengths of the steel both in the rolling direction and perpendicular to the rolling direction increases with the decreases in the thickness of steel sheets, while the ductility of the steel decreases with the decreases in the thickness of steel sheets. The material properties perpendicular to the rolling direction are significantly different from those in the rolling direction. The local percent elongation in both directions is much higher than the uniform percent elongation. The failure of the coupons did not appear to be brittle. The local percent elongation for all the 22, 24, 26, and 28 gage steel coupons is less than 13.0%, while the uniform percent elongation is less than 1.3%. The average ratio of tensile-to-yield strength is less than 1.05.

In conclusion, it appears, based on the available information in the literature, that the members (mainly beam and connections) made of the A653 Structural Grade 80 steel may be designed based on a stress level that is higher than 75% of specified yield and tensile strengths of the steel.

6. FUTURE RESEARCH WORK

The research work reported herein is the first phase of an overall research project on Strength of Flexural Members Using Structural Grade 80 of A653 and Grade E of A611 Steels, sponsored by the American Iron and Steel Institute. The future research work of the project is described as follows.

Based on the findings of the preliminary study, an experimental program for testing flexural members made of A653 Structural Grade 80 steel is under development. Beam specimens has been designed and manufactured. Four different types of steel sheets, namely 22, 24, 26, and 28 gages with the thickness ranging from 0.029, 0.024, 0.017, and 0.015 inches, respectively, were used to make the beam specimens. Beam tests will be conducted at the Department of Civil Engineering of the University of Missouri-Rolla. The investigation will include the following tasks:

a. Conduct beam tests for determining section strength (i.e., effective yield moment, $M_n=S_e F_y$). Single-span one-point and two-point loading beam tests will be conducted to study the effect of high-strength low ductility A653 Structural Grade 80 steel on the effective yield moment. Beam specimens that consist of hat-shaped section without intermediate stiffeners have been designed such that the first yielding in the section can occur in the compression flange, in the tension flange, and in the compression and tension flanges simultaneously. Multi-span beam tests may be carried out to study possible partial moment redistribution and partial plastification of section at interior supports.

b. Conduct beam tests for determining web crippling strength including end-one-flange loading and interior-one-flange loading.

In addition, an initial experimental investigation on connections made of A653 Structural Grade 80 steel will be carried out following the beam tests. The research tasks include a preliminary study of screw

connections considering tensile and bearing capacities, an initial study of pull-out and pull-over strengths, a preliminary study of welded connections including arc spot welds and fillet welds.

Finally, all of the available test results will be evaluated and appropriate design criteria will be developed from the findings of the research work outlined above.

ACKNOWLEDGEMENTS

The research work reported herein was conducted at the Department of Civil Engineering at the University of Missouri-Rolla under the sponsorship of the American Iron and Steel Institute. Drs. Wei-Wen Yu and R.A. LaBoube are the directors of the project.

The financial assistance granted by the Institute and the technical guidance provided by members of the Subcommittee 24 - Flexural Members of the AISI Committee on Specifications for the Design of Cold-Formed Steel Structural Members and the AISI Staff (R.B. Haws and K.C. Slaughter) are gratefully acknowledged. The sub-committee members are: J.N. Nunnery (Chairman), R.E. Albrecht, R.L. Brockenbrough, R.E. Brown, C.R. Clauer, D.S. Ellifritt, S.J. Errera, J.M. Fisher, T.V. Galambos, M. Golovin, G.J. Hancock, A.J. Harrold, R.B. Haws, R.B. Heagler, D.L. Johnson, W.E. Kile, R.A. LaBoube, M.R. Loseke, R. Madsen, T.H. Miller, T.M. Murray, T.B. Pekoz, D.C. Perry, R.M. Schuster, P.A. Seaburg, W.L. Shoemaker, T. Sputo, T.W. Trestain, and W.W. Yu.

All of the steel sheet materials used for the coupon tests and beam specimens were kindly donated by the Wheeling Corrugating Company, Wheeling, West Virginia. Mr. F. C. Rosenberger from the Wheeling-Pittsburgh Steel Corporation Steubenville Plant and Mr. R.E. Brown from the Wheeling Corrugating Company are acknowledged for their technical advice.

Thanks are also due to J.J. Bradshaw, S.D. Gabel, and J.M. McCracken, staff of the Department of Civil Engineering, for their technical support and to Mr. Chiu-Jen Ku for his assistance in the preparation and performance of the coupon tests and the preparation of the report.

REFERENCES

American Iron and Steel Institute. (1991). "Load and Resistance Factor Design Specification for Cold-Formed Steel Structural Members," March 16, 1991 Edition.

American Iron and Steel Institute. (1986). "Specification for the Design of Cold-Formed Steel structural Members," August 19, 1986 Edition with December 11, 1989 Addendum.

ASTM A370, "Standard Methods and Definitions for Mechanical Testing of Steel Products," Annual Book of ASTM Standards.

ASTM E8, "Tension Testing of Metallic Materials," Annual Book of ASTM Standards.

ASTM A446, "Standard Specification for Steel Sheet, Zinc coated (Galvanized) by the Hot-Dip Process, Physical (Structural) Quality," Annual Book of ASTM Standards.

ASTM A611, "Standard Specification for Steel, Cold-Rolled Sheet, Carbon, Structural," Annual Book of ASTM Standards.

ASTM A653/A653M-94, (SO Grades 33, 37, 40, 50, and 80; HSLA Grades 50 and 60), Steel Sheet, Zinc-Coated (Galvanized) or Zinc-Iron alloy-Coated (Galvanized) by the Hot-Dip Process.

Bernard, E.S., Bridge, R.Q., and Hancock, G.J. (1992a). "Intermediate Stiffeners in Cold-Formed Profiled Steel Decks, Part 1-'V' Shaped Stiffeners," Research Report No. R653, Centre for Advanced Structural Engineering, School of Civil and Mining Engineering, University of Sydney, Australia, April.

Bernard, E.S., Bridge, R.Q., and Hancock, G.J. (1992b). "Intermediate Stiffeners in Cold-Formed Profiled Steel Decks, Part 2-'Flat Hat' Shaped Stiffeners," Research Report No. R658, Centre for Advanced Structural Engineering, School of Civil and Mining Engineering, University of Sydney, Australia, August.

Bernard, E.S., Bridge, R.Q., and Hancock, G.J. (1993a). "Intermediate Stiffeners in Cold-Formed Profiled Steel Decks, Part 3-Condeck Rolled Panels," Research Report No. R674, Centre for Advanced Structural Engineering, School of Civil and Mining Engineering, University of Sydney, Australia, August.

Bernard, E.S., Bridge, R.Q., and Hancock, G.J. (1993b). "Intermediate Stiffeners in Cold-Formed Profiled Steel Decks, Part 4-Bondek Rolled Panels," Research Report No. R675, Centre for Advanced Structural Engineering, School of Civil and Mining Engineering, University of Sydney, Australia, August.

Bernard, E.S., Bridge, R.Q., and Hancock, G.J. (1993c). "Design of Decking Panels with Intermediate Stiffeners," Research Report No. R676, Centre for Advanced Structural Engineering, School of Civil and Mining Engineering, University of Sydney, Australia, August.

Daudet, L.R., and Klippstein, K.H. (1994). "Stub Column Study Using Welded, Cold-Reduced Steel," Proceedings of the 12th International Specialty Conference on Cold-Formed Steel Structures, St. Louis, Missouri, October 18-19, pp. 285-302.

Davies, J.M., and Cowen, J.S. (1994). "Pallet Racking Using Cold-Reduced Steel," Proceedings of the 12th International Specialty Conference on Cold-Formed Steel Structures, St. Louis, Missouri, October 18-19, pp. 641-655.

Dhalla, A.K., Errera, S., and Winter, G. (1971a). "Connections in Thin Low-Ductility Steels," Journal of the Structural Division, ASCE, Vol. 97, No. ST10, October, pp. 2549-2566.

Dhalla, A.K. and Winter, G. (1971b). "Influence of Ductility on the Structural Behavior of Cold-Formed Steel Members," Report No. 336, Cornell University, June.

Dhalla, A.K., and Winter, G. (1971c). "Ductility Criteria and Performance of Low Ductility Steels for Cold-Formed Members," Proceedings of the 1st Specialty Conference on Cold-Formed Steel Structures, University of Missouri-Rolla, August, pp. 22-30.

Dhalla, A.K., and Winter, G. (1974a). "Steel Ductility Measurements," Journal of the Structural Division, ASCE, Vol. 100, No. ST2, February, pp. 427-444.

Dhalla, A.K., and Winter, G. (1974b). "Suggested Steel Ductility Requirements," Journal of the Structural Division, ASCE, Vol. 100, No. ST2, February, pp. 445-462.

Dodd, B. and Bai, Y. (1987). "Ductile Fracture and Ductility, with Application to Metalworking," Academic Press.

Glauz, R.S. (1990). "Cold-Formed Steel Design Program, User's manual,"

Hancock, G. (1995). "Structural Ductility of G550 Steel to AS 1397," Unpublished paper.

Kile, W. (1995). "RIBUMR," STRUCTUNEERING INC.

Kwon, Y.B. and Hancock, G.J. (1992). "Design of Channels against Distortional Buckling," Research Report No. R660, Centre for Advanced Structural Engineering, School of Civil and Mining Engineering, University of Sydney, Australia, October.

Kwon, Y.B. and Hancock, G.J. (1991). "Strength Tests of Cold-Formed Channel Sections Undergoing Local and Distortional Buckling," Research Report No. R640, Centre for Advanced Structural Engineering, School of Civil and Mining Engineering, University of Sydney, Australia, June.

Macadam, J.N., Brockenbrough, R.L., LaBoube, R.A., Pekoz, T., and Schneider, E.J. (1988). "Low-Strain-Hardening Ductile-Steel Cold-Formed Members," Proceedings of the 9th International Specialty Conference on Cold-Formed Steel Structures, St. Louis, Missouri, November 8-9, pp. 459-487.

Mahendran, M. (1992). "Contrasting Behavior of Thin Steel Claddings under Simulated Cyclonic Wind Loading," Proceedings of the 11th International Specialty Conference on Cold-Formed Steel Structures, St. Louis, Missouri, October 20-21, pp. 245-256.

Mahendran, M. (1994). "Profiled Steel Roof Claddings under High Wind Forces," Steel Structures, Journal of Singapore Structural Steel Society, Vol. 5, No. 1, December, pp. 95-106.

Maricic, A. (1979). "Cold-Formed Structures of High Strength Steel," Thin-Walled Structures--Recent Technical Advances and Trends in Design, Research and Construction, International Conference at the University of Strathclyde, Glasgow, April 3-6, pp. 386-397.

MRI. (1978). "Structural Test of Butler Building BR-II Wall/Roof Panels," Midwest Research Institute (MRI) report, Project No. 5-1068-L (16), Midwest Research Institute, October 13.

Pan, L.C., and Yu, Wei-Wen. (1988). "High Strength Steel Members with Unstiffened Compression

Elements," Proceedings of the 9th International Specialty Conference on Cold-Formed Steel Structures, St. Louis, Missouri, November 8-9, pp. 489-511.

Pekoz, T. (1986). " Development of a Unified Approach to the Design of Cold-Formed Steel Members," Proceedings of the 8th International Specialty Conference on Cold-Formed Steel Structures, St. Louis, MO, pp. 77-84.

Pekoz, T. and McGuire, W. (1979). "Welding of Sheet Steel," Report SG 79-2, Committee of Sheet Steel Producers, AISI, January.

Salaheldin, M.M., and Schmidt, L.C. (1992). "Profiled Sheet Behavior under Concentrated Load," Proceedings of the 11th International Specialty Conference on Cold-Formed Steel Structures, St. Louis, Missouri, October 20-21, pp. 197-215.

Seleim, S.S., and LaBoube, R.A. (1994). "Behavior of Low-Ductile Steels in Cold-Formed Steel Connections," Report (unpublished), Department of Civil Engineering, University of Missouri-Rolla.

Tondelli Engineering (1991). "PANEL86, User's Guide,"

Xu, Y.L. (1995). "Fatigue Performance of Screw-Fastened Light-Gauge-Steel Roofing Sheets," Journal of Structural Engineering, ASCE, Vol. 121, No.3, March, pp. 389-398.

Yu, Wei-Wen. (1991). "Cold-Formed Steel Design," Second Edition, John Wiley & Sons. Inc..

APPENDIX

Table 2.3.1 Comparison of V Stiffener Specimen Test Results with the M_u Calculated by AISI Specification (1991) [Bernard et al. (1993c)]

Specimen	Mode[♭]	M_u (test) kNm	$M_u^!$ (code) kNm	$\frac{M_{u,\,test}}{M_{u,\,code}}$
ST21A	L	3.39	2.790	1.215
ST21B	L	2.97	2.799	1.061
ST22A	L	3.56	2.924	1.218
ST22B	L	3.16	2.939	1.075
ST23A	L	2.65	2.162	1.226
ST23B	L	2.38	2.163	1.100
IST43A	D+L	3.85	3.716	1.036
IST44A	D+L	4.00	3.895	1.027
IST44B	D+L	3.68	3.843	0.958
IST45B	D+L	3.88	3.877	1.001
IST46A	D+L	4.59	4.735	0.969
IST47A	D+L	4.56	4.410	1.034
IST47B	D+L	4.57	4.467	1.023
IST48B	D+L	4.54	4.647	0.977
IST48A	L	5.42	5.814	0.932
IST410A	L	5.75	6.101	0.942
IST410B	L	5.14	5.672	0.906
IST412B	L	5.59	6.059	0.923
			Mean	1.035
			σ	0.101

[♭] L = Local only; L+D = Local then Distortional;
D = Distortional only; D+L = Distortional then Local
[!] Calculated by AISI, 1991

Table 2.3.2 Comparison of Flat-Hat Specimen Test Results with the M_u Calculated by AISI Specification (1991) [Bernard et al (1993c)]

Specimen	Mode[♭]	M_u (test) kNm	$M_u^!$ (code) kNm	$\frac{M_{u,\,test}}{M_{u,\,code}}$
TS3A1	D+D2	2.96	2.919	1.014
TS3A2	D+D2	2.93	3.048	0.961
TS3A3	D+L	2.96	3.262	0.907
TS3A4	L+D	3.52	3.746	0.939
TS3A5	L+D	4.10	4.538	0.903
TS3A6	L+D	3.87	4.502	0.860
TS3B4	L+D	3.63	3.583	1.013
TS3B5	L+D	4.01	4.019	0.998
TS3B6	L	4.04	4.414	0.915
			Mean	0.946
			σ	0.055

[♭] L = Local only; L+D = Local then Distortional; D+D2 = 1st & 2nd mode Distortional; D+L = Distortional then Local
[!] Calculated by AISI, 1991

Table 2.3.3 Comparison of V Stiffener Specimen Test Results with the M_u Calculated by Eurocode 3/Annexe A [Bernard et al. (1993c)]

Specimen	Mode[♭]	M_u (test) kNm	$M_u^{\dagger}$ (EC3) kNm	$\frac{M_{u,\,test}}{M_{u,\,EC3}}$
ST21A	L	3.39	2.780	1.219
ST21B	L	2.97	2.791	1.064
ST22A	L	3.56	2.907	1.225
ST22B	L	3.16	2.922	1.081
ST23A	L	2.65	2.151	1.232
ST23B	L	2.38	2.152	1.106
IST43A	D+L	3.85	3.056	1.260
IST44A	D+L	4.00	3.258	1.228
IST44B	D+L	3.68	3.043	1.209
IST45B	D+L	3.88	3.226	1.203
IST46A	D+L	4.59	3.917	1.173
IST47A	D+L	4.56	3.713	1.228
IST47B	D+L	4.57	3.819	1.197
IST48B	D+L	4.54	4.007	1.133
IST48A	L	5.42	4.322	1.254
IST410A	L	5.75	4.739	1.213
IST410B	L	5.14	4.254	1.208
IST412B	L	5.59	4.747	1.178
			Mean	1.189
			σ	0.057

[♭] L = Local only; L+D = Local then Distortional;
D = Distortional only; D+L = Distortional then Local
[†] Calculated by EC3/ Annexe A

Table 2.3.4 Comparison of Flat-Hat Specimen Test Results with the M_u Calculated by Eurocode 3/Annexe A [Bernard et al. (1993c)]

Specimen	Mode[♭]	M_u (test) kNm	$M_u^{\dagger}$ (EC3) kNm	$\frac{M_{u,\,test}}{M_{u,\,EC3}}$
TS3A1	D+D2	2.96	2.468	1.199
TS3A2	D+D2	2.93	2.592	1.130
TS3A3	D+L	2.96	2.736	1.082
TS3A4	L+D	3.52	3.010	1.169
TS3A5	L+D	4.10	3.182	1.288
TS3A6	L+D	3.87	3.164	1.223
TS3B4	L+D	3.63	2.952	1.230
TS3B5	L+D	4.01	3.234	1.240
TS3B6	L	4.04	3.253	1.242
			Mean	1.200
			σ	0.064

[♭] L = Local only; L+D = Local then Distortional; D+D2 = 1st & 2nd mode Distortional; D+L = Distortional then Local
[†] Calculated by EC3/ Annexe A

Table 2.3.5 Comparison of V Stiffener Specimen Test Results with the M_u Calculated by Australia Standard AS1538 [Bernard et al. (1993c)]

Specimen	Mode[b]	M_u (test) kNm	$M_u^!$ (AS1538) kNm	$\frac{M_{u,\,test}}{M_{u,\,AS1538}}$
ST21A	L	3.39	3.276	1.035
ST21B	L	2.97	3.289	0.903
ST22A	L	3.56	3.400	1.047
ST22B	L	3.16	3.418	0.924
ST23A	L	2.65	2.502	1.059
ST23B	L	2.38	2.504	0.950
IST43A	D+L	3.85	3.369*	1.143
IST44A	D+L	4.00	3.352*	1.193
IST44B	D+L	3.68	3.352*	1.098
IST45B	D+L	3.88	3.367*	1.152
IST46A	D+L	4.59	3.466*	1.324
IST47A	D+L	4.56	3.391*	1.345
IST47B	D+L	4.57	3.408*	1.341
IST48B	D+L	4.54	3.427*	1.325
IST48A	L	5.42	5.549	0.977
IST410A	L	5.75	5.855	0.982
IST410B	L	5.14	5.438	0.945
IST412B	L	5.59	5.825	0.959
			Mean	1.095
			σ	0.154

[b] L = Local only; L+D = Local then Distortional;
D = Distortional only; D+L = Distortional then Local
[!] Calculated by AS1538-1988
* Stiffener inadequate by AS1538

Table 2.3.6 Comparison of Flat-Hat Specimen Test Results with the M_u Calculated by Australia Standard AS1538 [Bernard et al. (1993c)]

Specimen	Mode[b]	M_u (test) kNm	$M_u^!$ (AS1538) kNm	$\frac{M_{u,\,test}}{M_{u,\,AS1538}}$
TS3A1	D+D2	2.96	2.611*	1.134
TS3A2	D+D2	2.93	2.642*	1.109
TS3A3	D+L	2.96	2.630*	1.125
TS3A4	L+D	3.52	4.287	0.821
TS3A5	L+D	4.10	4.210	0.974
TS3A6	L+D	3.87	4.220	0.917
TS3B4	L+D	3.63	2.628*	1.381
TS3B5	L+D	4.01	4.140	0.969
TS3B6	L	4.04	4.140	0.976
			Mean	1.045
			σ	0.163

[b] L = Local only; L+D = Local then Distortional; D+D2 = 1st & 2nd mode Distortional; D+L = Distortional then Local
[!] Calculated by AS1538-1988
* Stiffener inadequate by AS1538

Table 2.3.7 Comparison of Test Results with the M_u Calculated by Unified Approach (Pekoz 1986) (with Partially Effective Webs by AISI Specification) [Bernard et al. (1993c)]

Specimen[‡]	Mode[♭]	M_u (test) kNm	$M_u^{\dagger}$ (Pekōz) kNm	$\frac{M_{u,\,test}}{M_{u,\,Pekoz}}$
TS3A4	L+D	3.52	2.189	1.608
TS3A5	L+D	4.10	2.929	1.400
TS3A6	L+D	3.87	2.980	1.299
TS3B4	L+D	3.63	1.810	2.006
TS3B5	L+D	4.01	2.447	1.639
TS3B6	L	4.04	3.095	1.305
			Mean	1.543
			σ	0.270

[♭] L = Local only; L+D = Local then Distortional; D+D2 = 1st & 2nd mode Distortional; D+L = Distortional then Local
[‡] No local buckling moment found in numerical study for specimens TS3A1-3. [†] Calculated by Unified Approach

Table 2.3.8 Comparison of Test Results with the M_u Calculated by Modified Effective Section Method (with Partially Effective Webs by AISI Specification) [Bernard et al. (1993c)]

Specimen	Mode[♭]	M_u (test) kNm	$M_u^{\dagger}$ (MES) kNm	$\frac{M_{u,\,test}}{M_{u,\,MES}}$	M_{le} kNm	M_{de} kNm	$\frac{M_{le}}{M_{de}}$
IST43A	D+L	3.85	2.506	1.536	-	1.930	-
IST44A	D+L	4.00	2.838	1.409	2.940	2.588	1.14
IST44B	D+L	3.68	2.445	1.505	-	1.780	-
IST45B	D+L	3.88	2.752	1.410	-	2.413	-
IST46A	D+L	4.59	3.568	1.286	3.597	3.999	0.90
IST47A	D+L	4.56	3.376	1.351	3.410	3.771	0.90
IST47B	D+L	4.57	3.281	1.393	3.440	3.385	1.02
IST48B	D+L	4.54	3.568	1.272	3.550	4.067	0.87
			Mean	1.395			
			σ	0.094			
IST48A	L	5.42	4.317	1.255	3.980	6.533	0.61
IST410A	L	5.75	4.945	1.163	4.364	8.952	0.49
IST410B	L	5.14	4.200	1.224	3.878	6.305	0.62
IST412B	L	5.59	4.925	1.135	4.416	8.861	0.50
			Mean	1.194			
			σ	0.055			
			Total Mean	1.328			
			σ	0.127			

[♭] L = Local only; L+D = Local then Distortional; D = Distortional only; D+L = Distortional then Local
[†] Calculated by MES Method

Table 2.3.9 Comparison of Test Results with the M_u Calculated by Modified Effective Section Method (with Partially Effective Webs by AISI Specification) [Bernard et al. (1993c)]

Specimen	Mode[b]	M_u (test) kNm	$M_u^\dagger$ (MES) kNm	$\frac{M_{u,\,test}}{M_{u,\,MES}}$	M_{le} kNm	M_{de} kNm	$\frac{M_{le}}{M_{de}}$
TS3A1	D+D2	2.96	2.229	1.328	-	1.498	-
TS3A2	D+D2	2.93	2.424	1.209	2.296	1.598	1.44
TS3A3	D+L	2.96	2.916	1.015	2.612	2.763	0.95
			Mean	1.184			
			σ	0.158			
TS3A4	L+D	3.52	3.256	1.081	2.414	3.572	0.68
TS3A5	L+D	4.10	3.486	1.176	2.367	4.709	0.50
TS3A6	L+D	3.87	3.470	1.115	2.398	4.350	0.55
TS3B4	L+D	3.63	3.116	1.165	2.423	3.502	0.69
TS3B5	L+D	4.01	3.341	1.200	2.374	4.344	0.55
TS3B6	L	4.04	3.510	1.151	2.365	5.073	0.47
			Mean	1.148			
			σ	0.043			
			Total Mean	1.160			
			σ	0.088			

[b] L = Local only; L+D = Local then Distortional; D+D2 = 1st & 2nd mode Distortional; D+L = Distortional then Local

† Calculated by MES Method

Table 3.1.1 Ultimate Tested Moments and Calculated Effective Moments for the Australia Single-Span Deck Panels [Bernard et al. (1992a)]

	$M_{u,test}$ (k-in)	$M_{y,91\ code}$ (k-in)	$M_{y,86\ code}$ (k-in)	$M_{n,60\ ksi}$ (k-in)	$M_{u,test}/M_{y,86\ code}$	$M_{u,test}/M_{n,60\ ksi}$
ST21A	30.01	24.70	23.95	18.70	1.25	1.60
ST21B	26.29	24.78	25.37	19.82	1.04	1.33
ST22A	31.51	25.88	26.59	20.96	1.19	1.50
ST22B	27.97	26.01	26.77	21.11	1.04	1.32
ST23A	23.46	19.14	18.50	14.66	1.27	1.60
ST23B	21.07	19.15	18.60	14.73	1.13	1.43
Mean					1.15	1.46
σ					0.101	0.125

1 k-in= 0.113 kN-m

Table 3.2.1 Ultimate Tested Pressures and Calculated Uniformly Distributed Loads for Butler Deck Panels

Specimen	Number of Span	Span Length (in)	Load	$W_{u,test}$ (psf)	$W_{y,86\ code}$ (psf)	$W_{n,60\ ksi}$ (psf)	$W_{u,test}/W_{y,86\ code}$	$W_{u,test}/W_{n,60\ ksi}$
1	3	90	pos.	37.70	35.26	28.57	1.07	1.32
2	3	90	neg.	55.00	39.69	30.40	1.39	1.81
3	2	90	pos.	37.40	28.21	22.85	1.33	1.64
4	2	90	neg.	55.00	31.75	24.32	1.73	2.26
5	4	60	pos.	89.20	74.15	60.07	1.20	1.48
6	4	60	neg.	97.20	83.46	63.94	1.17	1.53
Mean							1.32	1.67
σ							0.233	0.331

1 psf=0.0479 kN/m^2, 1 inch=25.4 mm

Table 4.4.1 Material Properties of 22 Gage Sheet Steel (Long Coupons)

Specimen	Thickness t (in)	Average Width (in)	0.2% Offset Yield Strength F_y (ksi)	Tensile Strength F_u (ksi)	Tensile-to-Yield Ratio F_u/F_y	Local Elongation in 1/2-in Gage Length (%)	Uniform Elongation Outside Fracture (%)	Elongation in 2-in Gage Length (%)
LT22-L1	0.029	0.502	110.7	110.8	1.00	12.80	0.80	3.38 (3.32)
LT22-L2	0.029	0.503	108.1	110.1	1.02	10.60	1.00	3.27 (3.56)
LT22-M1	0.029	0.501	104.1	108.1	1.04	10.60	1.60	4.05 (4.13)
LT22-M2	0.029	0.502	101.7	106.3	1.05	11.70	1.70	4.29 (3.96)
LT22-R1	0.029	0.501	103.2	107.4	1.04	12.50	1.50	3.94 (4.05)
LT22-R2	0.029	0.501	103.5	107.3	1.04	13.65	1.15	3.94 (4.08)
Average	0.029	0.502	105.2	108.3	1.03	11.98	1.29	3.81
TT22-L1	0.029	0.501	122.5	123.9	1.01	6.95	0.65	* (2.16)
TT22-L3	0.029	0.500	121.0	122.1	1.01	7.45	0.35	1.81 (1.87)
TT22-R3	0.029	0.500	114.9	116.4	1.01	7.75	0.25	1.90 (1.93)
TT22-R4	0.029	0.499	115.5	118.4	1.03	7.00	0.40	1.95 (2.03)
Average	0.029	0.500	118.5	120.2	1.02	7.29	0.41	1.96

1 ksi=6.895 MPa, 1 inch=25.4 mm

Table 4.4.2 Material Properties of 24 Gage Sheet Steel (Long Coupons)

Specimen	Thickness t (in)	Average Width (in)	0.2% Offset Yield Strength F_y (ksi)	Tensile Strength F_u (ksi)	Tensile-to-Yield Ratio F_u/F_y	Local Elongation in 1/2-in Gage Length (%)	Uniform Elongation Outside Fracture (%)	Elongation in 2-in Gage Length (%)
LT24-L1	0.024	0.499	115.8	119.1	1.03	8.85	1.15	2.89 (2.82)
LT24-L2	0.024	0.500	*	*	*	9.70	1.30	* (3.08)
LT24-M1	0.024	0.499	111.1	116.6	1.05	8.15	1.65	3.24 (3.28)
LT24-M2	0.024	0.500	112.2	116.7	1.04	9.15	1.65	* (3.50)
LT24-R1	0.024	0.497	112.9	117.4	1.04	10.05	0.75	2.99 (2.91)
LT24-R2	0.024	0.499	112.1	116.7	1.04	10.10	0.90	2.97 (3.06)
Average	0.024	0.499	112.8	117.3	1.04	9.33	1.23	3.11
TT24-L1	0.024	0.500	123.6	126.8	1.03	6.00	0.60	1.64 (1.70)
TT24-L2	0.024	0.500	124.3	127.7	1.03	7.10	0.30	1.61 (1.60)
TT24-R1	0.024	0.500	124.2	126.2	1.02	6.05	0.35	1.54 (1.55)
TT24-R2	0.024	0.499	121.7	125.6	1.03	6.45	0.15	1.60 (1.61)
Average	0.024	0.500	123.5	126.6	1.03	6.40	0.35	1.60

1 ksi=6.895 MPa, 1 inch=25.4 mm

Table 4.4.3 Material Properties of 26 Gage Sheet Steel (Long Coupons)

Specimen	Thickness t (in)	Average Width (in)	0.2% Offset Yield Strength F_y (ksi)	Tensile Strength F_u (ksi)	Tensile-to-Yield Ratio F_u/F_y	Local Elongation in 1/2-in Gage Length (%)	Uniform Elongation Outside Fracture (%)	Elongation in 2-in Gage Length (%)
LT26-L1	0.017	0.499	116.8	120.3	1.03	8.00	1.00	2.58 (2.89)
LT26-L2	0.017	0.500	113.8	119.6	1.05	10.35	0.85	2.91 (2.83)
LT26-M1	0.017	0.499	113.8	117.8	1.04	8.50	0.90	2.72 (2.60)
LT26-M2	0.017	0.499	115.2	120.2	1.04	9.45	0.35	2.33 (2.33)
LT26-R1	0.017	0.498	114.7	119.9	1.05	9.95	0.85	2.42 (3.02)
LT26-R2	0.017	0.499	114.1	118.6	1.04	8.55	0.65	2.34 (2.32)
Average	0.017	0.499	114.7	119.4	1.04	9.13	0.77	2.55
TT26-L1	0.017	0.499	129.0	132.7	1.03	*	*	*
TT26-L2	0.017	0.498	127.7	131.6	1.03	4.10	0.50	1.07 (1.12)
TT26-R1	0.017	0.497	130.3	133.3	1.02	3.45	0.35	1.23 (1.10)
TT26-R2	0.017	0.496	127.9	131.6	1.03	*	*	*
Average	0.017	0.498	128.7	132.3	1.03	3.78	0.43	1.15

1 ksi=6.895 MPa, 1 inch=25.4 mm

Table 4.4.4 Material Properties of 28 Gage Sheet Steel (Long Coupons)

Specimen	Thickness t (in)	Average Width (in)	0.2% Offset Yield Strength F_y (ksi)	Tensile Strength F_u (ksi)	Tensile-to-Yield Ratio F_u/F_y	Local Elongation in 1/2-in Gage Length (%)	Uniform Elongation Outside Fracture (%)	Elongation in 2-in Gage Length (%)
LT28-L1	0.015	0.500	114.5	119.8	1.05	7.60	1.20	2.79 (2.77)
LT28-L2	0.015	0.500	114.8	121.6	1.06	8.55	1.05	2.81 (2.65)
LT28-M1	0.015	0.499	114.7	119.7	1.05	7.00	1.20	2.62 (2.51)
LT28-M2	0.015	0.499	114.8	121.1	1.05	8.90	0.90	2.77 (2.66)
LT28-R1	0.015	0.498	114.9	120.5	1.05	7.35	1.05	2.42 (2.25)
LT28-R2	0.015	0.499	114.6	117.4	1.02	7.95	0.85	2.57 (2.37)
Average	0.015	0.499	114.7	120.0	1.05	7.89	1.04	2.66
TT28-L1	0.015	0.499	129.2	130.1	1.01	*	*	*
TT28-L2	0.015	0.498	128.2	129.2	1.01	*	*	*
TT28-R1	0.015	0.496	127.0	130.2	1.03	2.90	0.50	1.22 (1.17)
TT28-R2	0.015	0.497	128.0	130.1	1.02	4.65	0.35	1.28 (1.43)
Average	0.015	0.497	128.1	129.9	1.02	3.78	0.43	1.25

1 ksi= 6.895 MPa, 1 inch=25.4 mm

Table 4.4.5 Material Properties of 22 Gage Sheet Steel (Short Coupons)

Specimen	Thickness t (in)	Average Width (in)	0.2% Offset Yield Strength F_y (ksi)	Tensile Strength F_u (ksi)	Tensile-to-Yield Ratio F_u/F_y	Local Elongation in 1/2-in Gage Length (%)	Uniform Elongation Outside Fracture (%)	Elongation in 2-in Gage Length (%)
LT22-L1S	0.029	0.501	104.0	107.3	1.03			3.17 (3.09)
LT22-L2S	0.029	0.502	105.2	108.3	1.03			3.57 (3.40)
LT22-L3S	0.029	0.502	104.7	108.2	1.03			3.31 (3.30)
LT22-M1S	0.029	0.502	101.0	106.6	1.06			4.12 (4.20)
LT22-M2S	0.029	0.502	101.5	106.2	1.05			3.86 (3.92)
LT22-R1S	0.029	0.501	104.6	108.1	1.03			3.39 (3.40)
LT22-R2S	0.029	0.501	106.6	109.2	1.02			4.24 (4.29)
Average	0.029	0.502	103.9	107.7	1.04			3.67
TT22-L1S	0.029	0.501	117.6	119.7	1.02			2.16 (1.90)
TT22-L2S	0.029	0.501	117.7	120.0	1.02			2.14 (1.91)
TT22-R1S	0.029	0.502	121.7	122.7	1.01			1.82 (1.80)
TT22-R2S	0.029	0.502	121.2	122.3	1.01			1.84 (1.89)
Average	0.029	0.502	119.6	121.2	1.02			1.99

1 ksi=6.895 MPa, 1 inch=25.4 mm

Table 4.4.6 Material Properties of 24 Gage Sheet Steel (Short Coupons)

Specimen	Thickness t (in)	Average Width (in)	0.2% Offset Yield Strength F_y (ksi)	Tensile Strength F_u (ksi)	Tensile-to-Yield Ratio F_u/F_y	Local Elongation in 1/2-in Gage Length (%)	Uniform Elongation Outside Fracture (%)	Elongation in 2-in Gage Length (%)
LT24-L1S	0.024	0.493	109.8	115.2	1.05			2.69 (2.69)
LT24-L2S	0.024	0.495	109.1	116.1	1.06			2.79 (2.76)
LT24-R1S	0.024	0.496	108.7	116.8	1.07			2.76 (2.66)
LT24-R2S	0.024	0.496	112.8	117.4	1.04			2.53 (2.56)
Average	0.024	0.495	110.1	116.4	1.06			2.69
TT24-L1S	0.024	0.492	125.6	128.0	1.02			1.76 (1.75)
TT24-L2S	0.024	0.493	126.2	128.0	1.01			1.75 (1.80)
TT24-R1S	0.024	0.495	126.2	129.3	1.02			1.80 (1.96)
TT24-R2S	0.024	0.495	126.0	128.8	1.02			1.80 (1.80)
Average	0.024	0.494	126.0	128.5	1.02			1.78

1 ksi=6.895 MPa, 1 inch=25.4 mm

Table 4.4.7 Material Properties of 26 Gage Sheet Steel (Short Coupons)

Specimen	Thickness t (in)	Average Width (in)	0.2% Offset Yield Strength F_y (ksi)	Tensile Strength F_u (ksi)	Tensile-to-Yield Ratio F_u/F_y	Local Elongation in 1/2-in Gage Length (%)	Uniform Elongation Outside Fracture (%)	Elongation in 2-in Gage Length (%)
LT26-L1S	0.017	0.497	110.0	114.4	1.04			2.47 (2.35)
LT26-L2S	0.017	0.497	112.9	114.6	1.02			2.43 (2.45)
LT26-R1S	0.017	0.501	113.6	117.7	1.04			2.42 (2.51)
LT26-R2S	0.017	0.501	113.4	116.9	1.03			2.28 (2.21)
Average	0.017	0.499	112.5	115.9	1.03			2.40
TT26-L1S	0.017	0.502	130.8	133.1	1.02			*
TT26-L2S	0.017	0.500	129.1	132.3	1.02			1.37 (1.21)
TT26-L3S	0.017	0.500	129.1	132.6	1.03			1.31 (1.35)
TT26-R1S	0.017	0.501	129.6	132.4	1.02			1.27 (1.35)
TT26-R2S	0.017	0.500	129.9	132.7	1.02			1.34 (1.35)
Average	0.017	0.501	129.7	132.6	1.02			1.32

1 ksi=6.895 MPa, 1 inch=25.4 mm

Table 4.4.8 Material Properties of 28 Gage Sheet Steel (Short Coupons)

Specimen	Thickness t (in)	Average Width (in)	0.2% Offset Yield Strength F_y (ksi)	Tensile Strength F_u (ksi)	Tensile-to-Yield Ratio F_u/F_y	Local Elongation in 1/2-in Gage Length (%)	Uniform Elongation Outside Fracture (%)	Elongation in 2-in Gage Length (%)
LT28-L1S	0.015	0.500	114.1	117.7	1.03			2.65 (2.45)
LT28-L2S	0.015	0.500	113.4	116.7	1.03			2.99 (2.89)
LT28-R1S	0.015	0.500	108.0	114.8	1.06			2.76 (2.55)
LT28-R2S	0.015	0.500	108.4	115.2	1.06			2.68 (2.45)
Average	0.015	0.500	111.0	116.1	1.05			2.77
TT28-L1S	0.015	0.500	128.7	130.3	1.01			1.30 (1.25)
TT28-L2S	0.015	0.500	128.2	131.0	1.02			1.29 (1.25)
TT28-R1S	0.015	0.500	127.0	129.7	1.02			1.55 (1.55)
TT28-R2S	0.015	0.499	125.3	129.4	1.03			1.36 (1.26)
Average	0.015	0.500	127.3	130.1	1.02			1.38

1 ksi=6.895 MPa, 1 inch=25.4 mm

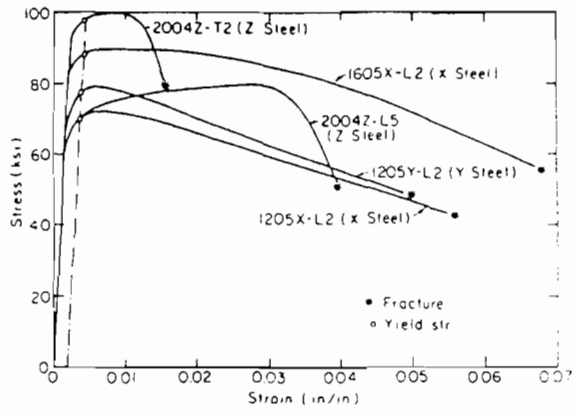

Fig. 2.2.1 Stress-Strain Curve of X, Y, and Z Steels, 2 in. (50.8 mm) Gage Length (Note: 1 ksi=6.895 MPa) [Dhalla and Winter (1971b)]

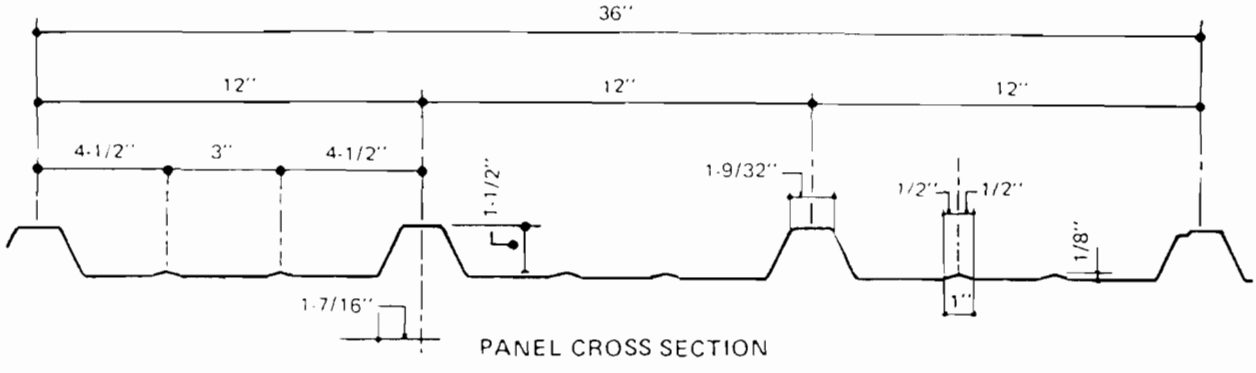

Fig. 2.3.1 Geometry of Butler BR-II Rib Sheet Steel Panels [MRI (1978)]

Test Program

Profile Type	Span Length ℓ in (mm)	Aspect Ratio b/ℓ
A	59 (1500) 55.1 (1400) 38.9 (990) 35.4 (900)	0.50 0.54 0.77 0.84
B	55.1 (1400) 35.4 (900)	0.50 0.77

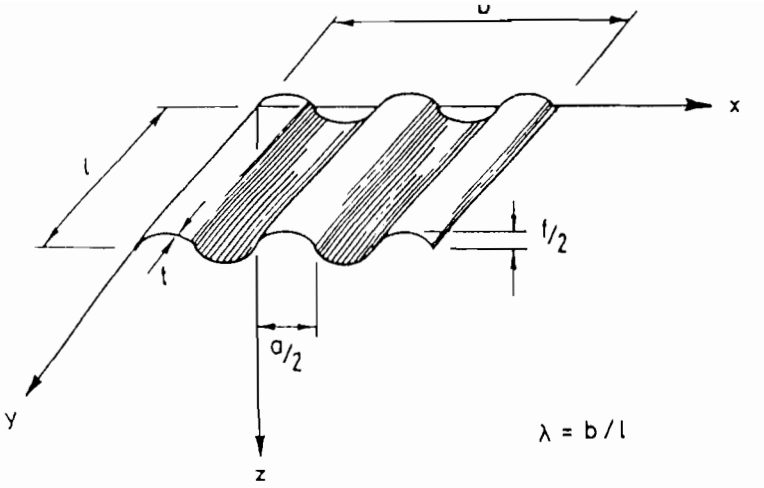

Geometrical Properties

Geometric Properties	Profile Type A in (mm)	Profile Type - B in (mm)
Basic Thickness t	0.0165 (0.42)	0.0165 (0.42)
Wave length a	3.0 (76)	3.44 (87.5)
Depth of profile f	0.67 (17)	0.944 (24)
Full panel width b	29.9 (760)	27.55 (700)

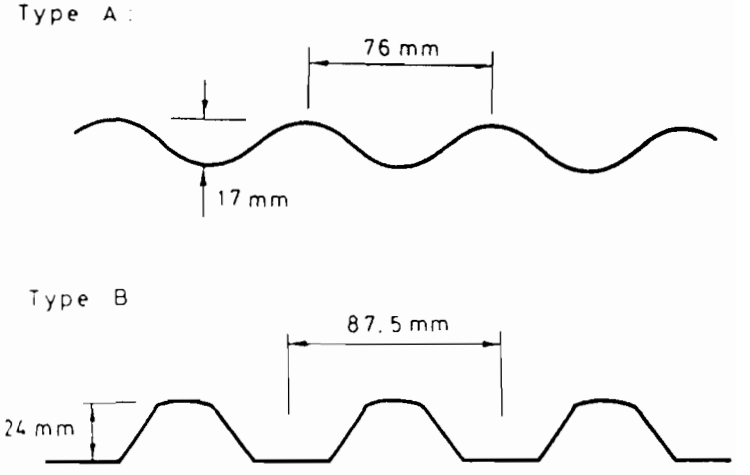

Fig. 2.3.2 Test Program and Geometrical Properties of Profiled Sheets [Salaheldin and Schmidt (1992)]

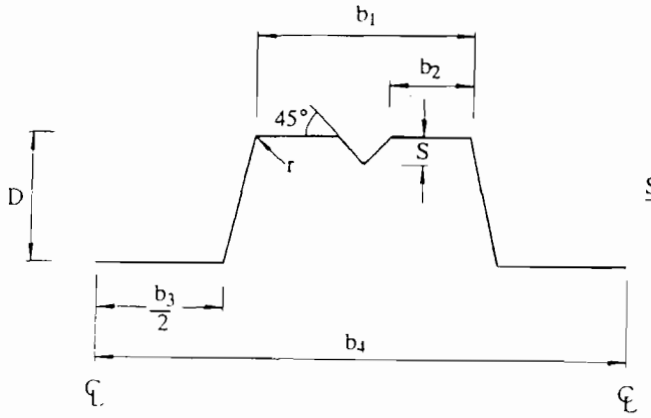

Specimens with stiffeners

b_1=3.50"
b_2=3.03" to 3.38"
$b_3/2$=1.60"
b_4=7.73"
D=2.13"
S=0.118" to 0.472"

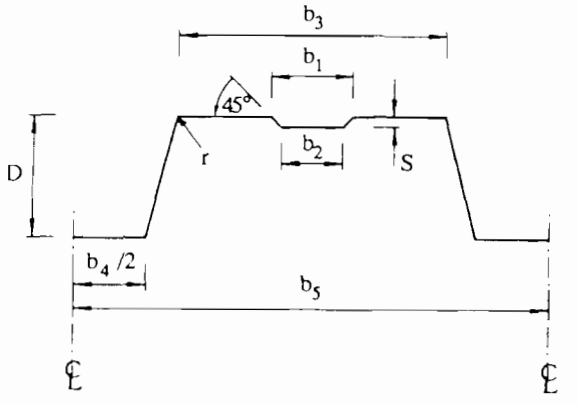

b_1=1.57"
b_3=5.30"
$b_4/2$=1.60"
b_5=9.33"
D=2.19"
S=0.039" to 0.236"

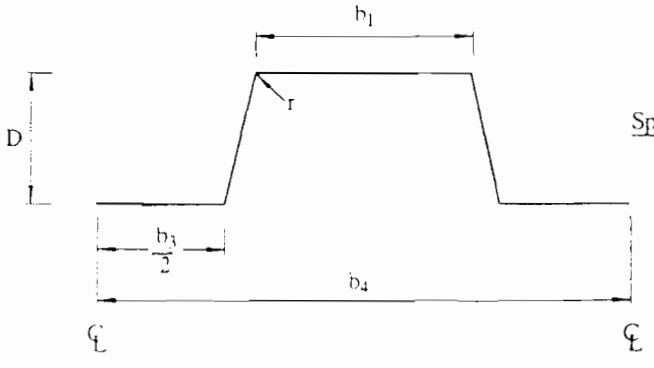

Specimens without stiffeners

b_1=1.75", 3.50", and 5.30"
$b_3/2$=1.60"
b_4=7.73"
D=2.13"

Fig. 2.3.3 Geometry and Nominal Dimensions of One Rib of V Stiffener and Flat-Hat Stiffener Specimens [Bernard et al. (1992a)(1992b)]

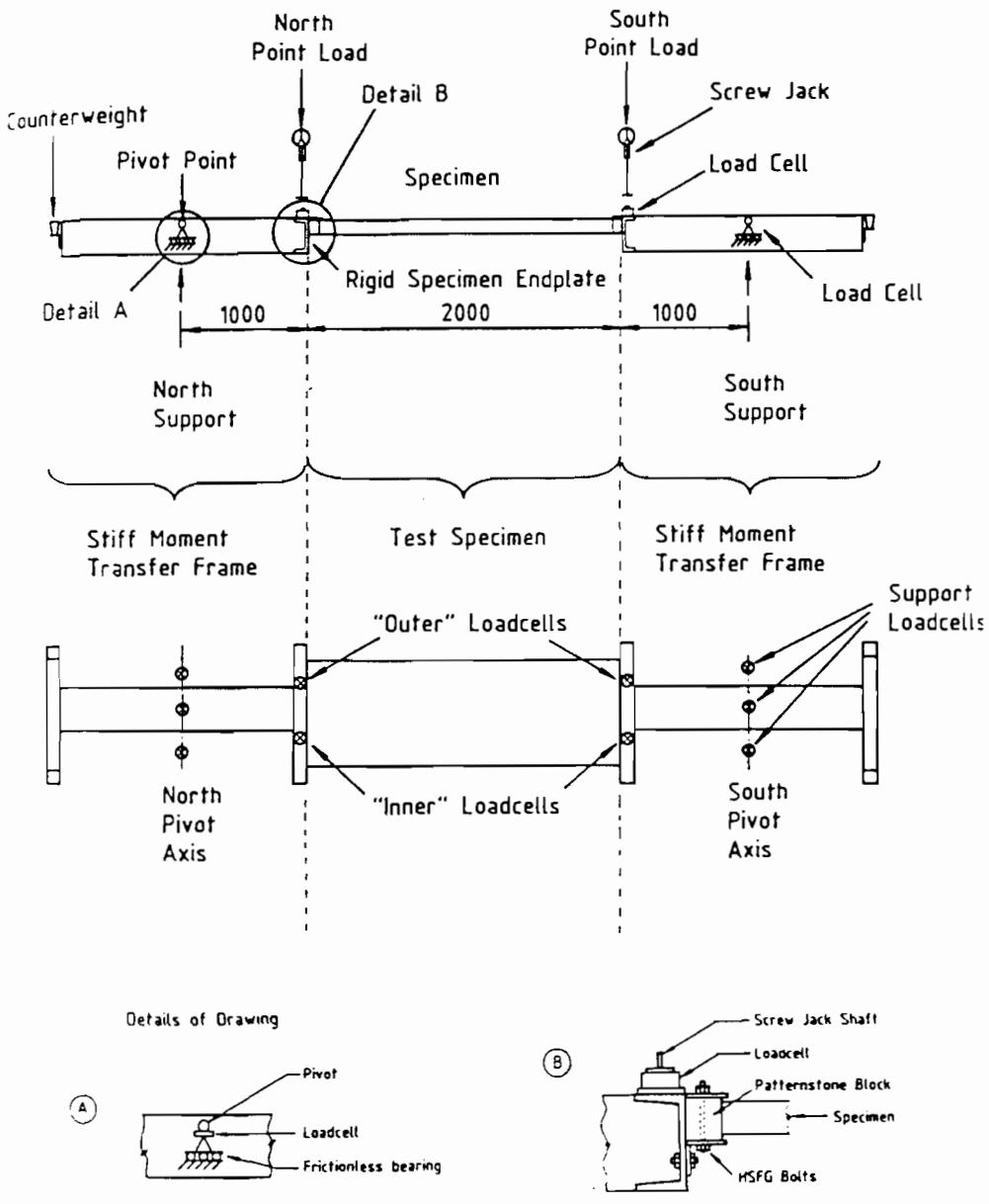

Fig. 2.3.4 Test Rig, Elevation and Plan of Test Setup [Bernard et al. (1992a)(1992b)]

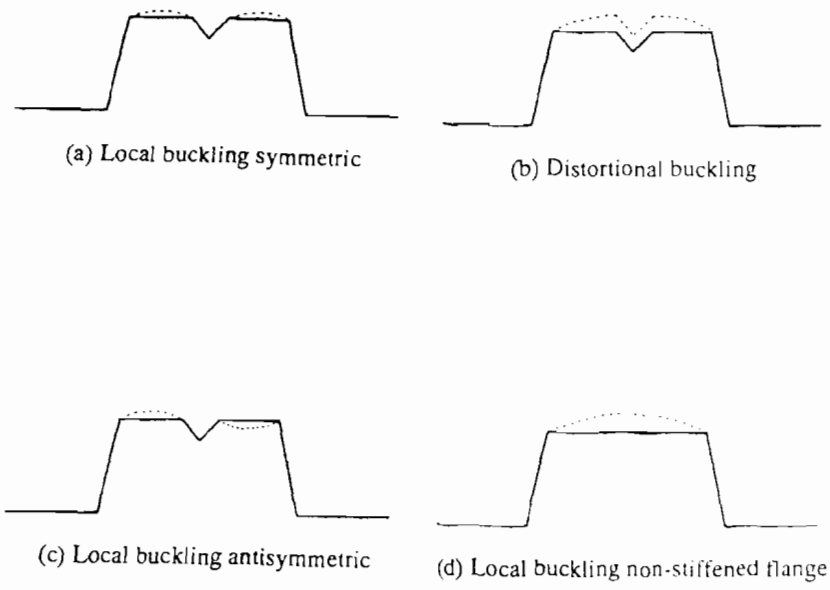

Fig. 2.3.5 Buckling Modes of V Stiffener Specimens Encountered in Test Program [Bernard et al. (1992a)]

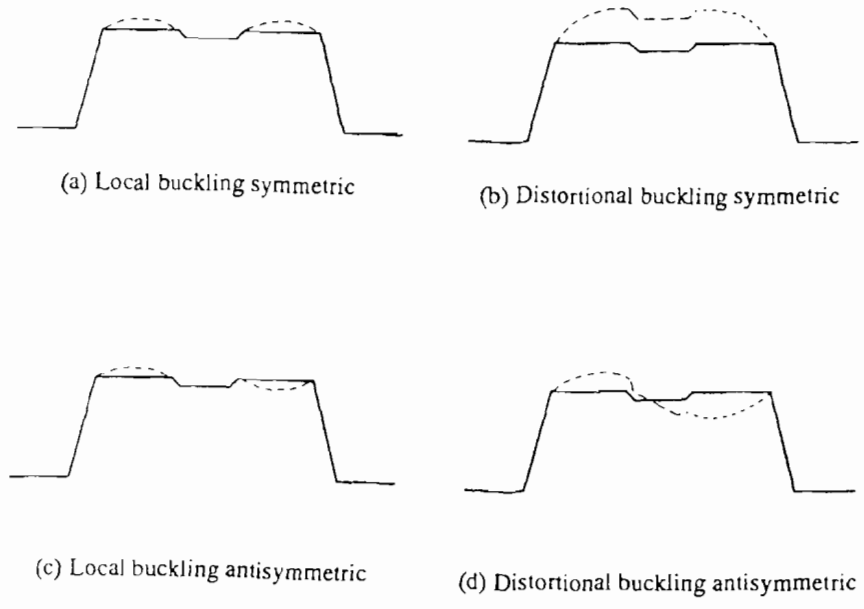

Fig. 2.3.6 Buckling Modes of Flat-Hat Stiffener Specimens Encountered in Test Program [Bernard et al. (1992b)]

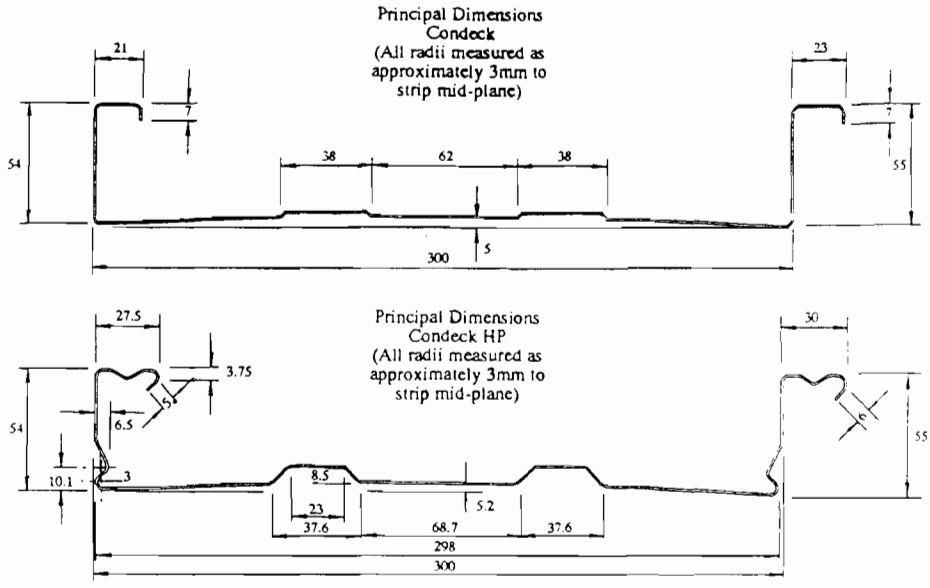

Fig. 2.3.7 Geometry and Dimensions of Condeck Specimens [Bernard et al. (1993a)]

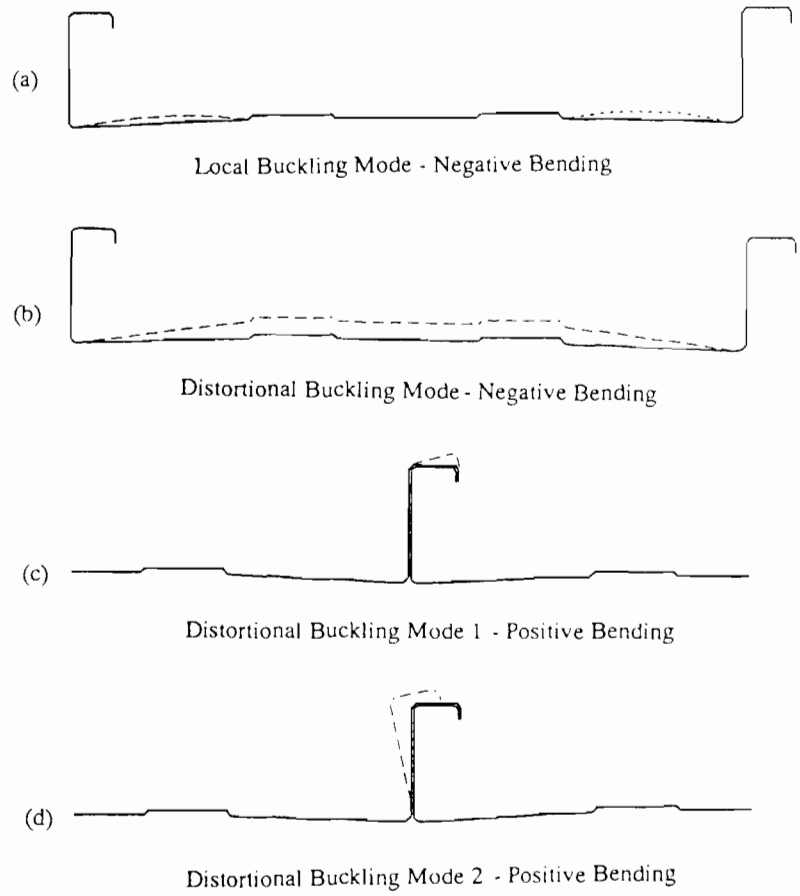

Fig. 2.3.8 Buckling Modes of Condeck Specimens as Determined by Numerical Analysis [Bernard et al. (1993a)]

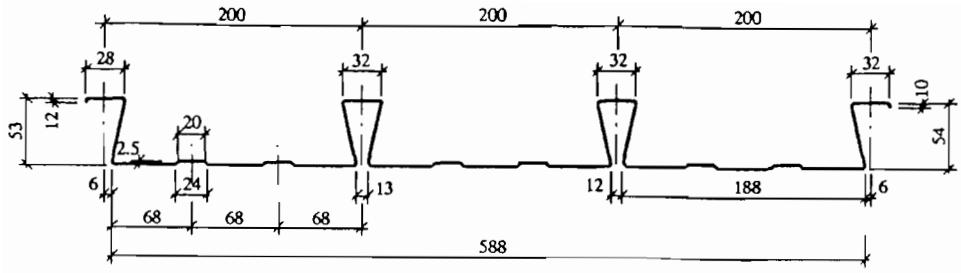

BONDEK 1
Dovetail and
Stiffener Radii
estimated = 2mm

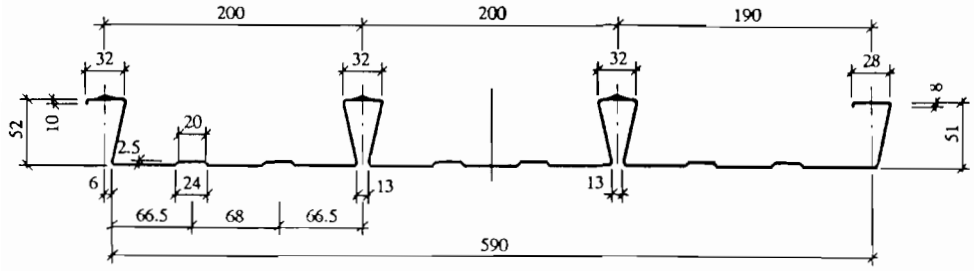

BONDEK 2
Dovetail and
Stiffener radii
as above

Fig. 2.3.9 Geometry and Dimensions of Bondek Specimens [Bernard et al. (1993b)]

a) Local Buckling mode in negative bending.

c) Local Buckling mode in positive bending.

b) Distortional Buckling mode in negative bending.

d) Distortional Buckling mode in positive bending.

Fig. 2.3.10 Buckling Modes of Bondek Specimens as Determined by Numerical Analysis [Bernard et al. (1993b)]

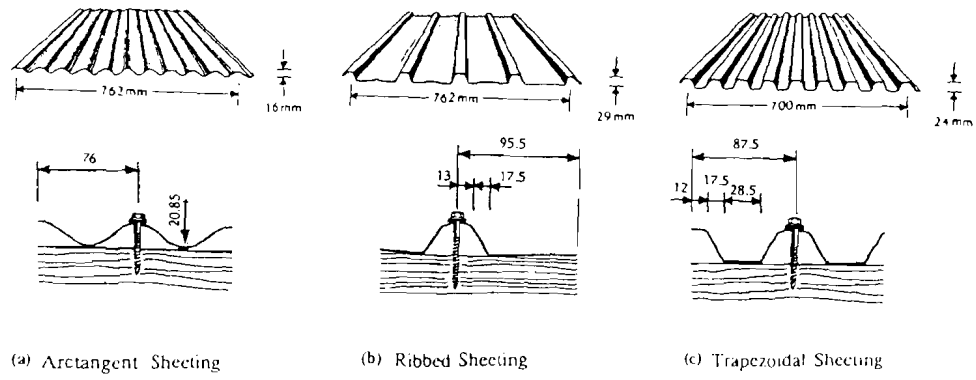

Fig. 2.3.11 Roofing Sheets and Fasteners Used in Tests [Xu (1995)]

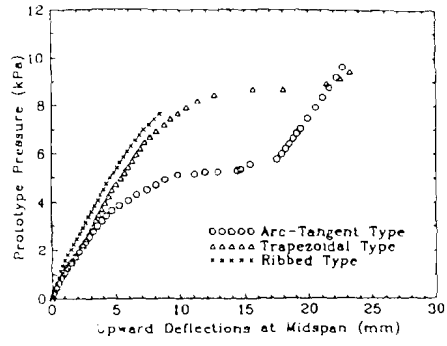

Fig. 2.3.12 Static Load-Deflection Curves [Xu (1995)]

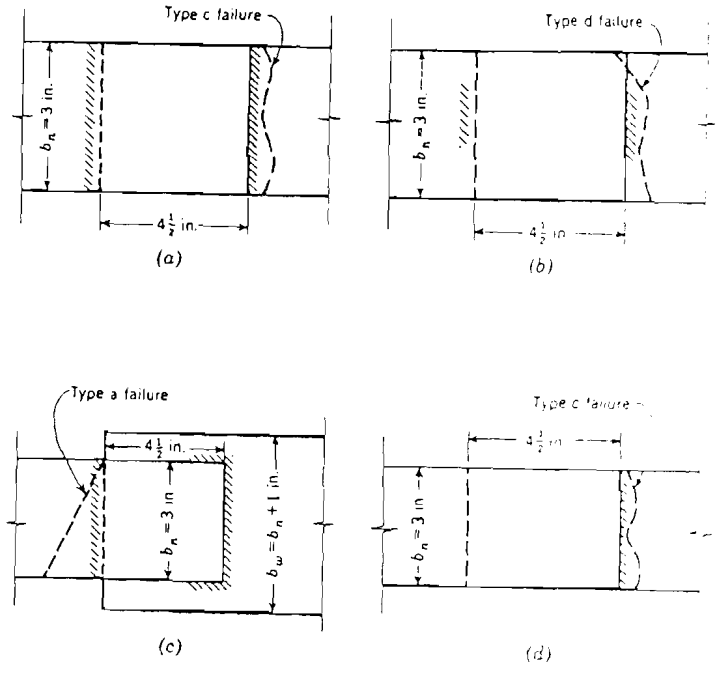

Fig. 2.4.1 Transverse Fillet Weld Specimens (a) Single Lap, Full Length Weld; (b) Single Lap, Partial Width Weld; (c) Single Lap, Unsymmetric Weld; and (d) Double Lap, Full Width Weld [Dhalla and Winter (1971b)]

Coord	ST21A	ST21A	ST21B	ST21B	ST22A	ST22A	ST22B	ST22B	ST23A	ST23A	ST23B	ST23B
#	x	y	x	y	x	y	x	y	x	y	x	y
1	0.000	0.085	0.000	0.073	0.000	0.057	0.000	0.012	0.000	0.144	0.000	0.075
2	1.339	0.000	1.329	0.000	1.378	0.000	1.368	0.000	1.437	0.000	1.516	0.000
3	2.087	2.077	2.047	2.108	1.959	2.140	1.969	2.150	2.096	2.112	2.185	2.091
4	3.839	2.057	3.780	2.091	5.472	2.150	5.482	2.118	7.352	2.047	7.470	1.978
5	4.498	-0.085	4.488	-0.051	6.093	-0.014	6.004	-0.057	8.130	-0.077	8.268	-0.140
6	7.726	-0.110	7.697	-0.014	9.321	0.004	9.232	-0.094	11.378	-0.120	11.496	-0.114
7	8.406	2.022	8.435	2.104	9.951	2.148	9.803	2.108	11.959	1.990	12.224	1.967
8	10.148	2.039	10.167	2.106	13.474	2.159	13.317	2.195	17.293	1.963	17.530	1.933
9	10.906	-0.102	10.925	-0.012	14.114	0.008	13.917	0.065	18.150	-0.120	18.388	-0.171
10	14.075	-0.118	14.085	-0.024	17.343	0.012	17.126	0.008	21.368	-0.156	21.565	-0.150
11	14.852	1.980	14.872	2.083	17.953	2.134	17.785	2.157	21.978	1.963	22.224	1.976
12	16.575	1.980	16.585	2.061	21.506	2.116	21.309	2.148	27.372	1.965	27.470	2.024
13	17.362	-0.136	17.343	-0.077	22.077	-0.047	21.880	-0.022	28.100	-0.136	28.258	-0.093
14	20.591	-0.156	20.531	-0.016	25.295	-0.043	25.098	0.008	29.488	-0.059	29.606	-0.077
15	21.132	1.974	21.201	2.118	25.906	2.130	25.669	2.179				
16	22.982	1.969	22.923	2.124	29.419	2.083	29.193	2.201				
17	23.642	-0.132	23.671	0.004	29.961	-0.061	29.744	0.067				
18	25.335	-0.053	25.079	0.087	31.339	-0.030	31.122	0.100				

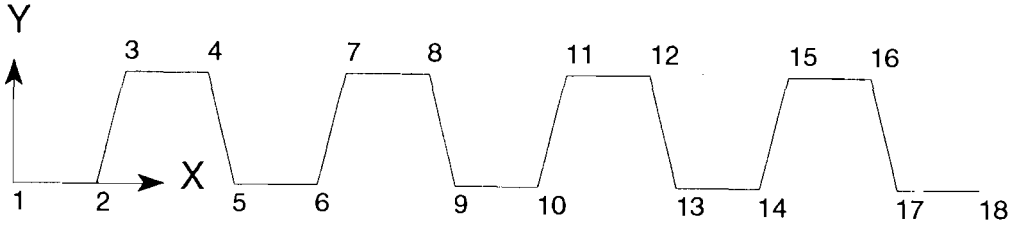

Fig. 3.1.1 Coordinate for the End Sections of the Six Panels Tested in Australia [Bernard et al. (1992a)]

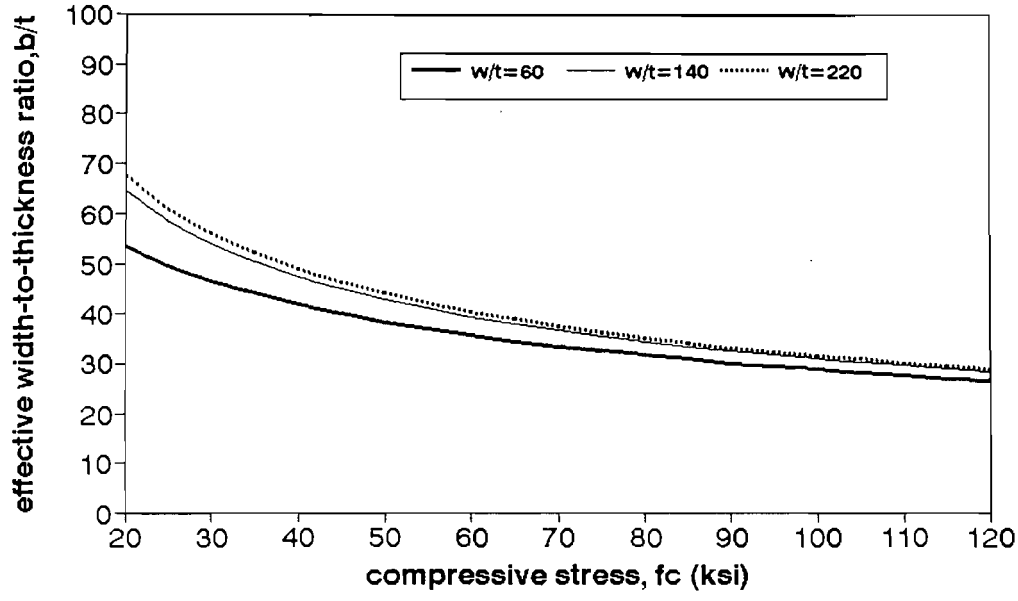

Fig. 3.3.1 Effective Width-to-Thickness Ratio vs. Compressive Stress

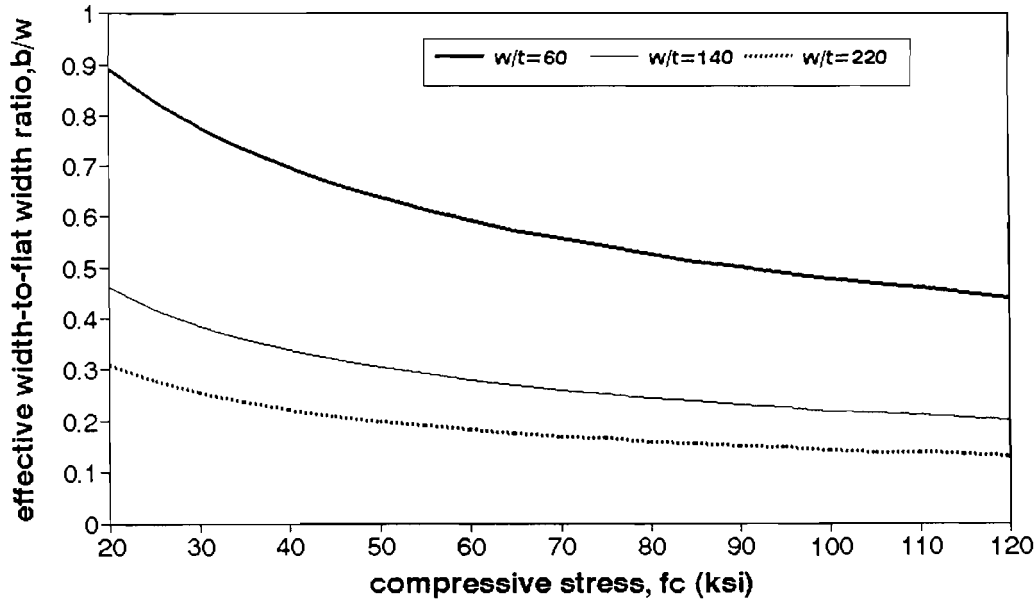

Fig. 3.3.2 Effective Width-to-Flat Width Ratio vs. Compressive Stress

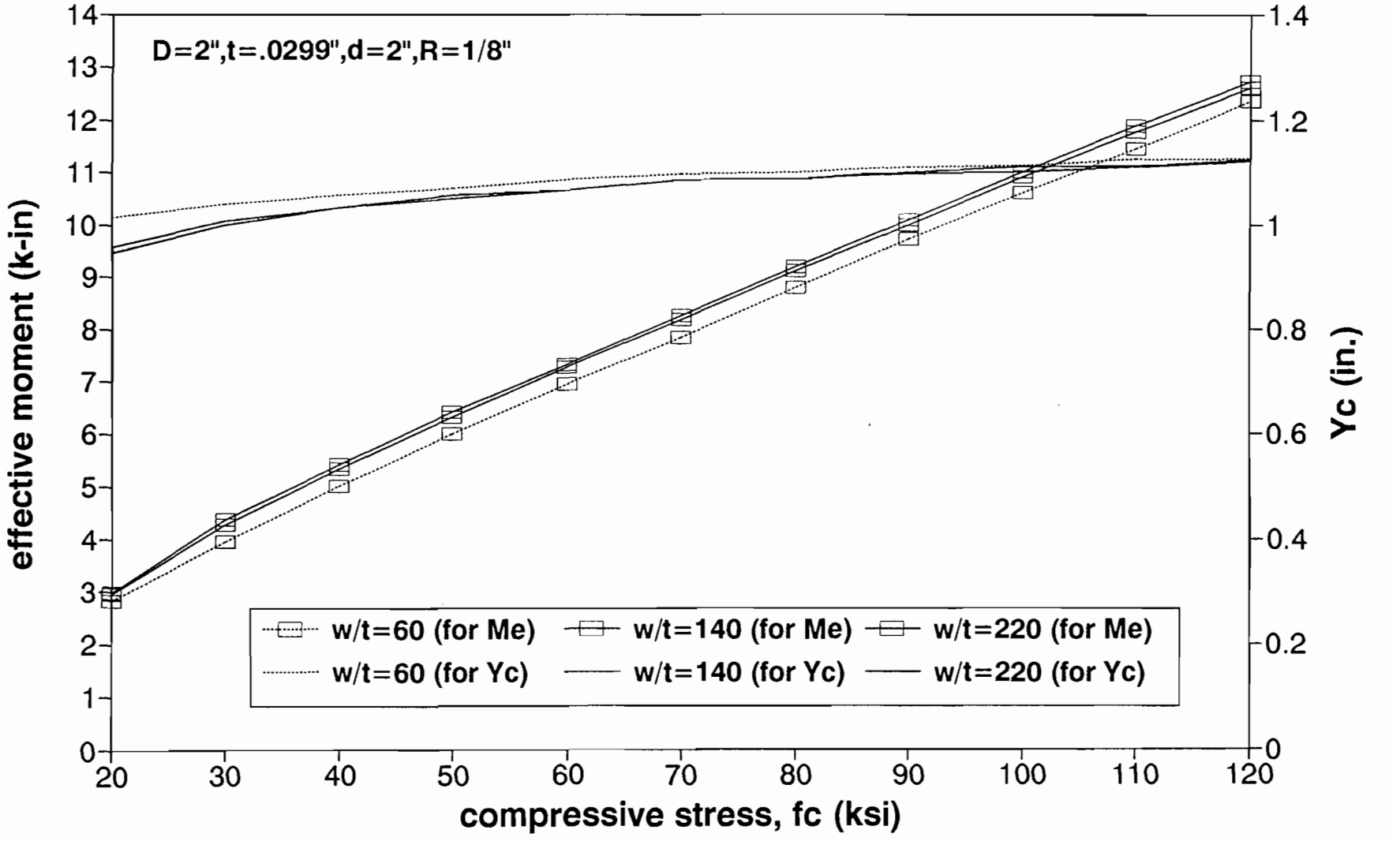

Fig. 3.3.3 Effective Moment and Distance Y_c vs. Compressive Stress

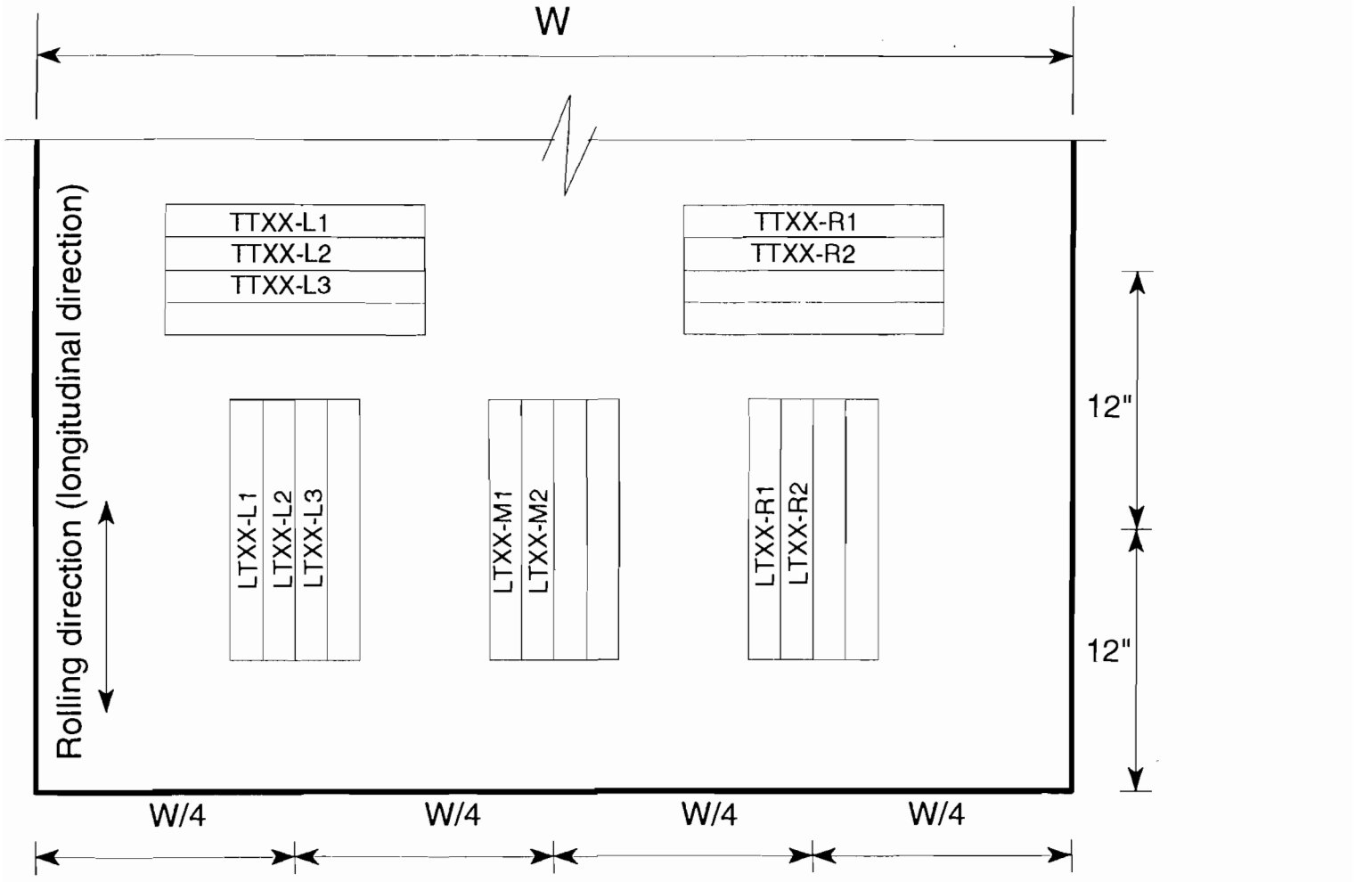

Fig. 4.2.1 Layout of Coupons Cut from Virgin Steel Sheet

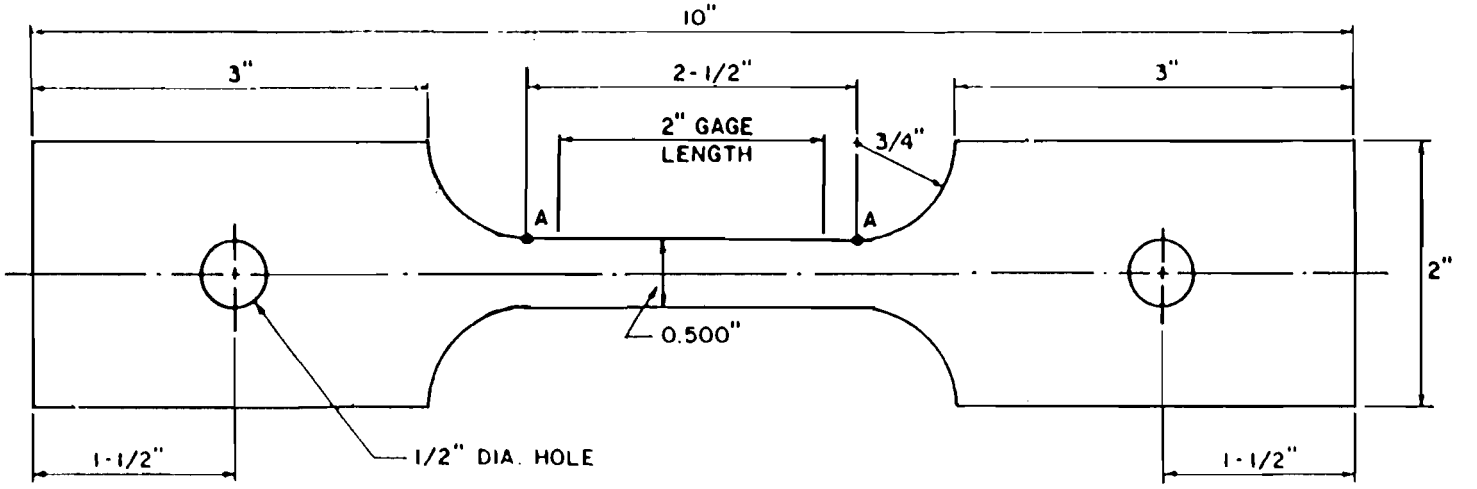

Fig. 4.2.2 Nominal Dimensions of Tension Coupons

Fig. 4.3.1 MTS 880 Test System

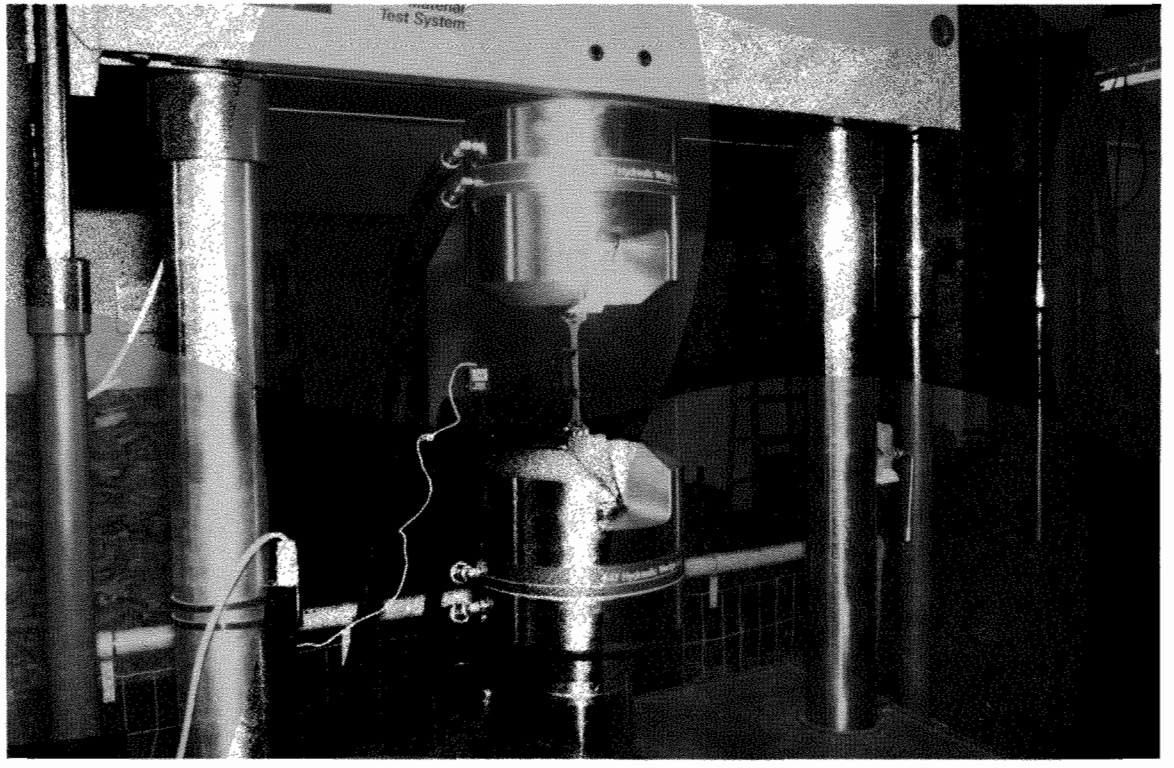

Fig. 4.3.2 Grips in MTS 880 Test Frame

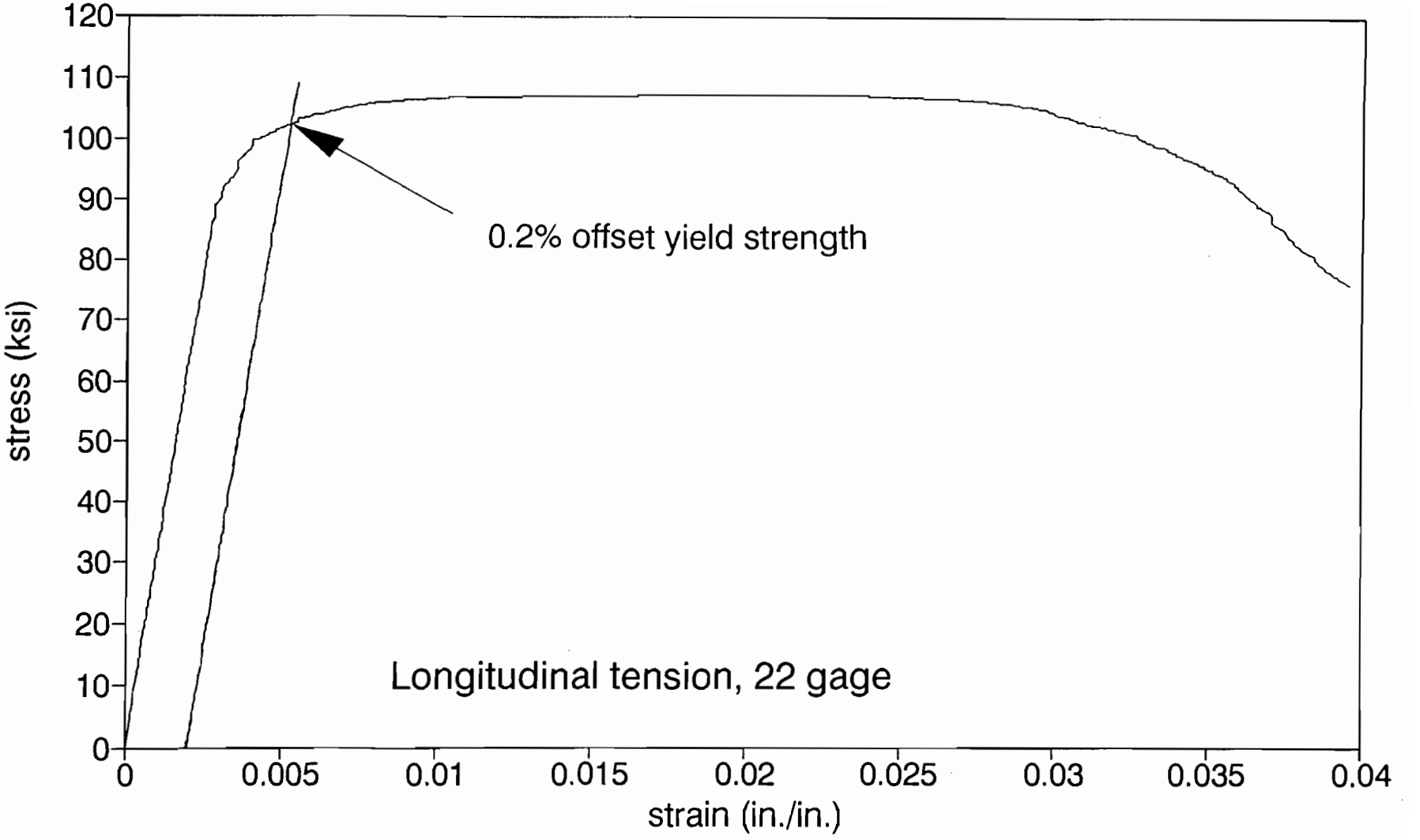

Fig. 4.4.1 Determining 0.2% Offset Yield Strength in Longitudinal Direction

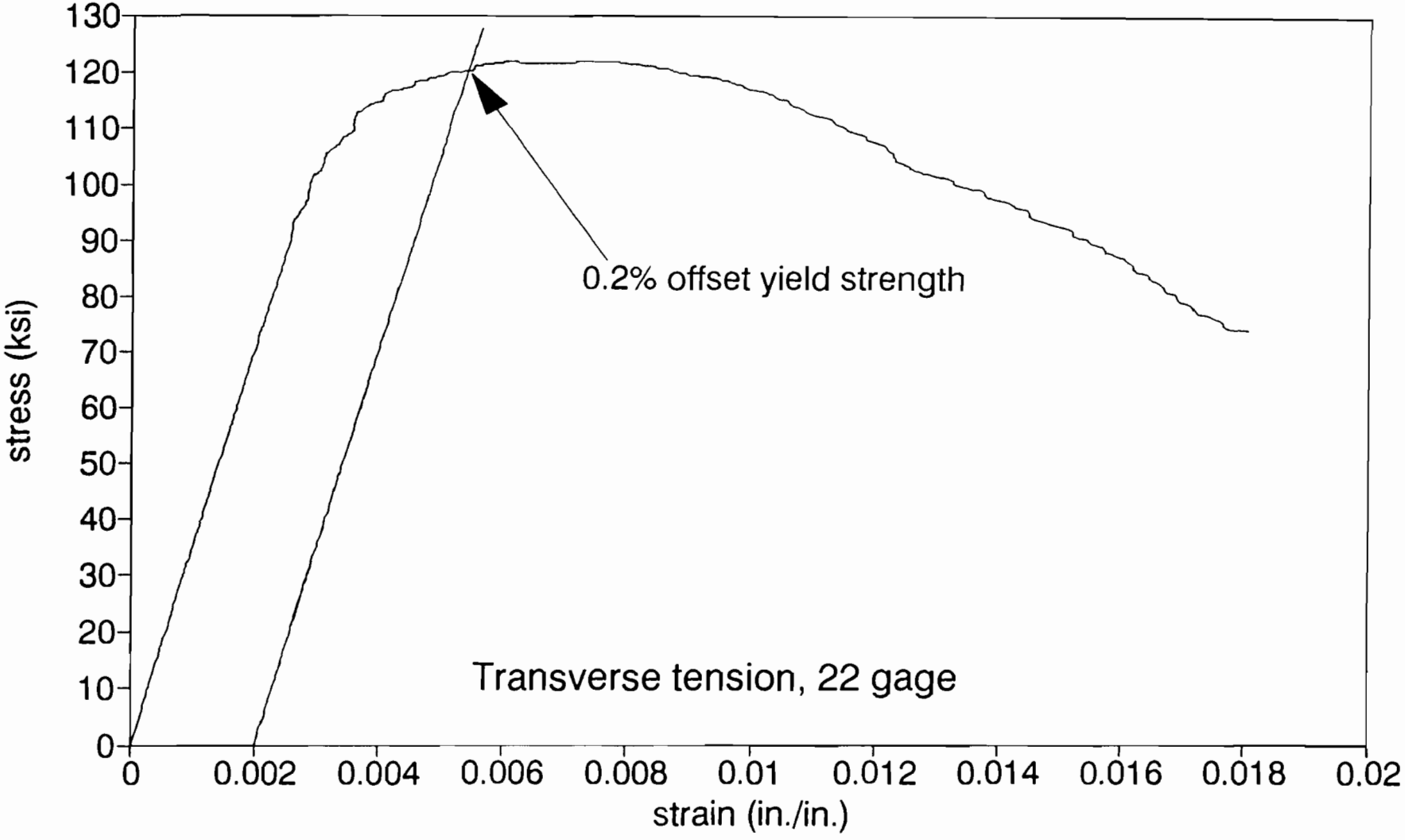

Fig. 4.4.2 Determining 0.2% Offset Yield Strength in Transverse Direction

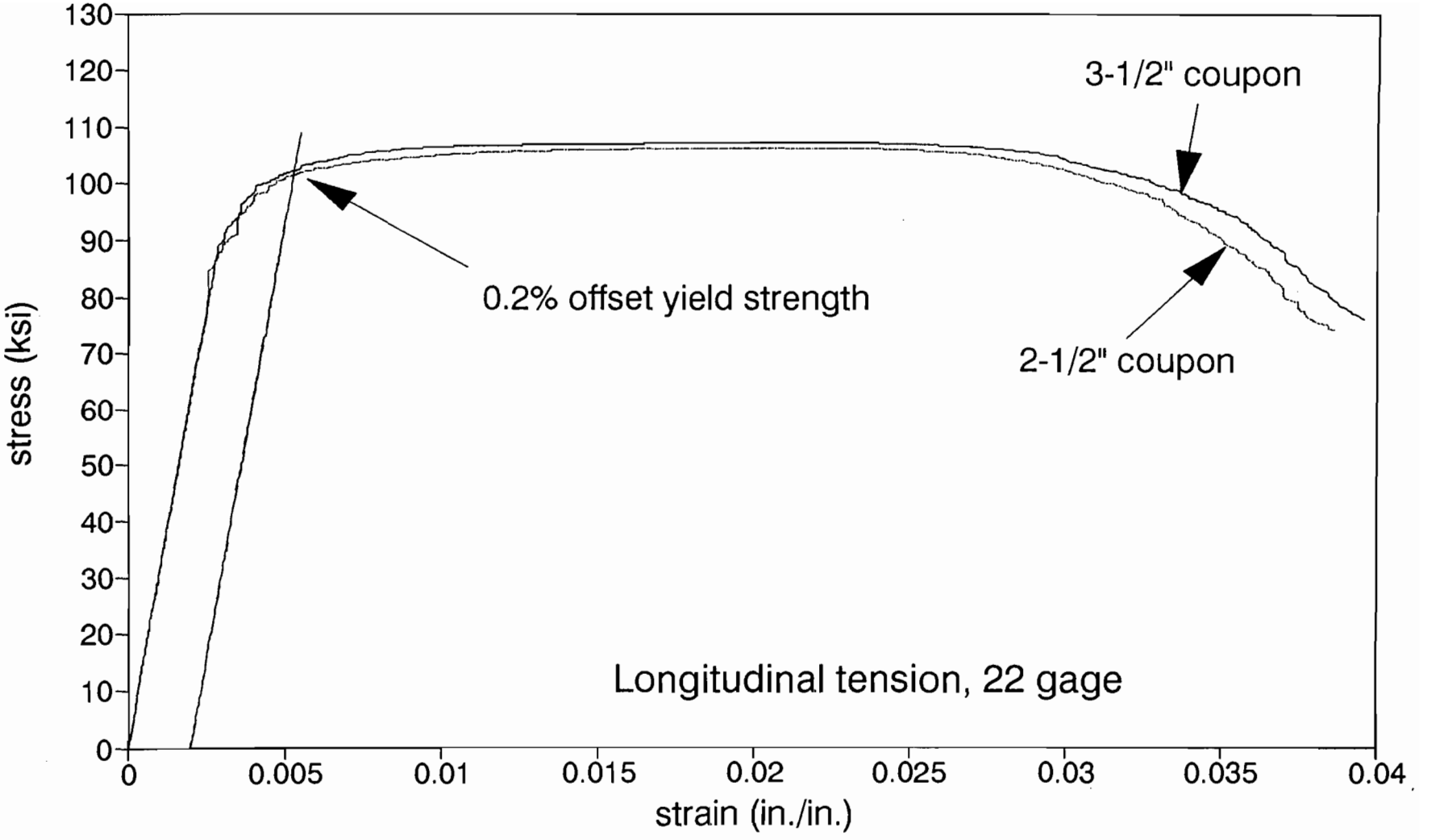

Fig. 4.4.3 Comparison of Stress-Strain Curves for Long and Short Coupons in Longitudinal Direction

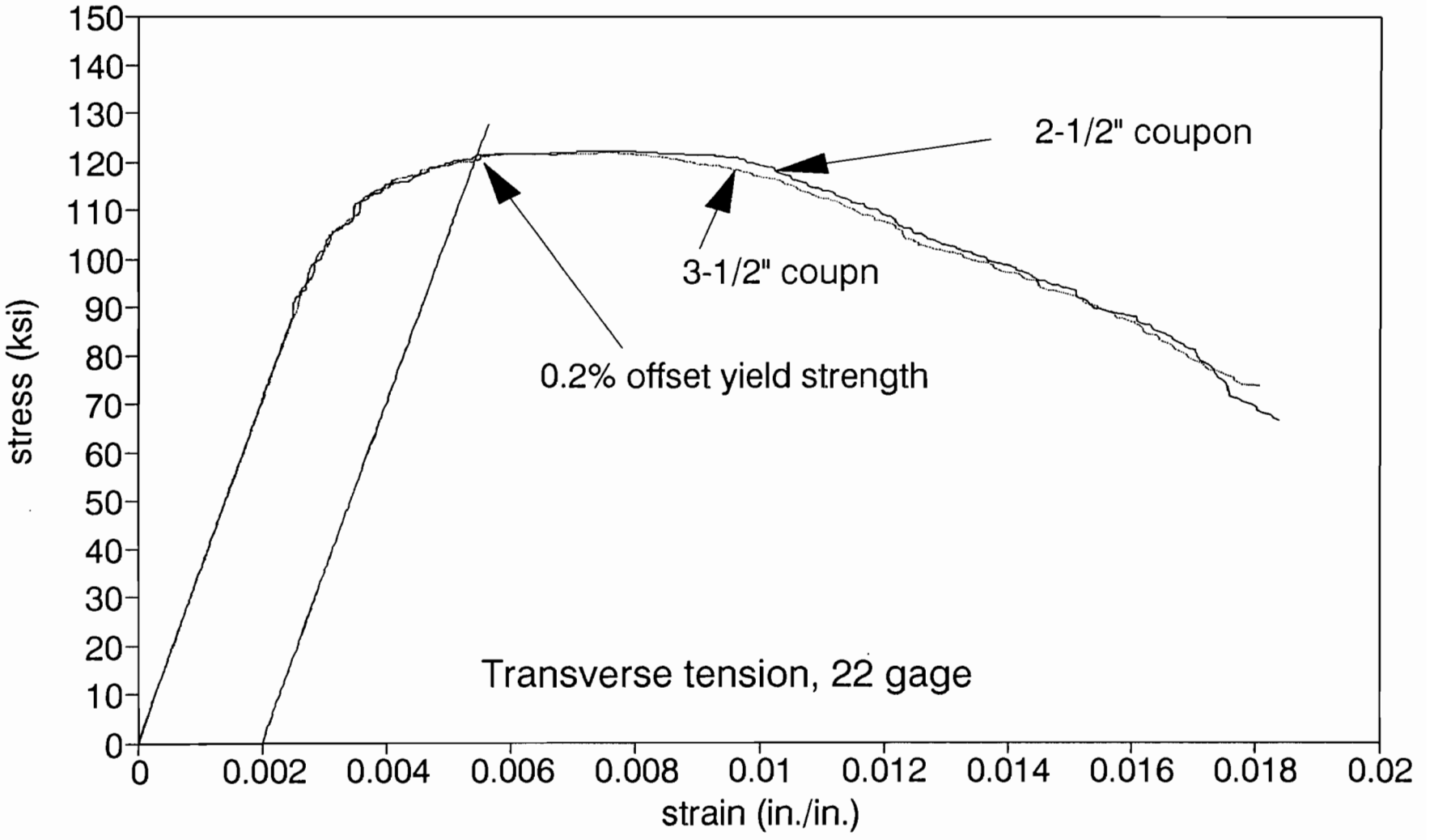

Fig. 4.4.4 Comparison of Stress-Strain Curves for Long and Short Coupons in Transverse Direction

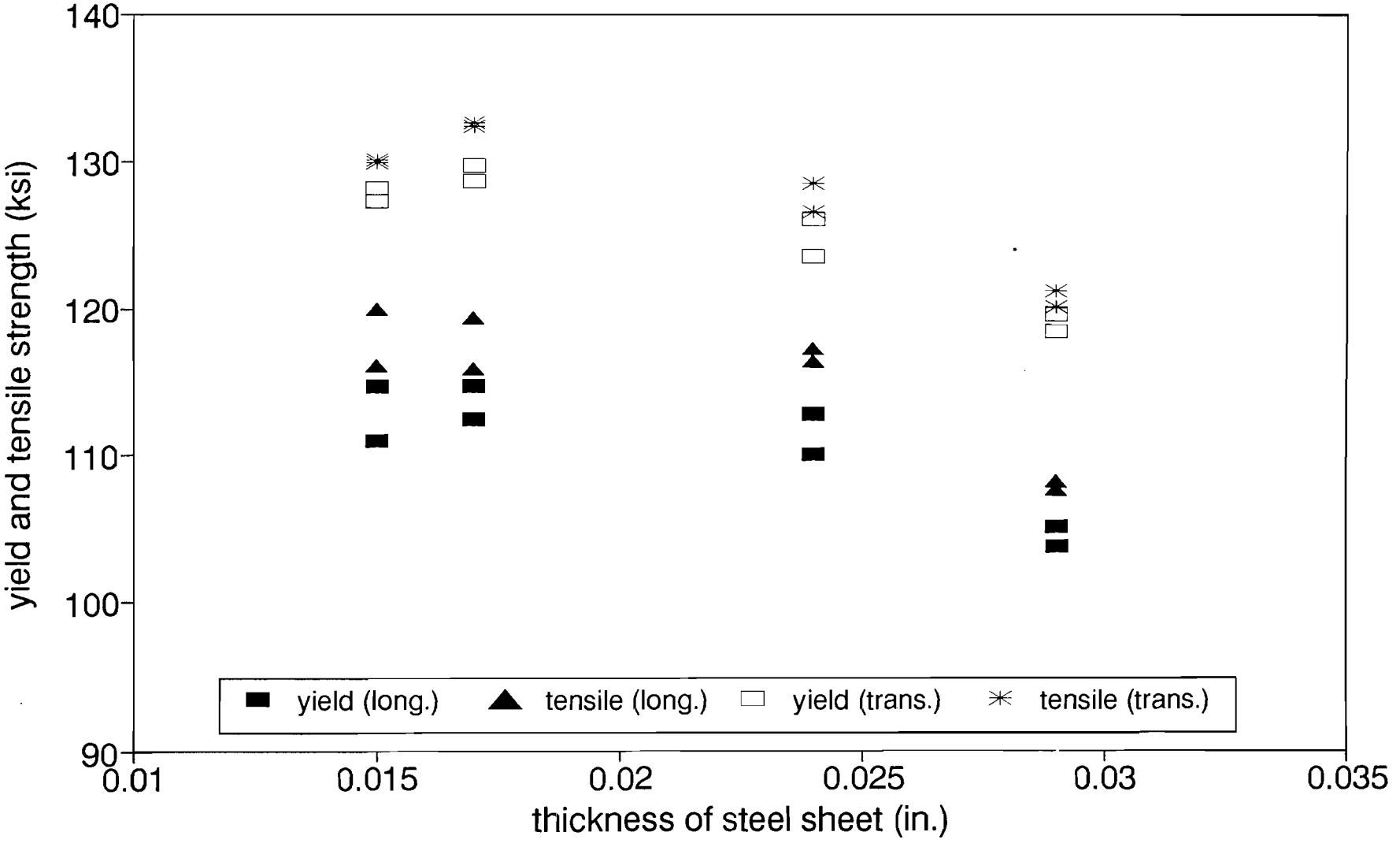

Fig. 4.4.5 Yield and Tensile Strengths vs. Thickness of Steel Sheet

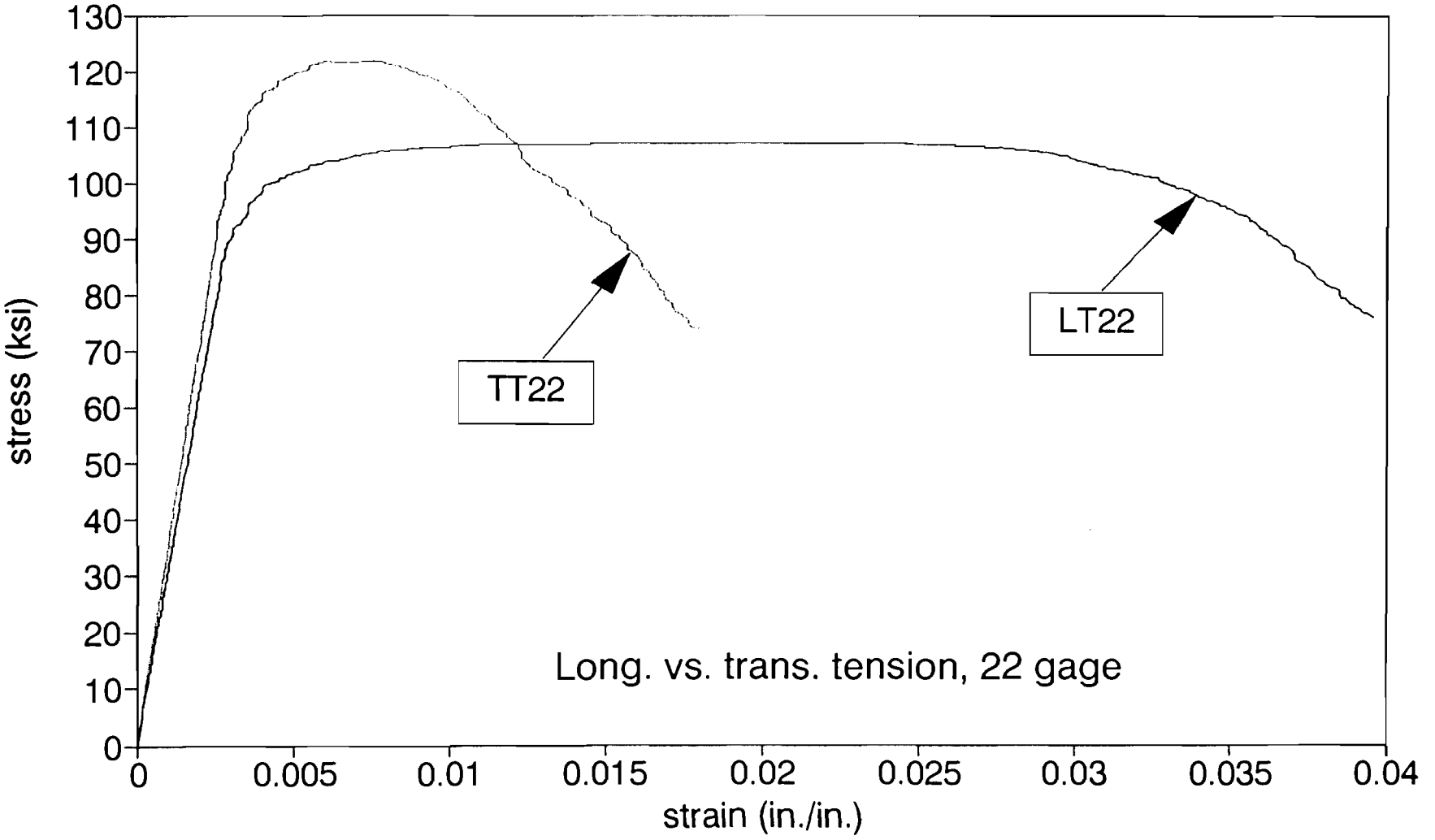

Fig. 4.4.6 Comparison of Stress-Strain Curves of 22 Gage Sheet Steel in Longitudinal and Transverse Direction

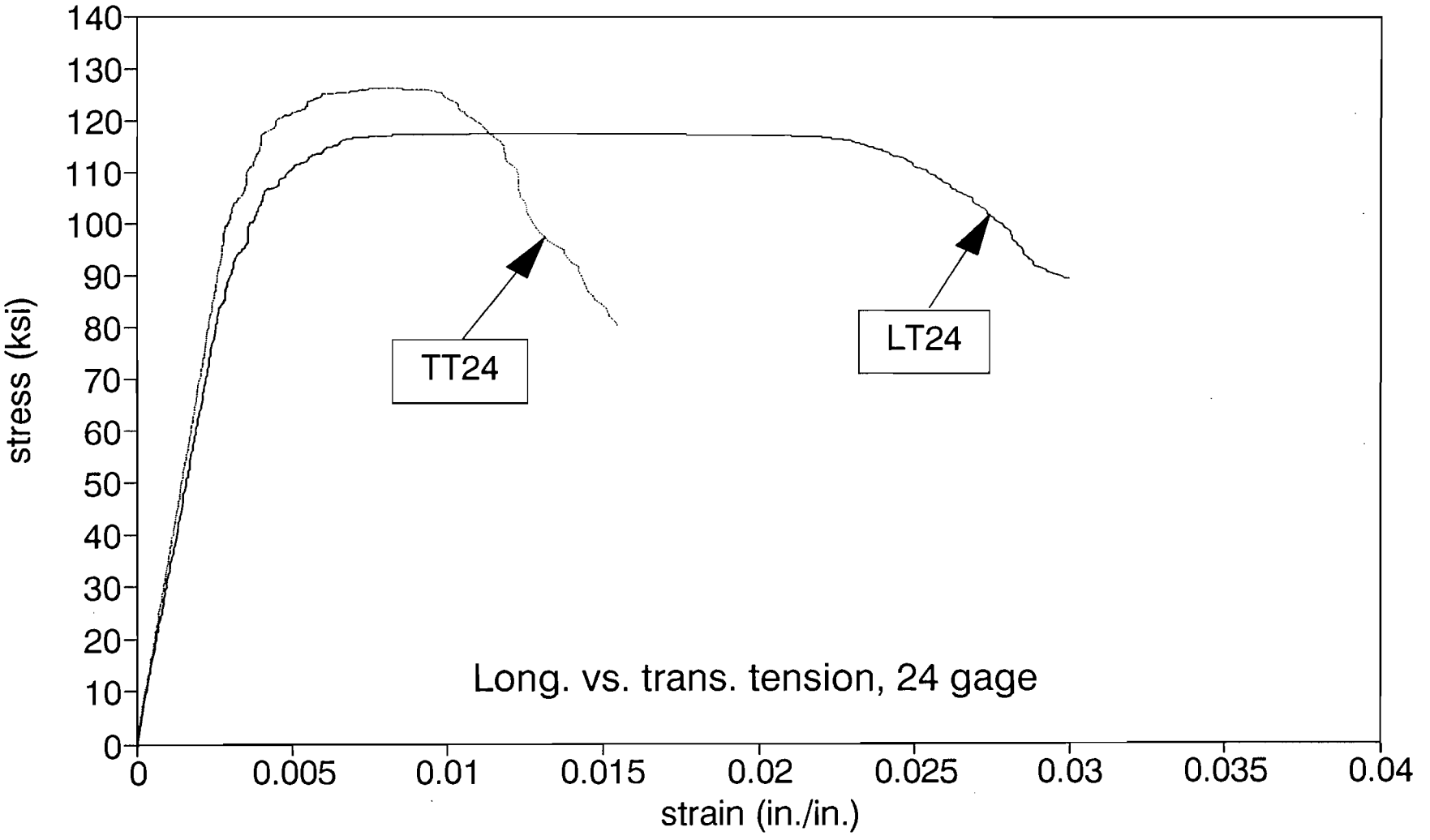

Fig. 4.4.7 Comparison of Stress-Strain Curves of 24 Gage Sheet Steel in Longitudinal and Transverse Direction

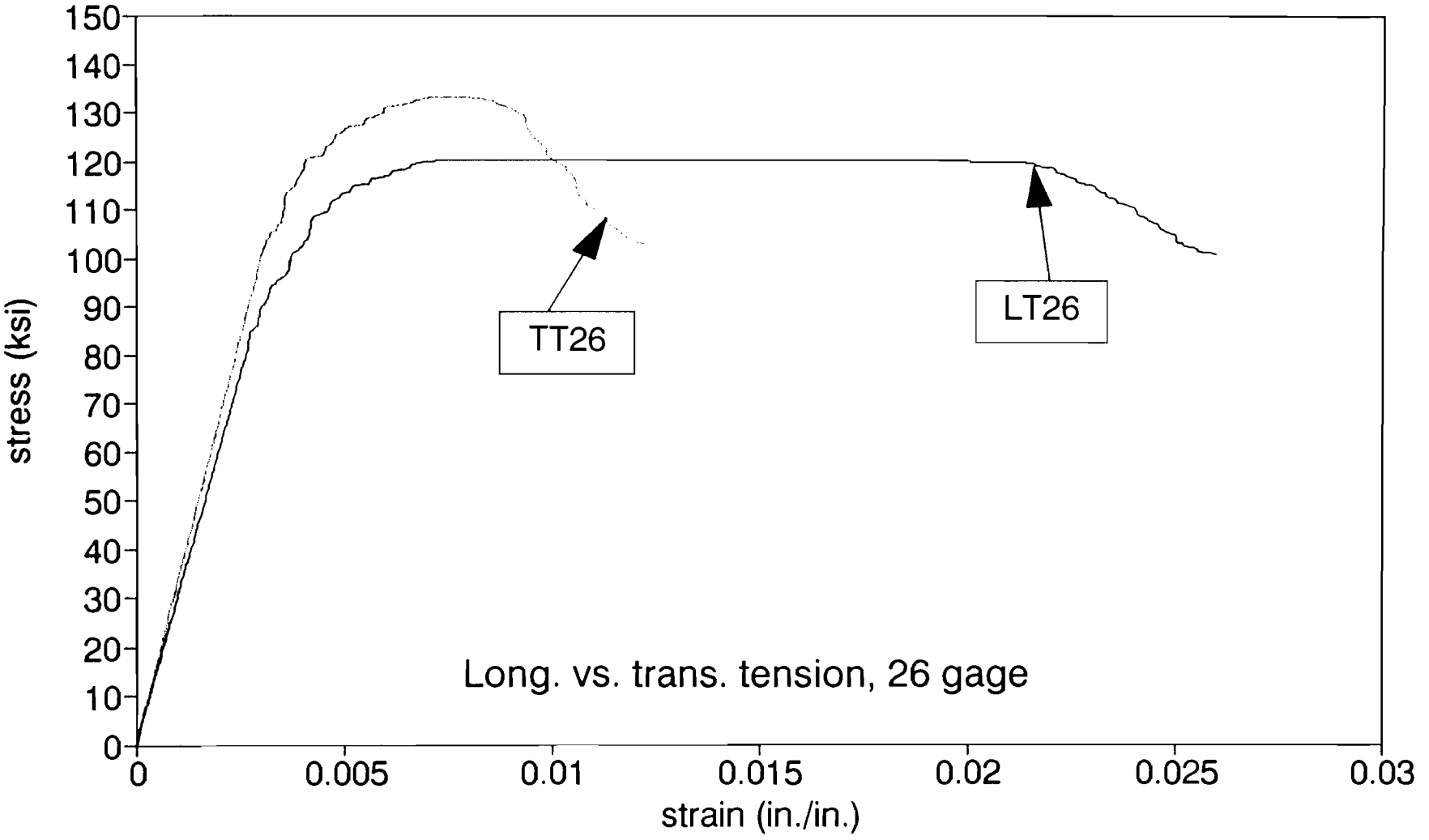

Fig. 4.4.8 Comparison of Stress-Strain Curves of 26 Gage Sheet Steel in Longitudinal and Transverse Direction

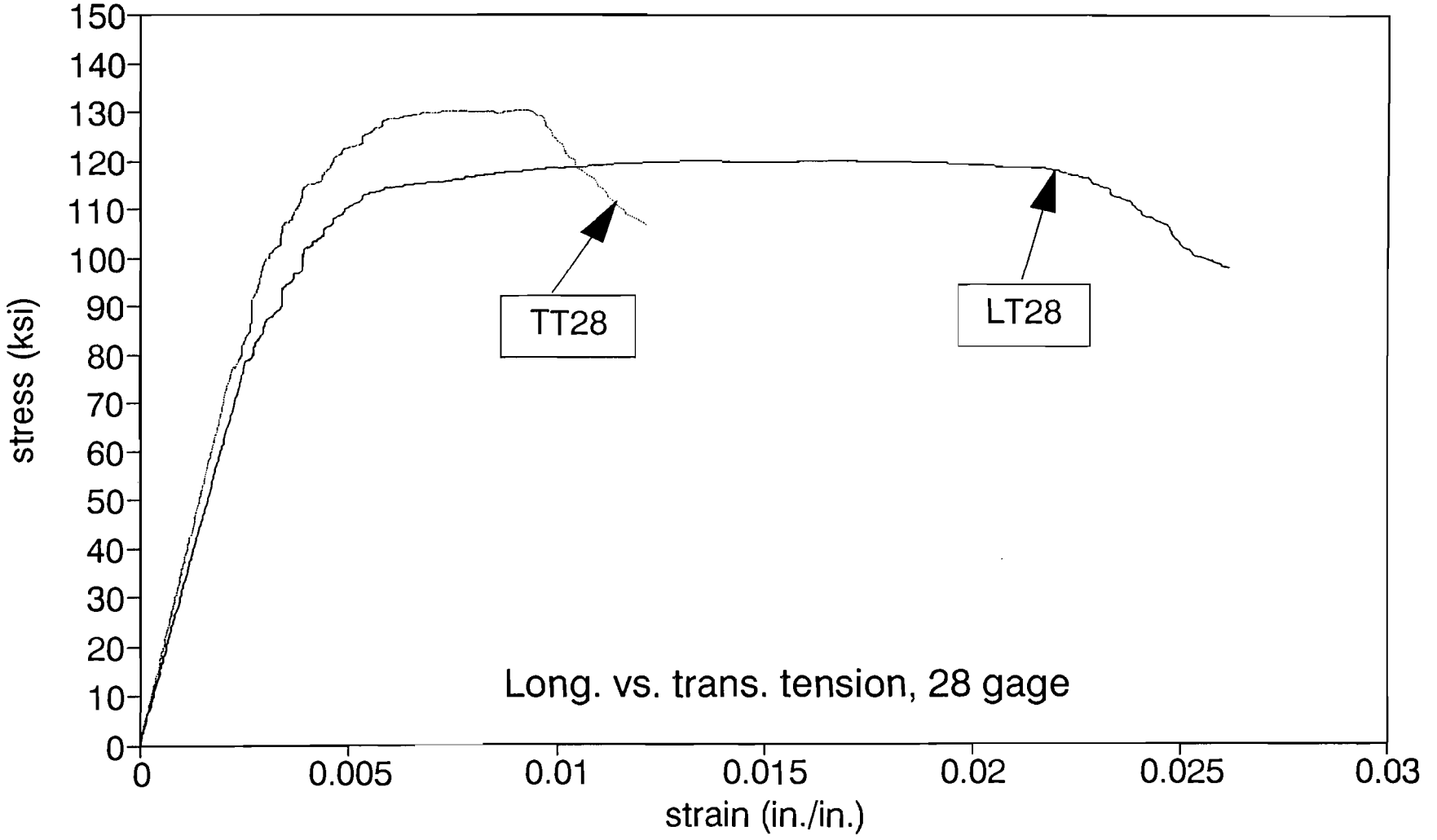

Fig. 4.4.9 Comparison of Stress-Strain Curves of 28 Gage Sheet Steel in Longitudinal and Transverse Direction

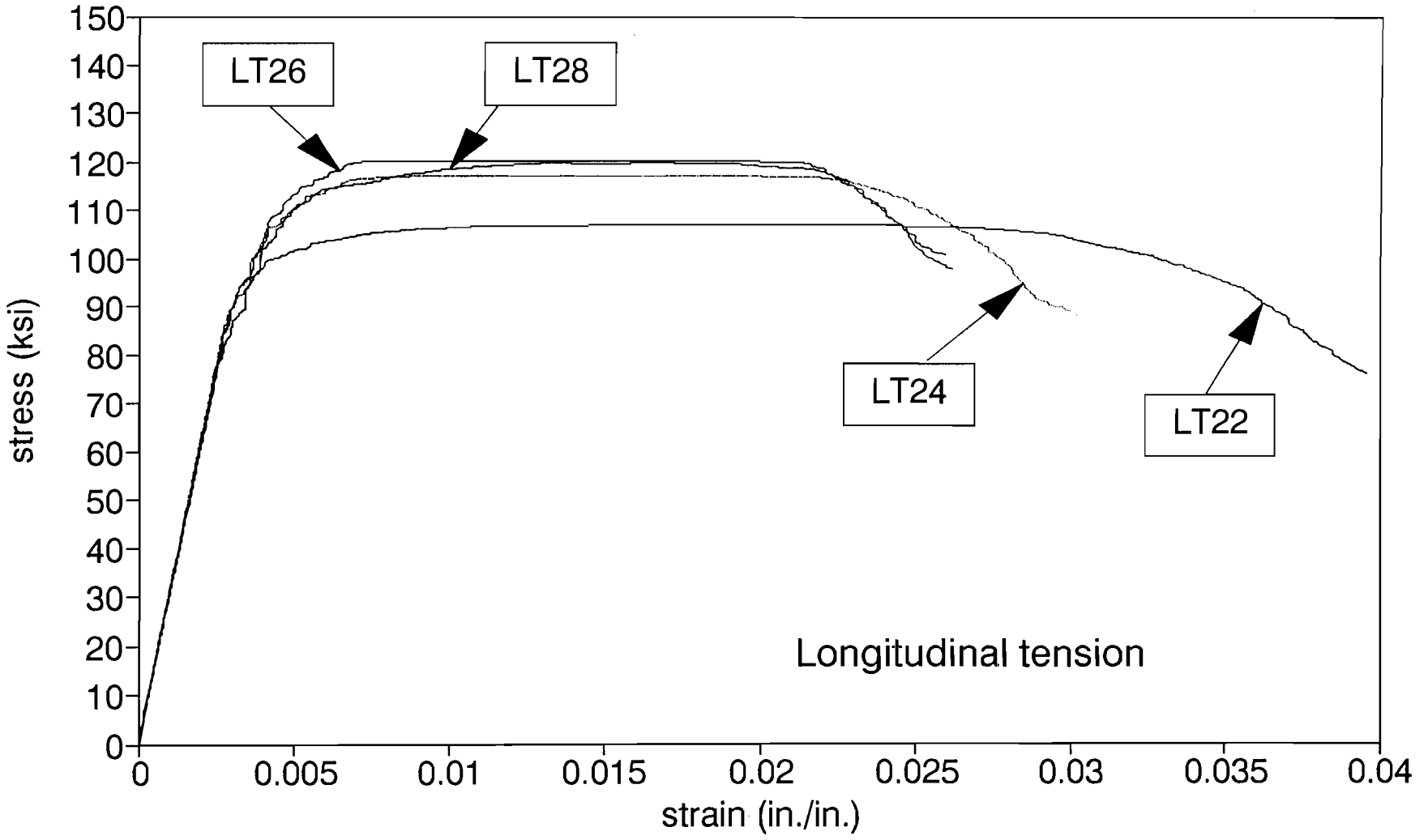

Fig. 4.4.10 Comparison of Stress-Strain Curves of Four Sheet Steels in Longitudinal Direction

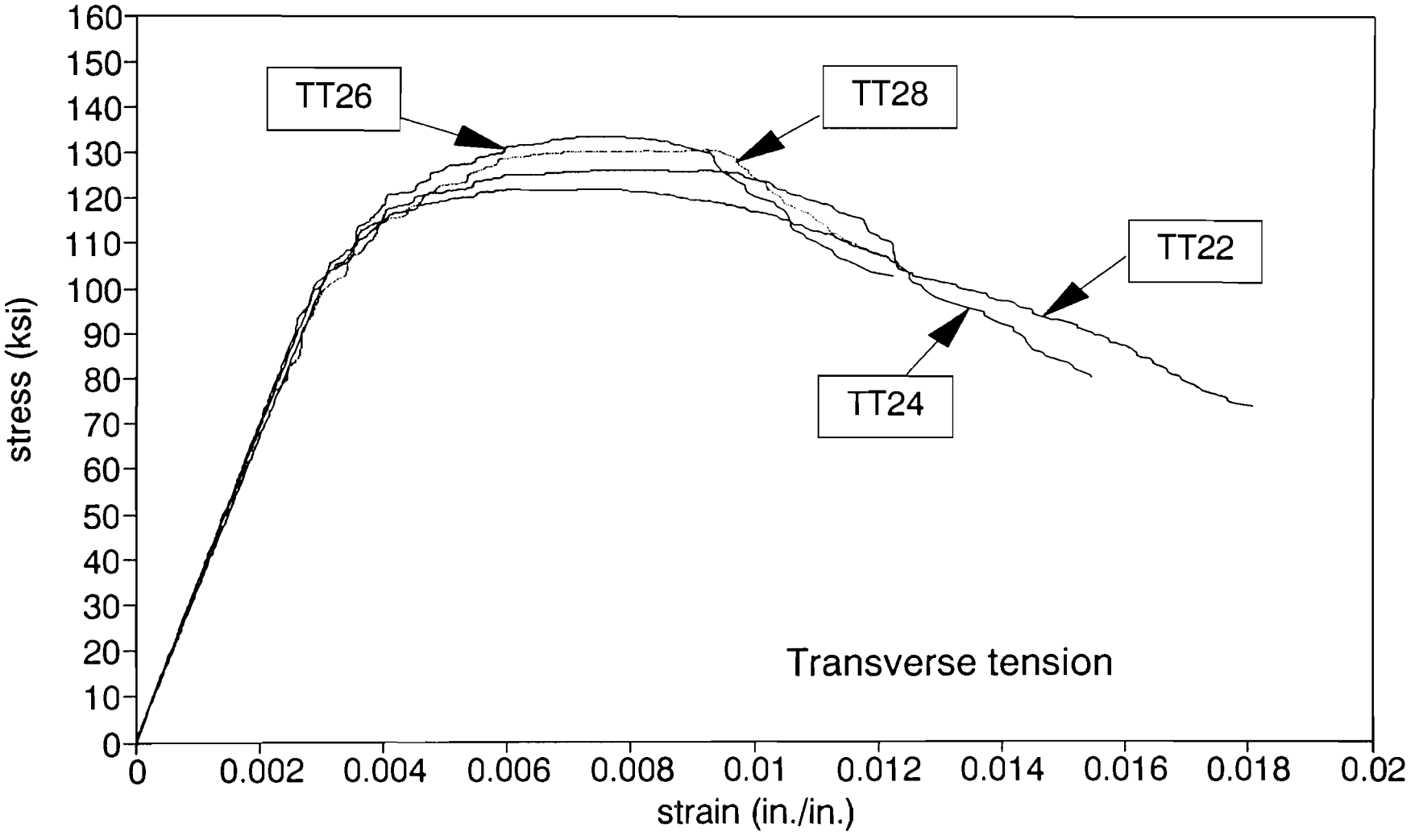

Fig. 4.4.11 Comparison of Stress-Strain Curves of Four Sheet Steels in Transverse Direction

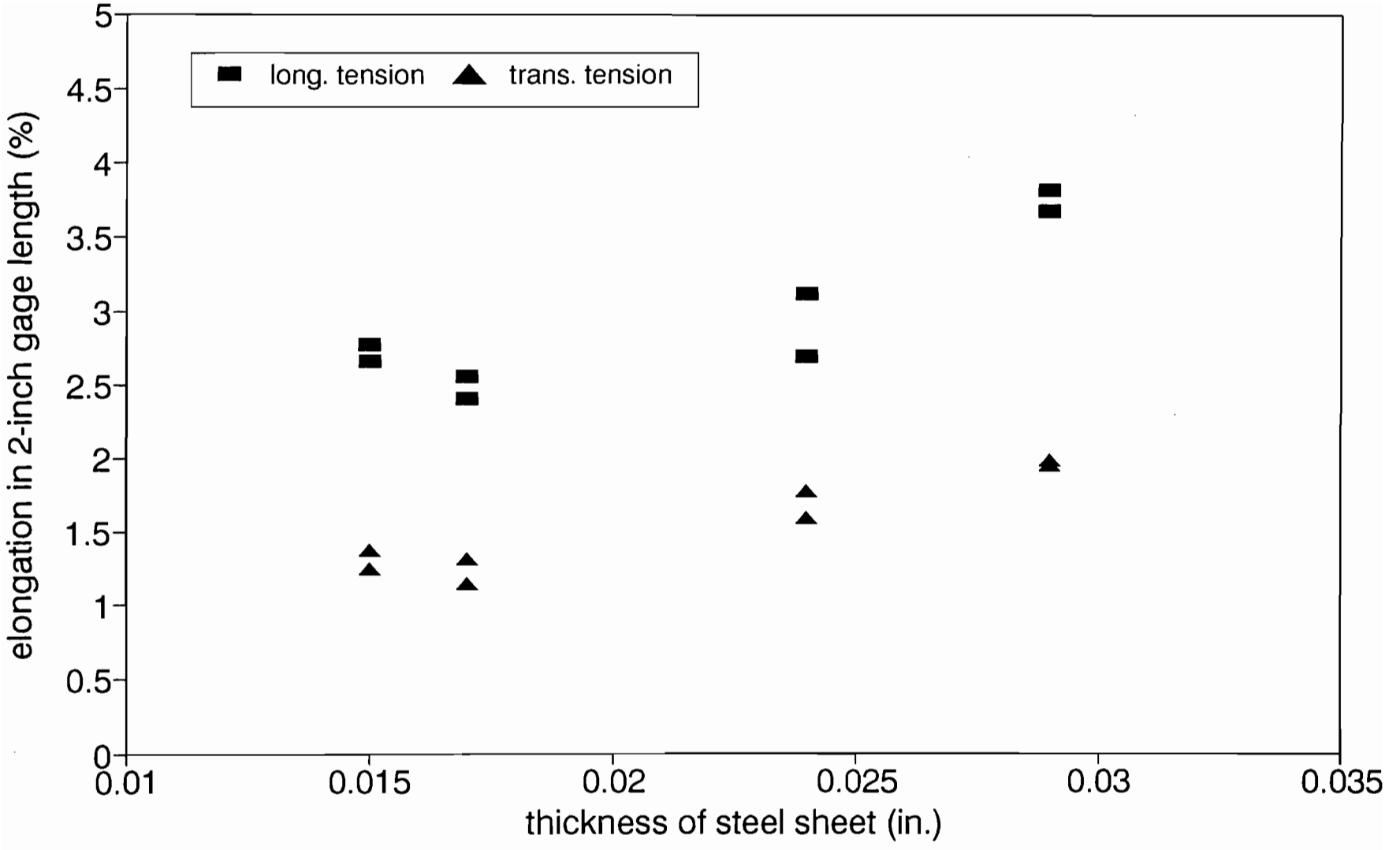

Fig. 4.4.12 Elongation in 2-Inch Gage Length vs. Thickness of Steel Sheet

Fig. 4.4.13 Failure of Long Coupons

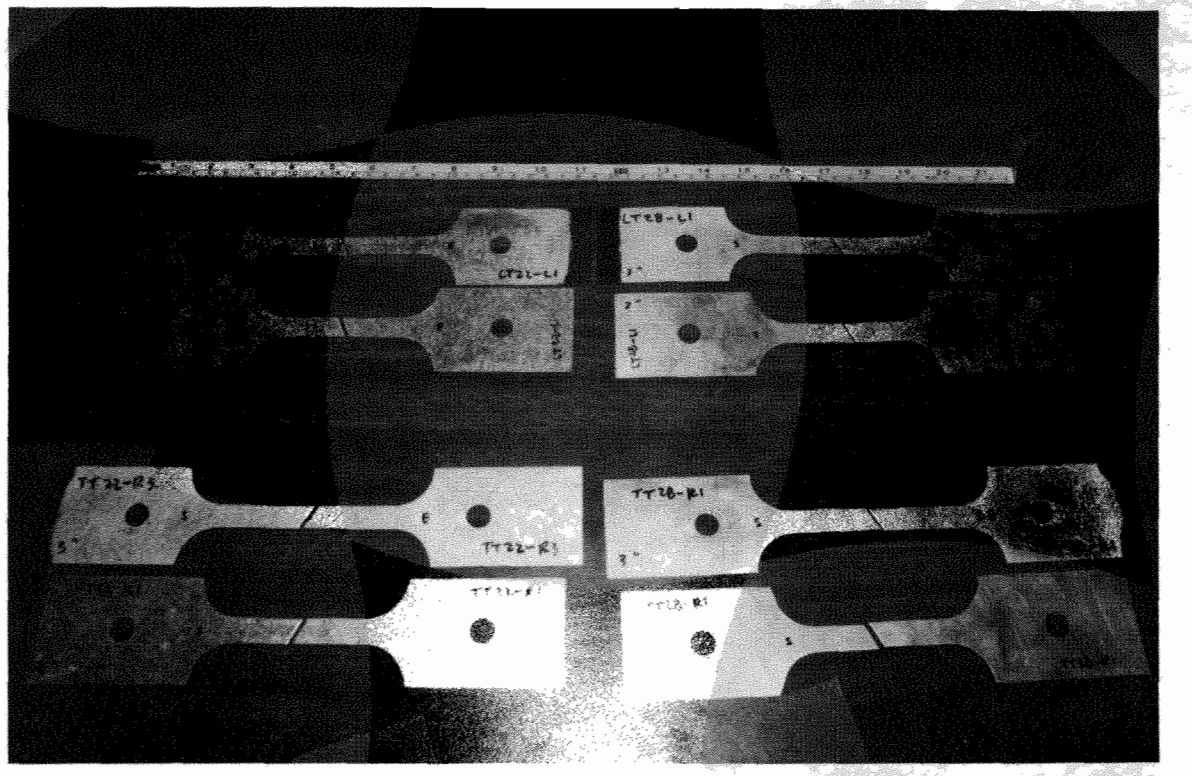

Fig. 4.4.14 Comparison of Failures between Long and Short Coupons

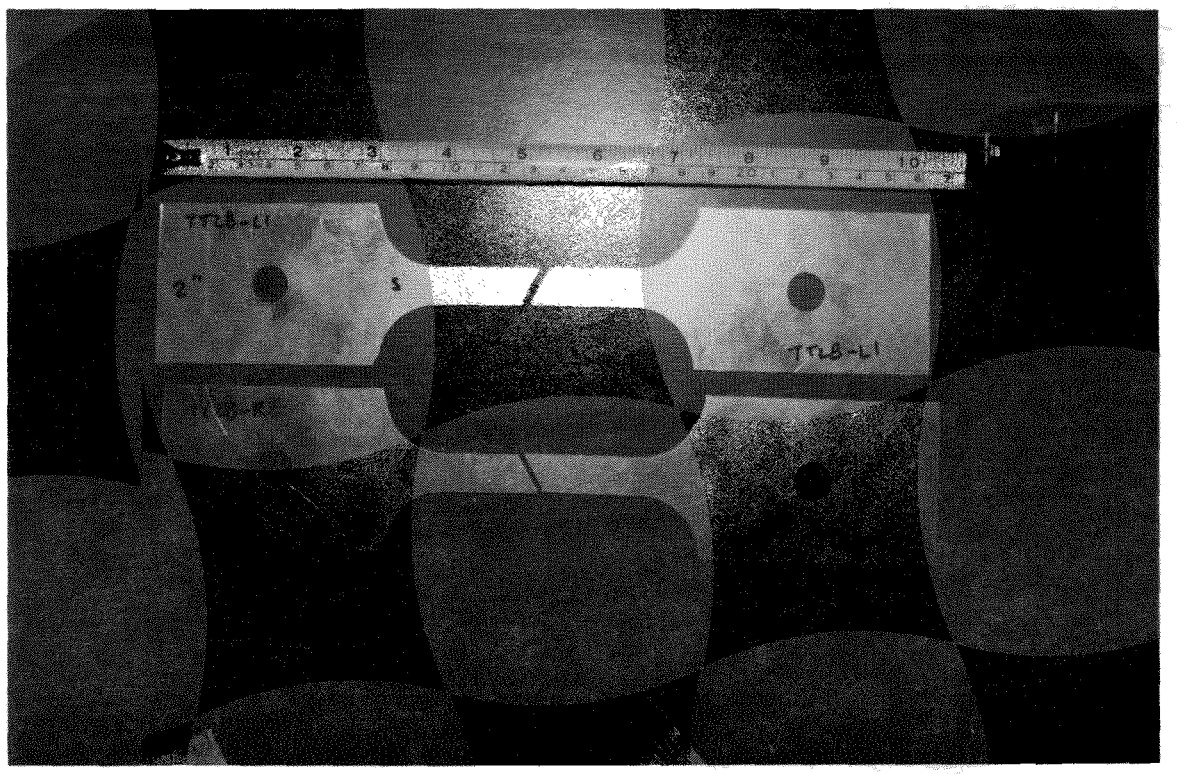

Fig. 4.4.15 Partial Brittle Failure at the Edge of Necking

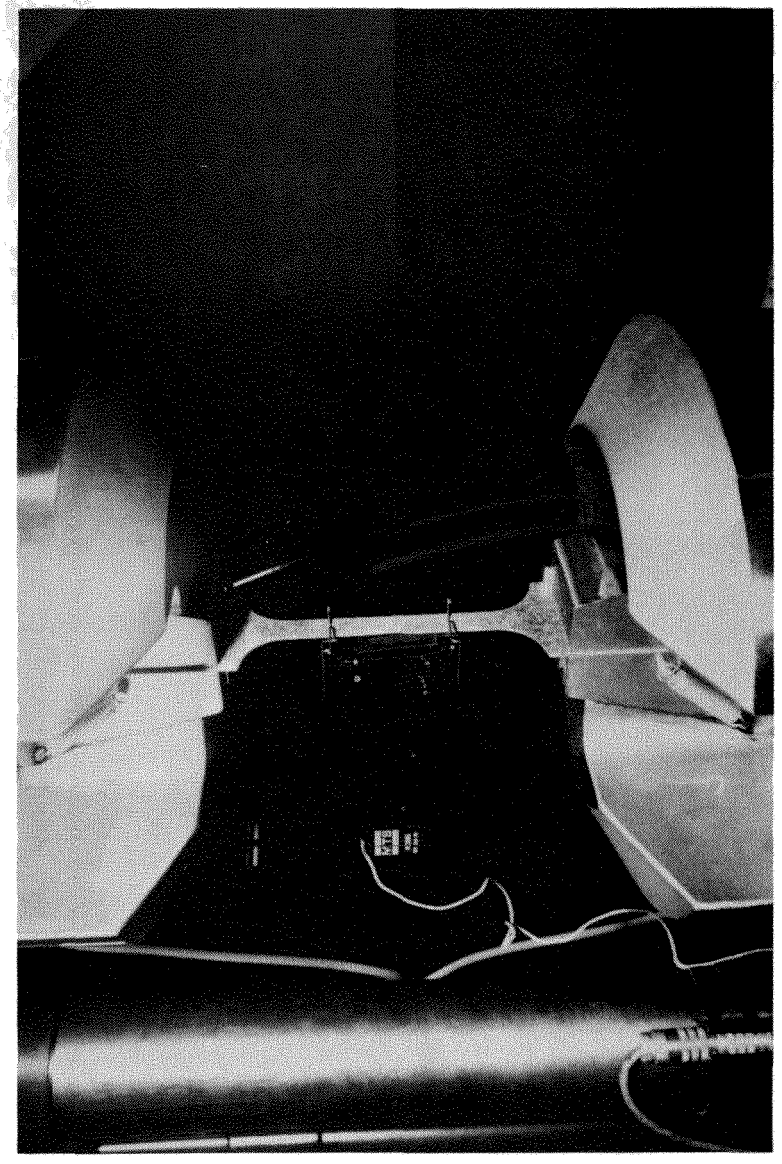

Fig. 4.4.16 Formation of Necking Prior to Fracture

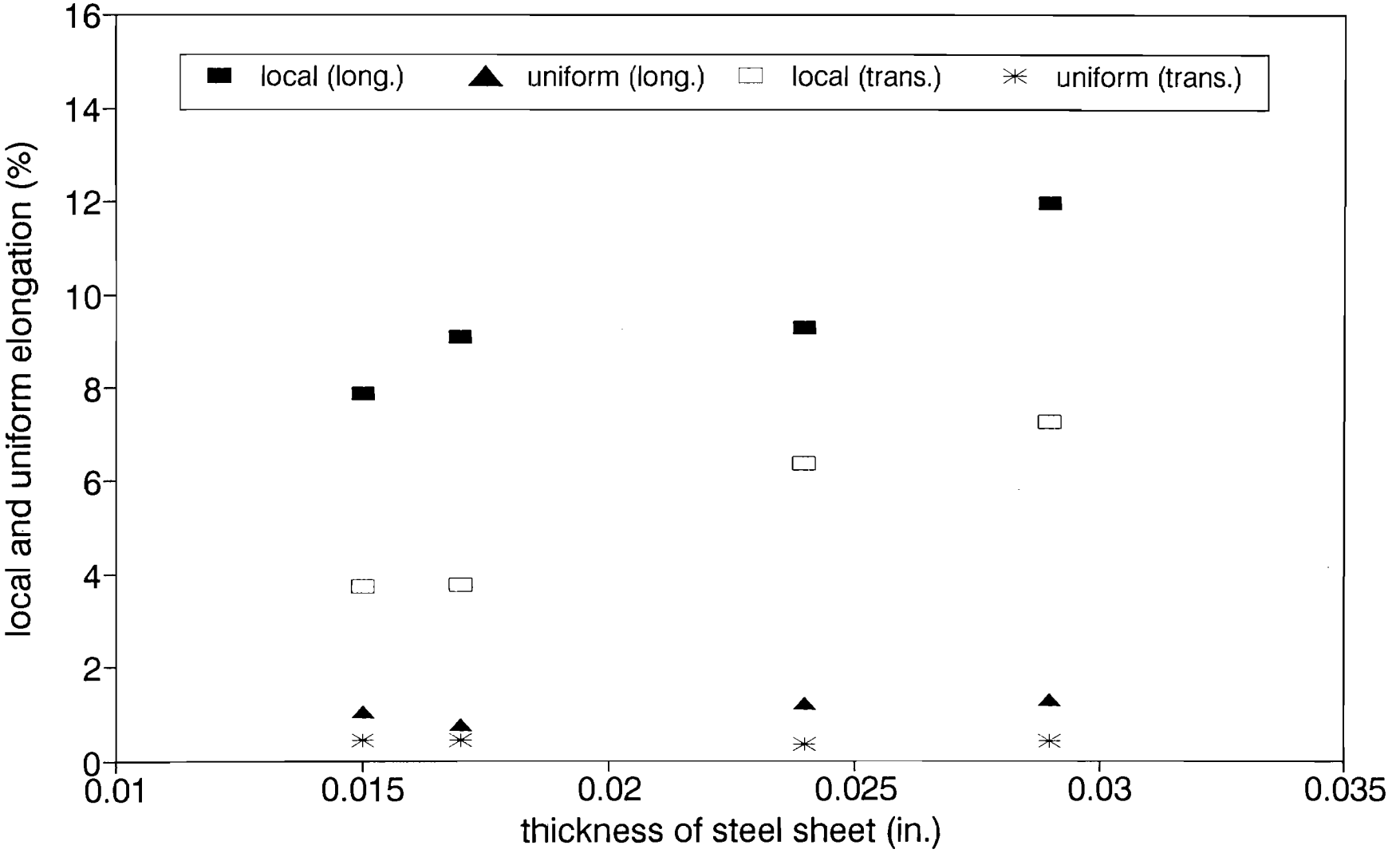

Fig. 4.4.17 Local and Uniform Elongations vs. Thickness of Steel Sheet